



National Library of Canada

Bibliothèque nationale du Canada

0-315-05526-X

Canadian Theses Division / Division des thèses canadiennes

Ottawa, Canada
K1A 0N4

53420

PERMISSION TO MICROFILM — AUTORISATION DE MICROFILMER

Please print or type — Écrire en lettres moulées ou dactylographier.

Full Name of Author — Nom complet de l'auteur

JEFFREY JOHN EDWARD HAYES

Date of Birth — Date de naissance

MARCH 19 1957

Country of Birth — Lieu de naissance

CANADA

Permanent Address — Résidence fixe

43 JEFFERSON ST APT 2
BANGOR, ME, 04401
USA

Title of Thesis — Titre de la thèse

A STUDY OF THE DOUBLE GALAXY
IN ABELL CLUSTER 1775

University — Université

ST. MARY'S UNIVERSITY, HALIFAX, NS.

Degree for which thesis was presented — Grade pour lequel cette thèse fut présentée

MASTER OF SCIENCE (M.Sc.)

Year this degree conferred — Année d'obtention de ce grade

1982

Name of Supervisor — Nom du directeur de thèse

G. A. WELCH

Permission is hereby granted to the NATIONAL LIBRARY OF CANADA to microfilm this thesis and to lend or sell copies of the film.

L'autorisation est, par la présente, accordée à la BIBLIOTHÈQUE NATIONALE DU CANADA de microfilmer cette thèse et de prêter ou de vendre des exemplaires du film.

The author reserves other publication rights, and neither the thesis nor extensive extracts from it may be printed or otherwise reproduced without the author's written permission.

L'auteur se réserve les autres droits de publication; ni la thèse ni de longs extraits de celle-ci ne doivent être imprimés ou autrement reproduits sans l'autorisation écrite de l'auteur.

Date

18/6/82

Signature



National Library of Canada
Collections Development Branch

Canadian Theses on
Microfiche Service

Bibliothèque nationale du Canada
Direction du développement des collections

Service des thèses canadiennes
sur microfiche

NOTICE

The quality of this microfiche is heavily dependent upon the quality of the original thesis submitted for microfilming. Every effort has been made to ensure the highest quality of reproduction possible.

If pages are missing, contact the university which granted the degree.

Some pages may have indistinct print especially if the original pages were typed with a poor typewriter ribbon or if the university sent us a poor photocopy.

Previously copyrighted materials (journal articles, published tests, etc.) are not filmed.

Reproduction in full or in part of this film is governed by the Canadian Copyright Act, R.S.C. 1970, c. C-30. Please read the authorization forms which accompany this thesis.

THIS DISSERTATION
HAS BEEN MICROFILMED
EXACTLY AS RECEIVED

Ottawa, Canada
K1A 0N4

AVIS

La qualité de cette microfiche dépend grandement de la qualité de la thèse soumise au microfilmage. Nous avons tout fait pour assurer une qualité supérieure de reproduction.

S'il manque des pages, veuillez communiquer avec l'université qui a conféré le grade.

La qualité d'impression de certaines pages peut laisser à désirer, surtout si les pages originales ont été dactylographiées à l'aide d'un ruban usé ou, si l'université nous a fait parvenir une photocopie de mauvaise qualité.

Les documents qui font déjà l'objet d'un droit d'auteur (articles de revue, examens publiés, etc.) ne sont pas microfilmés.

La reproduction, même partielle, de ce microfilm est soumise à la Loi canadienne sur le droit d'auteur, SRC 1970, c. C-30. Veuillez prendre connaissance des formules d'autorisation qui accompagnent cette thèse.

LA THÈSE A ÉTÉ
MICROFILMÉE TELLE QUE
NOUS L'AVONS REÇUE

A STUDY OF THE DOUBLE GALAXY
IN ABELL CLUSTER 1775



By Jeffrey J. E. Hayes

Submitted as a Partial Requirement
for the Degree of Master of Science
in Astronomy from St. Mary's University

© Halifax, October A.D. 1981

ABSTRACT

Photographic and photoelectric photometry are used to obtain intensity profiles of the A1775 double galaxy. The intensity profiles are fitted to the standard ($c = 2.25$) King models, from which composite models are constructed. The apparent core radii of the SE and NW components are found to be 2.4 kpc and 3.9 kpc respectively ($H_0 = 75$ km/sec/Mpc). The composite models consist of isophotal contour maps and a modelled surface brightness profile along the line joining the two components. The models constructed do not fit the data very well in the outer portions of the brightness profile, in that they overestimate the amount of light coming from these regions. On the basis of the models however, it seems unlikely that the A1775 system is a superposition of two unrelated galaxies, but is more likely to be some sort of interacting system. The nature of the interaction, however, cannot be answered, nor can the existence of a large diffuse halo be demonstrated on the basis of the present data.

TABLE OF CONTENTS

Acknowledgements	1
Section I: Introduction	2
Section II: Previous Studies	3
Section III: Observations and Data Reduction.	14
Section IV: King Models and Model Fitting.	33
Section V: Composite Models	56
Section VI: Discussion and Conclusions	77
Notes to Appendices.	82
Appendix 1: Programme GALAXY	83
Appendix 2: Programme PROFIL	84
Appendix 3: Background on King Models.	87
Appendix 4: Programme REDUCE	95
Appendix 5: Programme MODEL.	96
References	97

ACKNOWLEDGEMENTS

This writer would like to thank first and foremost Dr. G. A. Welch, without whose help this study would not have been possible. The writer would also like to thank Dr. J. N. Scrimger, who acted as interim advisor while Dr. Welch was on sabbatical leave.

Thanks are also due to Dr. I. R. King for supplying the points which define the isothermal models and Dr. John Huchra at the Centre for Astrophysics for supplying unpublished spectroscopic data of the A1775 system. Mr. T. J. Deveau, who supplied and allowed the writer to use his computer programme that digitizes microdensitometry tracings and Mr. G. Collins who supplied the author with a linear interpolation routine are also to be thanked. Thanks are also extended to Mr. R. Brooks and Ms. L. Burgoyne who helped to prepare the figures and to calibrate the surface brightnesses, respectively.

SECTION I: INTRODUCTION

The double galaxy in Abell Cluster 1775 has been studied by Chincarini et al (1977) and by Hintzen (1979). The conclusions reached in these two papers are quite different. Chincarini et al determined that the A1775 system forms a bound, closed system of extremely large mass, while Hintzen found that the system was not bound, but the superposition of two elliptical galaxies. The aim of this study is to use photographic and photoelectric photometry of the A1775 system as a starting point for the construction of composite models for the light distribution of the system.

The models chosen for the fitting process are those of King (1966), and it is upon the goodness of the fit of these composite models to the observations that it may be possible to determine which hypothesis (either Chincarini et al's or Hintzen's) most accurately describes the A1775 system.

Section II of this study will deal with the observations and conclusions of earlier investigations of the A1775 system. Section III will be concerned with the present data and its reduction to a point where model fitting is possible. Section IV will be concerned with the King models and the procedure used to fit the models to the observations. Section V will discuss the construction of the composite model, of the A1775 system, while Section VI will discuss the conclusions which may be drawn from the modelling of the A1775 double, and suggestions for further study.

SECTION II: PREVIOUS STUDIES

The double galaxy in A1775 has been studied before by two separate investigating teams. Chincarini et al in 1971 concluded that the A1775 system is a bound one, where the two components are in mutual orbit. The mass of the system was estimated to be $\sim 2 \times 10^{13} M_{\odot}$, making it one of the most massive known.

Hintzen's (1979) study concluded that the A1775 system was not bound, but a superposition of possibly unrelated elliptical galaxies.

The evidence cited by each of the above studies will be recapitulated. The evidence that Chincarini et al cite will be discussed first.

On the basis of photometry and spectroscopy, Chincarini et al concluded that the A1775 system is a single bound system. They base their claim on several pieces of evidence.

Firstly, the isophotes of the system show that the two components appear to be immersed in a common envelope. Secondly, microdensitometry indicates a deficiency of surface brightness at the minimum between the two components when compared to the sum of the surface brightnesses at an equal distance on either side.

According to Chincarini et al the deficiency of surface brightness is expected if the two components are bound, for the following reason. An optical dust-free double system would give no such deficiency of surface brightness. Consider two identical point masses. The gravitational potential midway between them is weaker than the sum at identical distances on either side. If it is assumed that the mass distribution within the bound double system tends to be located at a position with stronger potential, and the surface brightness is a mass-density indicator, then the observed deficiency can be plausibly accounted for.

In addition to the above, Chincarini et. al. also cite the colour and late-type absorption-line spectrum of the system. Both give no indication of any violent activity, which might be expected if one were observing a colliding pair of galaxies.

Also, on 48-inch Schmidt plates, the two components of this system (see Figure 1a) are the brightest objects within a circular area whose radius is at least 25 times the individual angular diameter of each nucleus. If one considers the probability of such a chance superposition of galaxies within the cluster, the odds are approximately 1 in 1000.

Using these arguments, Chincarini et. al. conclude that the system in A1775 is one in which the two components are bound. If one assumes that the components are in circular orbits, and with the observed difference in radial velocities of 1720 km/sec (see Table I), the lower limit to the mass is $\sim 2 \times 10^{13} M_{\odot}$. This would make it one of the most massive systems known.

Hintzen's (1979) paper is considered next, along with the evidence he cites to support his conclusion that the system in A1775 is not a bound system.

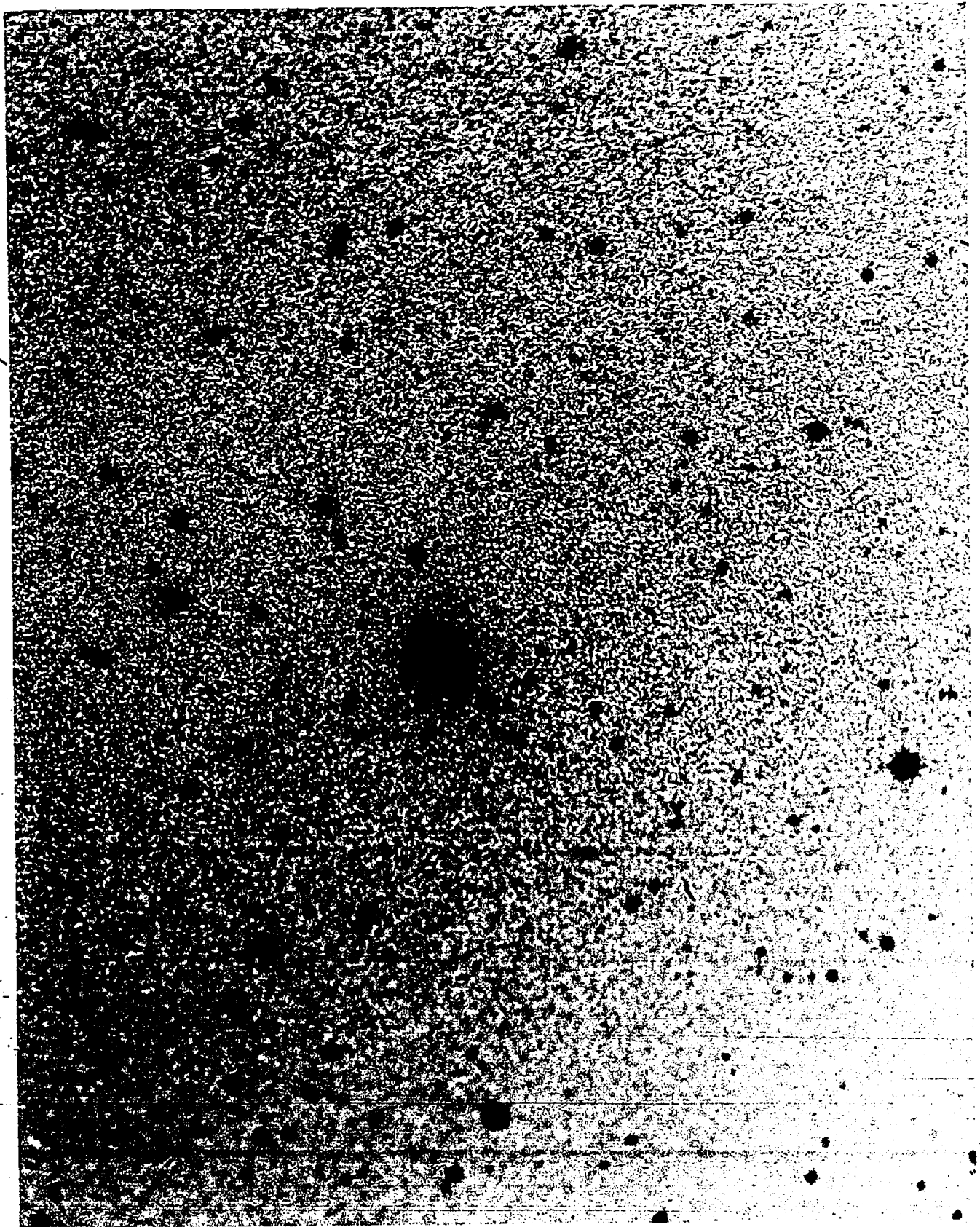
First, Hintzen cites the velocity dispersion of the cluster of galaxies. He finds the mean velocity of nine galaxies in the cluster, including the two components of the system to be 20859 km/sec, with a very large velocity dispersion of 1522 km/sec. Hintzen says there are two ways to explain this dispersion (one of the largest measured).

Either the cluster itself has a very large intrinsic velocity dispersion, or there are two clusters of galaxies superimposed along the line of sight. Due to the fact that the two components of the system are the brightest and largest galaxies in the central region of the A1775

Figure 1a. The Al775 system orientation:



103aD. plate 20^{min} exposure; scale = 1 cm = 25.6^μ



cluster, Hintzen concludes that the probability of the superposition of two large galaxies, one each in a cluster of high and low velocity dispersion respectively, to be small. Hintzen, therefore, considers the single cluster model. The difference between the models of Chincarini et. al. and Hintzen is that the former conclude that the system is bound, while the latter does not. The counter-arguments that Hintzen uses against Chincarini et. al.'s conclusions follow.

The velocities of the individual components of the A1775 system are 797 km/sec and 853 km/sec below and above the mean velocity of the cluster for the SE and NW components respectively. This indicates that it is not necessary for the two components to be bound, as the difference between their velocities are comparable to the velocity dispersion of the cluster and can be attributed to the individual random motions of the galaxies within the cluster.

Next, considering the fact that the region midway between the two components is not as bright as one would expect from the addition of the intensities of two separate galaxies, Hintzen states that the argument upon which it is based is physically incorrect. The argument is that the material of the halo would be preferentially located near regions of strong gravitational potential. He continues his argument by saying that the halo or envelope material need not be bound to either of the components but could still be found to the system as a whole. Such material would be distributed within an equipotential surface containing both components of the system, and the volume between them. Therefore, if the A1775 system is bound, and if the halo structure is a common envelope of both components, one would expect the surface brightness to be greater than or equal to the superposition of two separate

galaxies. Hintzen concludes that the hypothesis that the A1775 system is bound has no physical support.

As to the cause of the observed effect, Hintzen suggests that the Kostinsky effect (Kodak 1967) could be the cause. The Kostinsky effect is photographic in nature and is one in which the heavily exposed images, such as the components on the plates used by Chincarini et. al., would exhaust the developer in the neighbourhood between the two components. The inter-component region would therefore be comparatively underdeveloped. This effect must be guarded against in any exposure of extended objects, such as galaxies. Hintzen notes that while rocking the plates during developing would reduce the effect, it might not eliminate it entirely.

Hintzen continues his critique of the conclusions drawn by Chincarini et. al. by answering their argument about the colour and spectrum not showing any signs of violent activity. As both components have the appearance of elliptical galaxies, their colours should be dominated by older population objects and contain very little inter-stellar gas. He therefore concludes that even in a high speed collision, one would not expect to find a difference in either the colour or the spectral characteristics. Replying to the argument that the chance superposition of two large galaxies found at the centre of a cluster is very low, Hintzen points out that numerous other investigators have noted the tendency of large galaxies to be located in the central regions of clusters of galaxies. He adds that White (1976), in his N-body models of clusters, found that mass concentrations develop as the number of galaxy-galaxy encounters increases. This leaves the most massive galaxies at the centre of the cluster. Therefore, in Hintzen's opinion, the two components of the A1775 system could be interacting, but not necessarily bound gravitationally.

Perhaps the most damaging piece of evidence against the idea that the A1775 double is bound is that the SE component has been found to be a tailed radio source by Miley and Harris (1977). These authors state that unless our ideas about the formation of tailed radio sources are wrong, there is no way that the A1775 system could be bound. This is because it is hard to see how two massive galaxies orbiting each other at a separation of only 30 kpc ($H_0 = 75$ km/sec/Mpc) could produce a straight 300 kpc long radio tail. Even if there were some inter-cluster medium or buoyancy, it would still be difficult to model the radio morphology (see Figure 1b). In the opinion of Miley and Harris, the existence of this long, straight radiotail indicates that the A1775 double is not bound.

To sum up, one has three possible models of the A1775 system. The first is that the A1775 double is a bound system, as forwarded by Chincarini et al. Second, that the A1775 double is formed by the collision of two elliptical galaxies, as forwarded by Hintzen. The third possibility is that the A1775 double is a superposition of two unrelated objects. The aim of this study is to try to distinguish between these three hypotheses by modelling the surface brightness distribution using the King models (1966) as fitting functions.

Consider the brightness distribution of the A1775 system if the system is bound. One might expect the halo to contribute an appreciable fraction of the light from both the outskirts and from between the two components. Also, the halo would be an integral part of the system, and one would expect the brightness distribution of the halo to fall off gradually over a large angular extent (e.g. Oemler 1978).

However, if the A1775 system is unbound, but interacting, there

Figure 1b. Radio contours of the A1775 system from Miley & Harris (1977). Orientation is;



(+) marks the position of the optical components.

26°44'

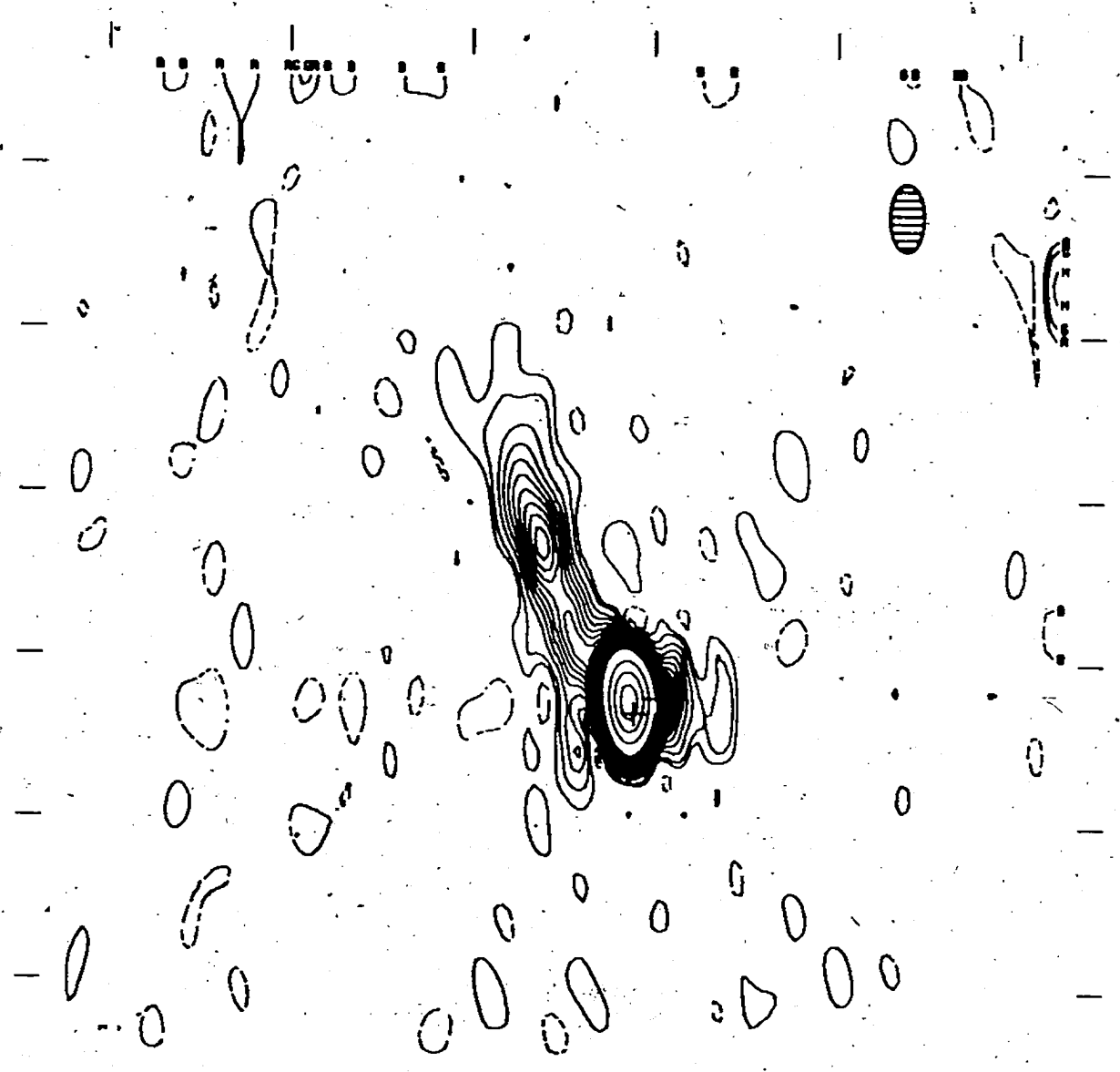
26°40'

26°36'

13H40M00S

13H39M40S

13H39M20S



are two points to be made. First, one would expect the components to have a small angular separation. Second, assuming that a King model is appropriate for interacting objects, then the halo may not be either as extensive as in the bound case, or contribute as much light to the overall surface brightness distribution. In view of the fact that King's quasi-isothermal spheres may not be appropriate to model tidal interactions, the most important factor in determining an interacting, but unbound system would be the angular separation between the components.

By the construction of composite models, one may be able to differentiate between the bounded and unbounded hypotheses outlined above. If a simple superposition of two scaled King models accurately describes the light distribution, then one may conclude that the A1775 system is unbounded; whereas if a more complex model is necessary to represent the contribution to the surface brightness by the halo, then one may say that the A1775 system is bound.

The composite models will be of two parts, consisting of an isophotal contour map, and an intensity profile along the line joining the two centres of light (called hereafter the system major-axis). A more complete and detailed discussion about the composite models will be found in Sections V and VI.

TABLE I

Observed Parameters of the A1775 System.

<u>Parameter</u>		<u>Reference</u>
Position	$\left\{ \begin{array}{l} \alpha = 13^{\text{h}} 36^{\text{m}} \\ \delta = +26^{\circ} 06' \end{array} \right.$ (e 1950)	
V_{rad}	14.1 ± 0.04 (46.6 diaphragm)	1
M_V	-23.7*	1
(B-V)	1.34 ± 0.01	1
Mass	$\approx 2 \times 10^{13} M_{\odot}$ (if bound)	1
V_{rad} {NW SE	22, 673 \pm 65 km/sec 20, 837 \pm 60 km/sec	2
Δv	1846 ± 125 km/sec	2
M/L	≥ 83 solar units if bound	1
Projected Separation	30 kpc*	1
Projected Linear Size	210 kpc*	1
Projected Length of SE radio tail	300 kpc*	3

Note: *value calculated with $H_0 = 75$ km/sec/Mpc

References; (1) Chincarini et. al. (1971)

(2) Huchra (1982)

(3) Miley & Harris (1977)

SECTION III: OBSERVATIONS AND DATA REDUCTION

3.1 Data

There are two forms of observations which were used in this study. There are photoelectric photometry and direct photography of the A1775 system. The direct photography will be discussed first.

3.2 Direct Photography

Five 48-inch Palomar Schmidt plates are used in this study. Four of the plates are in the V bandpass, with the fifth plate in the J bandpass. The four V plates were obtained by Dr. G. A. Welch in May 1970, and the J plate was obtained also by Dr. Welch in June 1971.

All five plates were calibrated in density by means of spot sensitometry. The sensitometry was applied immediately after exposure at the telescope, and the exposure time was one-half of the exposure time at the telescope. Filters were used to approximate the spectral range covered by the exposure at the telescope.

Four of the plates (three V bandpass and the J bandpass) were traced at St. Mary's University using the Department of Astronomy's Joyce-Lobel microdensitometer (Model MK III C.S.).

These plates were traced using a 2.4 density wedge. The fifth plate was traced previously by Dr. Welch using a 3.0 density wedge.

Table II lists the plates used in this study, along with the bandpass, filter, emulsion type and exposure times.

3.3 Photoelectric Photometry

The photoelectric data was obtained by Dr. Welch in February and March 1970 at Kitt Peak National Observatory. It was obtained using a 1P21 photocathode and DC electronics in conjunction with the #1 36-inch

TABLE II

Plate Material Used in This Study

Plate No.	Exposure Time	Emulsion	Filter	Bandpass	Date
PS 5719	20 min	103aD	Wratten 12	V	25/5/70
PS 5720	05 min	103aD	Wratten 12	V	25/5/70
PS 5724	20 min	103aD	Wratten 12	V	26/5/70
PS 5748	05 min	103aD	Wratten 12	V	29/5/70
PS 6864	120 min	IIIaJ	Wratten 4	J	21/6/71

telescope and the 84-inch telescope. Table III lists the photoelectric magnitudes, along with the diaphragm diameters, the filters used and the telescopes. Most of the photoelectric observations appear, in an averaged form in Chincarini et. al.'s paper (1971) (see their Table II), for each component of the A1775 system.

3.4 Data Reduction

A number of density tracings were obtained from each of the plates. The first series of tracings taken from each plate were those of the spot sensitometry. All 12 of the spots were traced, along with the clear-plate fog level. From the spot sensitometry, characteristic curves for each of the plates could be constructed.

The densities of the spots were determined by drawing a straight line through the clear plate level and the tops of the tracings of the spots. Measuring the difference (in the sense spot minus clear plate level) in densities gave the density co-ordinate of the characteristic curve. The intensity co-ordinate for each of the spots was provided by Dr. J. Kormendy. In addition to the sensitometry tracings, the plates were traced in 3 directions at various magnifications.

Each of the plates were traced on a line joining the two components referred to throughout the rest of this study as the system major axis, and through each of the components in a direction perpendicular to the system major axis. These latter two tracings are called the SE and NW minor axis; as the designation suggests, the minor axis were named for the positions of the components with respect to a point on the system major axis between them.

All of the plates were traced initially at a magnification of 10 in order to measure the density of the sky. The galaxy was centred on

7

f

TABLE III
Photoelectric Photometry of A1775 System

Component	Date	Diaphragm	V	σ_s^*	Comments
NW	14/3/70	18.3	15.41	0.03	KPNO 84-inch
NW	15/3/70	18.3	15.54	0.08	"
SE	14/3/70	18.3	15.26	0.02	"
SE	15/3/70	18.3	15.22	0.05	"
Both	02/2/70	46.6	14.1	0.04	KPNO #1 36-inch

*The formal standard deviation between settings of the diaphragm on the component in question.

these tracings. The plates were then retraced at higher magnifications (> 50), and then retraced at the low magnification. Such a procedure was carried out for all three axes.

The reason for retracing the axes at the low (10) magnification is two-fold. The first reason was to check that the plate did not move when the lever arm was changed in order to change the magnification. The second reason was to check for machine drift in the zero-point of the density level. It was found, by comparing the first and second low magnification tracings by eye, that there was no evidence for either plate movement or zero-point drift for all five plates.

The measured values of the magnification were found to be different than the nominal values engraved on the lever arms of the micro-densitometer. The measured values of the magnifications are needed as it is essential to know the precise value at which a density tracing was traced when a series of such tracings are averaged together.

The measured values of the magnifications were found by tracing a standard grid of lines incised on a piece of glass. A reticle from an eyepiece marked in 0.1 millimetre intervals was used as the standard grid. The reticle was traced using a given lever arm, and the distance between successive peaks on the tracing measured using a centimetre rule and estimating to the nearest 0.1 millimetre. These distances were measured peak to peak. The grid lines were measured on the Department of Astronomy's measuring engine. Table IV lists both the nominal and measured values of all the lever arms used in this investigation. In the remainder of this study the nominal values of the magnification will be quoted for ease of notation; however, it should be understood that the measured values of the magnification, as given in Table IV, were used in all the calculations.

TABLE IV
Nominal and Measure Value of Magnification
of Microdensitometer Arm

Nominal	Measured
10	10.08
50	51.86
100	104.07
200	199.30

The aperture which admits the light to the photocathode of the microdensitometer is used as a projection screen. Projected upon this aperture (or slit) is the portion of the plate which is being traced. The size of the aperture could be changed and its size was determined by the exposure time of the plate being traced. The slit width was chosen as a compromise between the best resolution of the object being traced and yet minimize the noise due to the individual grains within the emulsion. As the need for high resolution is greater in the short exposures, since the central regions are overexposed in the longer exposures, a small slit width was chosen. Conversely, the need to suppress the noise is greater in the longer exposures and one would not expect to find much fine detail in either the overexposed central regions or the faint outer regions. Table V lists the plates, and exposures, along with the projected slit width (both in microns and arc-seconds) and the magnification at which it was traced.

After the density tracings of the A1775 system were made, these tracings were digitized. The digitization process involved setting up a co-ordinate axis on each one of the tracings and noting the position of an origin of this co-ordinate system. While the precise origin of the co-ordinate axis was arbitrary, it was always in the lower left-hand corner of the microdensitometer tracings below the level of the sky.

Digitization consisted of measuring at one millimetre intervals, points along the length of the density tracings of the galaxy, with respect to the origin of the co-ordinate axis. The digitization process was carried out by a computer programme called GALAXY, written by Mr. T. J. Deveau, on the St. Mary's University PDP 11/70 in the BASIC language. The programme used a Textronix 4662 plotter in the data transmission mode.

TABLE V
Projected Slit Widths Used for
Microdensitometry

Plate Number	Projected Slit Width		Magnification
	μm	arc-sec	
PS 5719	70	4.70	100
PS 5720	35	2.35	200
PS 5724	70	4.70	100
PS 5748	35	2.35	200
PS 6864	140	9.41	50

Data files of (x, y) points were formed by the programme. Each of the (x,y) pairs correspond to a point on the density tracing of the system. The high magnification tracings and one of the low magnification tracings were digitized for each axis of the system (i.e. the system major axis and the NW and SE minor axes). This was done for all five plates.

It should be pointed out that stars and other galaxies were omitted where digitizing the low magnification tracings, as were regions surrounding the double galaxy itself in order to reduce the possible effects of a faint extended halo on the determination of the sky level.

The data files of (x,y) pairs were transmitted to the Dalhousie University Cyber 170/720 computer, where the remaining steps in the data reduction were carried out. More information on the programme GALAXY may be found in Appendix 1.

The next step in the data reduction was the conversion of the relative density tracings from the plates into plots of relative intensity versus radius with the galaxy. This process is performed by a FORTRAN computer programme called PROFILE. This computer programme uses as input the digitized data from the microdensitometer tracings and the characteristic curves. The programme also performs a linear regression on the data input from one of the low magnification tracings, to obtain the level of the sky. Standard deviations of the scatter about this line are printed out in the form of σ_{sky} . This standard deviation is important in determining the boundary of the matching region when a series of microdensitometer tracings are averaged (or stacked) together. As each density tracing is reduced, the computer programme produces two graphs. These graphs are in the form $\log_{10} r$ versus $\log_{10} I$ (I is the relative intensity with 3.00 being the brightest point and r is the

radial position in arc-seconds). The first plot shows the average of all the previous profiles and displays the current profile to be averaged in, shifted in $\log_{10} I$ to give the best fit with the previous average. The second plot shows the new average obtained.

During the averaging process the programme chooses a segment of each of the profiles to serve as a matching interval. The inner boundary of this interval is defined as the first point of the tracing to be averaged-in which is farther than the projected slit-width (used to trace the plate on the microdensitometer) from the centre of the system. The outer boundary is chosen as the distance at which $I = 5 \times \sigma_{\text{sky}}$. These boundary criteria for the matching intervals were used for the two short exposures and one of the 20 minute exposures. For the remaining 20 minute exposure and the J plate, the outer boundary was tightened up some-what to be the point at which $I = 10 \times \sigma_{\text{sky}}$. There was no preference in using one 20 minute exposure over another. It was necessary to raise the outer boundary criterion for the longer exposures because any values of intensity outside the range of the programme's capability (for example points found to have negative intensities within the matching region) would cause the programme to fail to run correctly for all the plates.

It should be pointed out that the plates used in this study are of small scale (67.2 mm^{-1}); all the exposures are limited in the radial direction. This is in the sense that the semi-axes of the profiles have less than 25 points in the matching region, and this presented some difficulties as the programme will not average in a profile with less than 25 points in the matching region. However, using the boundary criteria outlined above, stacked profiles of all the semi-axes of the

A1775 system, using all five plates were obtained. For a more complete discussion of the programme PROFIL, the reader is urged to consult the study of English (1979). A sample run of the programme profile is to be found in Appendix 2 of this study.

Another form of data used for this study are isophotometric tracings of the plate PS5724. There are two such tracings, and one of them is found in this study; Figure 2.

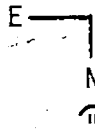
This form of data is important as it allows one to see more clearly the various regions of the system under study. By inspection of Figure 2, one notes that the A1775 system is composed of 2 components surrounded by, and possibly enclosed by, a halo. The halo is notable in two ways. First, the halo is very 'boxy' in shape. Second, the halo may not be as extensive as those of CD galaxies studied by Oemler (1976) and Dressler (1979). The angular extent of the halo of A1775 from the centre (i.e. the radius of the halo from one of the components) is some 45 to 50 arc seconds. The isophotometric tracings of the A1775 system were obtained by Dr. G. Welch in 1971 using a 2-dimensional scanning Joyce-Lobel microdensitometer at Michigan State University.

3.5 Errors in the Data Reduction

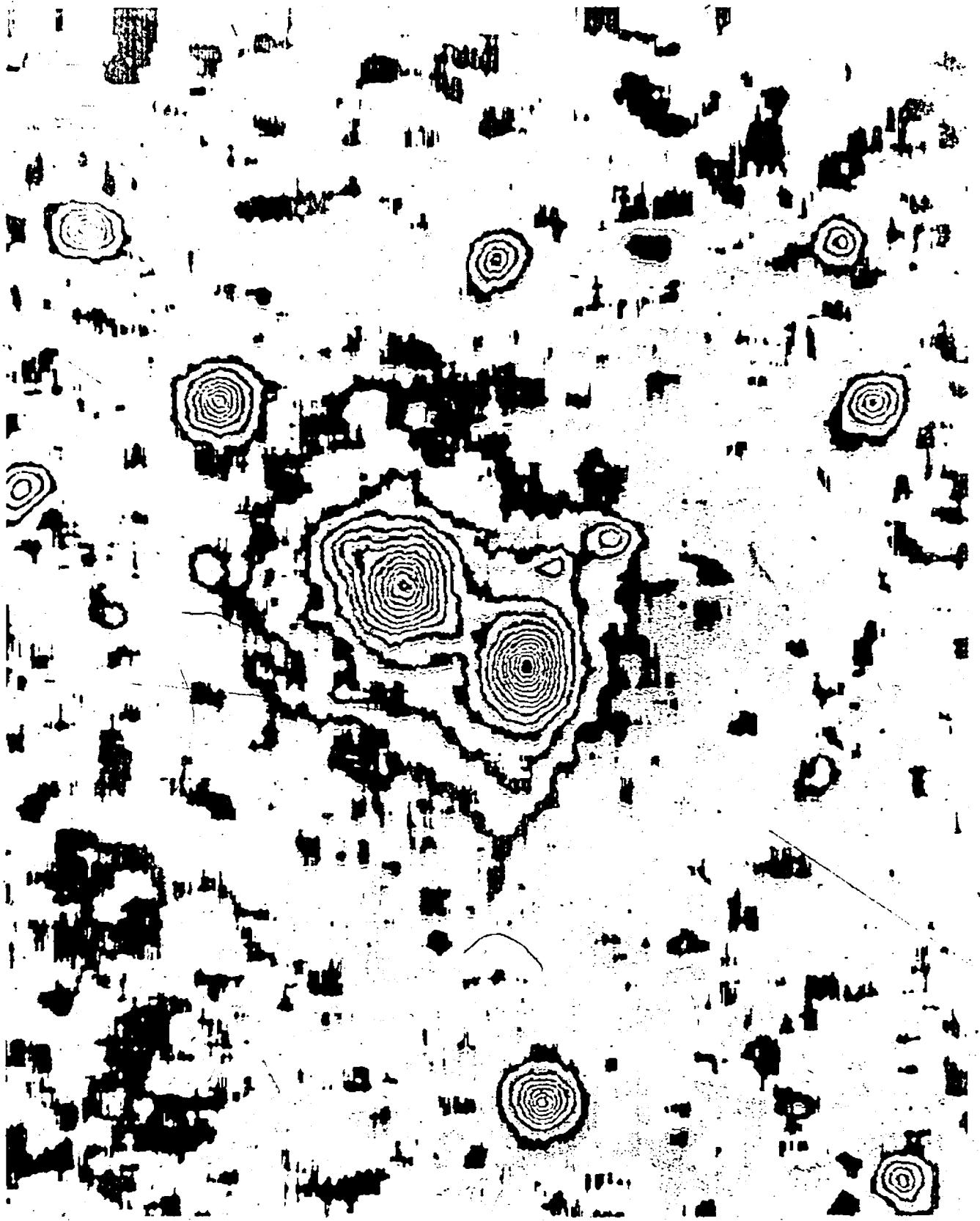
The most critical step in the data reduction process is the construction of the characteristic curve. Indeed the accuracy with which one can construct the characteristic curve will determine the errors in the intensity at a given position within the galaxy.

The plates used in this study were stacked together to form an average intensity-radius profile. The stacking process was carried out in an attempt to minimize errors incorporated when plotting the characteristic curves or errors in interpolating intensities using the curves.

Figure 2. Isoplates of A1775 system. Orientation



Scale = 1 cm = 7.45 from a 102aD 20^m plate.



Stacking of the tracings also help minimize the errors and uncertainties involved slit-smearing and seeing effects which would be recorded when the plates were traced. Therefore, by stacking the plates one could see, plate by plate, the run of intensity in comparison with other profiles as well as any deviations in the relative intensity which might appear in one of the profiles. For example, if one were to see an increase in relative intensity at a given radial position on only one of the five profiles, one would be inclined to disbelieve the increment in brightness as being an intrinsic property of the galaxy, but ascribe its nature to either an incorrectly plotted point on the characteristic curve or an inaccurate interpolation in the computer programme PROFIL.

Naturally, each of the plates will have a slightly different sensitivity and will have been traced on the microdensitometer under slightly different conditions, and the averaging process is performed to try to minimize these differences as much as possible.

By the process of stacking, one could see the differences in relative intensity caused by the differences in plate sensitivity, tracing conditions (slit smearing) and in interpolation of intensities using the different characteristic curves. Using the deviations in relative intensity from plate to plate allows one to attempt to quantify the uncertainties caused by all the above mentioned processes. This quantifying process was done in the following manner. A root mean square (RMS) deviation for the intensity was obtained by comparing the average of the 5 stacked plates with each separate profile at 12 radial positions for 2 typical semi-axes; namely, the NW semi-axes of the NW component (i.e. along the system major axis) and along the NE semi axes of the SE component. These RMS deviations are found in Table VI. One notes that the

TABLE VI

Deviations in the Stacking of Intensity Profiles

NW Component, NW Semi-axis

<u>Radius</u>		<u>RMS Deviation</u>	
r(in arc-sec)	$\text{Log}_{10} r$	Intensity (%-age)	Surface Brightness ₂ (mag/arc sec ²)
1.00	0.000	20	-0.19 +0.24
1.46	0.167	22	-0.22 +0.27
1.78	0.250	21	-0.21 +0.26
2.15	0.333	19	-0.19 +0.23
2.61	0.417	17	-0.17 +0.20
3.16	0.500	16	-0.16 +0.19
4.65	0.667	13	-0.13 +0.15
5.62	0.750	16	-0.16 +0.19
6.81	0.833	28	-0.27 +0.36
10.00	1.000	42	-0.38 +0.59
17.78	1.250	60	-0.51 +0.94
20.00	1.301	55	-0.48 +0.87

TABLE VI (cont.)

SE Component, NE Semi-axis

r(in arc-sec)	<u>Radius</u>		<u>RMS.Deviation</u>	
	$\text{Log}_{10}r$	Intensity (%-age)	Surface Brightness ₂ (mag/arc sec ²)	
1.00	0.000	25	-0.24 +0.31	
1.46	0.167	18	-0.18 +0.22	
1.78	0.250	10	-0.10 +0.11	
2.15	0.333	8	-0.08 +0.09	
2.61	0.417	12	-0.12 +0.14	
3.16	0.500	20	-0.19 +0.24	
4.65	0.667	18	-0.18 +0.22	
5.62	0.750	23	-0.23 +0.28	
6.81	0.833	20	-0.19 +0.24	
10.00	1.000	52	-0.45 +0.79	
17.78	1.250	33	-0.31 +0.43	
20.00	1.301	48	-0.43 +0.71	

minimum RMS deviation occurs in the range 1.5 to 7 arc seconds; this is the region of matching in the stacking process. This is reasonable, as one would expect the RMS deviation to be a minimum in this interval.

The values for the RMS deviations are somewhat larger for points interior radially and exterior radially from the matching region. The increase in the RMS deviation interior to the matching region, while due to all the above problems would also include differences in seeing and guiding of the plates, slit smearing and centering when the plates were traced on the microdensitometer. For points exterior to the matching region, the increase in the RMS deviation is attributable to the fact that one is at a very low light level, and one is tracing the galaxy out to where it is becoming fainter than the sky.

There is another source of error which will be included in the RMS deviations, and this will be the fact that the actual digitization process (using the Textronix 4662 plotter) will be repeatable only to a certain accuracy. It was found that the digitization process is repeatable to ± 0.15 millimetres, which corresponds to ± 0.05 arc-seconds on a tracing of magnification 200. While this error is not as great as those introduced due to the microdensitometry or even more so the characteristic curve, it will add its contribution to the RMS deviation.

There are two remaining reasons for stacking the profiles of the galaxy. First, it allows one to cover a larger range of surface brightness within the system, by using short exposures to delineate the central regions and the longer (> 5 minutes) to delineate the outer regions to the halo. Second, stacking allows one to increase the signal-to-noise ratio, which is tied into the discussion above.

3.6 Calibration of the Profiles in Magnitudes

The relative interaction used in the construction of the intensity profiles were converted into standard surface brightnesses via two methods in this study.

The first method uses the Newton-Ralphson iteration method to find a value for a constant which is added to the relative magnitudes of points on the profile to give a standard surface brightness in magnitudes per square arc-second. A more complete discussion of this method is found in English (1979).

The second method of calibrating the isophotal contours involves summing the relative magnitudes of each of the isophotal contours (see Figure 2), to find a constant, which when added to the faintest contour will convert the relative magnitudes into standard surface brightness.

Analytically this expression is of the form

$$-2.5 \sum_{i=1}^N \text{Log}_{10} (I_i + R) a_i + M_{pe} = \mu_{pe} \quad (\text{III-1})$$

where - I_i is the relative intensity of the i^{th} contour

- a_i is the area of the i^{th} contour

- R is the constant to be found

- M_{pe} is the apparent photo-electric mag of each component of the A1775 double in the V bandpass using a diaphragm of 9.2 arc-sec.

Two semi-axes of the A1775 system were calibrated using both of the methods outlined above. It was found that the two methods gave the same central surface brightnesses to within 0.08 mags/□ⁿ. Table VII lists the central surface brightnesses of the eight semi-axes, along with the averages each of the components.

TABLE VII

Measured Values of Central Surface Brightnesses of the A1775 System
 (in mags/ $\square^{\prime\prime}$)

SE Component

Semi-axis	NW	NE	SW	SE
Iteration Method	19.27	19.24	19.15	19.31
Analytic Method	-	-	-	19.40

NW Component

Semi-axis	NW	NE	SW	SE
Iteration Method	19.60	19.46	19.50	19.56
Analytic Method	-	-	19.44	-

Averaged Surface Brightnesses of the Components

SE Component	19.24
NW Component	19.53

SECTION IV: KING MODELS AND MODEL FITTING

4.1 King Models

The fitting functions used in this study are King's (1966) isothermal spheres.

King's models were developed in an attempt to form more realistic fitting function, and are a step away from the purely empirical function of deVaucouleurs (1959) and Hubble (1930). The King models are based upon the dynamics of the stars within the system, and assume a velocity distribution which is everywhere within the system isothermal and Gaussian. To alleviate the problem of an infinite mass inherent in an isothermal sphere, the Gaussian is truncated at a specific point corresponding to the escape velocity of the system.

The models were originally developed for use with globular star clusters, but have been found to describe elliptical galaxies reasonably well (King 1966, 1978).

The models have three parameters, two of which describe the core of the system. These two parameters are f_0 , the central surface brightness and r_{core} , the 'core-radius', at which the surface brightness has fallen to approximately one-half its central value. If one defines a limiting radius r_{tidal} , then one can define the third parameter, of the form

$$c = \log_{10} \left(\frac{r_{\text{tidal}}}{r_{\text{core}}} \right)$$

A series of numerical calculations defining the profiles of the King models have been made available by Dr. King (1980). All the models have similar cores, but behave differently in the outer regions.

Models with $c < 1.5$ are cut off sharply and of elliptical galaxies, only tidally limited objects such as the dwarf elliptical systems of the

Local Group are well described by them (Hodge 1971).

It is these models which also fit the globular clusters. In the range $1.5 < c < 2.0$, the models are similar to the $r^{1/2}$ deVaucouleurs relation. For $c > 2.0$, the central concentration becomes so large that a distinct outer halo is formed that is brighter than the deVaucouleurs relation. For $c \gg 2.0$, the surface brightness of the models approach the r^{-1} relation of the isothermal relation.

The King model used in this study has $c = 2.25$, the so-called 'standard' King models used by other investigators of elliptical galaxies (King 1966, Kormendy 1977, Dressler 1979).

The King model is used in this study in preference to either deVaucouleurs (1959) or Hubble's (1930) because each of these relations implies an infinite central space density, whereas the King models do not.

However, there are difficulties with King's models. The models are based upon the idealized Gaussian distribution, which while applicable to relaxed systems such as globular clusters, will not be applicable to galaxies. King's models were developed with tidally limited objects in mind, and elliptical galaxies are not limited, at least in the sense of the tidal interaction defined by King (1962; 1966).

There are other factors which differentiate elliptical galaxies from globular clusters, and these will be recapitulated briefly.

The profile of the halo of an elliptical galaxy in the framework of the King model is related to the high-energy tail of the velocity distribution in the centre of the galaxy. There is no reason to believe this true for elliptical galaxies. The models are based upon an isotropic velocity distribution. Again, there is no reason to believe this is true in the halo of an elliptical galaxy. Also, the models are self-gravitating,

whereas there is a growing body of evidence that the outer portions of elliptical galaxies are dominated by an unseen mass which is distributed differently than the visible material. If this is so, then the halo density distribution (and hence the velocity distribution) depends on both the gravitational potential and velocity distribution of this unseen material.

It has been recently pointed out by Illingsworth (1977) that the velocity dispersions in the cores of elliptical galaxies are not isotropic. If this is found to be true, then the dynamical model for King's models has no applicability to elliptical galaxies.

Finally, Schweizer (1979/81) recently pointed out that, except in galaxies in the Local Group, the central portions of galaxies are not being resolved. This would imply that King's models overestimate the core radii of galaxies (except in the Local Group) by an order of magnitude. While the dynamical construction of King's models are not affected by this fact, it does call into question any conclusions about the dynamics in the cores of elliptical galaxies.

Thus, while the dynamical significance of the 'standard' King model is in some doubt with respect to elliptical galaxies, they are used in preference to the relations of deVaucouleurs and Hubble because they do not fit the centres of elliptical galaxies well. A brief description of the dynamical calculations behind King's models is found in Appendix 3.

4.2 Model Fitting

The model fitting process consists of scaling the 'standard' King model to each of the intensity profiles for each of the eight semi-axes of the A1775 system. The scaling process is in both the radial and

intensity co-ordinates and the fitting process was carried out in two steps.

The first step involves plotting the eight averaged intensity profiles in the same scale as that of the 'standard' King model (the scale used was $\frac{1}{2}$ -inch for 0.10 in $\log_{10} r$). A sliding fit was made in the radial co-ordinate between the unscaled King model and the intensity profile in question. This was used to obtain the apparent core radius (in view of Schweizer's work, it would be inappropriate to denote this fitted value as the core radius - implying the intrinsic value). At the same time limits were found on this apparent core radius. This was found by finding where the sliding fit was only tolerable in both directions radially.

The points defining the given intensity profile, along with its the apparent core radius, and with the unscaled standard King model (in the form of points) were used as input to a computer programme which performed the second step in the model fitting process.

Three other parameters are also needed by this computer programme. These are arbitrary maximum and minimum trial values for the central intensity, and the number of steps desired between these two values.

The second step in the model fitting process was performed by a computer programme called REDUCE (see Appendix 4 for a listing of the code). The points defining a given intensity profile and the unscaled King model ($c = 2.25$) are entered into the programme logarithmically and are converted into linear co-ordinates. The radial co-ordinate of the King model is then scaled by using the value of the apparent core radius, found in the above procedure, and the King model is truncated at the outer-most point of the intensity profile. The King model is then scaled

for the central intensity. The central intensity of the King model is first set equal to the arbitrary minimum value of the intensity used as input to the programme. This intensity is then increased by a given amount (determined by the difference between the maximum and minimum intensity values and the number of steps) and the central intensity is stepped through a series of values, from the minimum to the maximum input values for the intensity. Thus a family of King models is formed, each with the same apparent core radius, but with different central intensities for each of the eight semi-axes of the A1775 system.

An interpolation between each of the King models and the points defining the observed intensity profile is then performed. The points defining a given scaled King model are numerically fitted by a cubic spline in a smooth curve. At each radial value of the observed intensity profile, a value of intensity on the King model is found by cubic spline interpolation. The observed and interpolated intensities are then compared at each radial position, and the differences (in the sense observed minus interpolated) calculated. A root mean square (RMS) deviation is calculated from these differences, and the total RMS deviation is divided by the central intensity of the King model in question. The ratio formed by this process indicates the goodness of fit of the scaled model to the observed profile. The interpolation process was carried out for each of the scaled King models in each family for all eight semi-axes. The smallest value of the ratio of RMS deviation over central intensity was considered to be the best fitting model with a given apparent core radius.

The entire interpolation process and the construction of families of King models outlined above was carried out for each of the eight semi-axes with different values of apparent core radius.

Each of the core radii found in the first step of the model fitting process was found to have an uncertainty of about ± 0.20 arc-seconds.

Each of the semi-axes of the A1775 system was fitted using a total of 5 values of apparent core radii from the maximum to minimum values of the uncertainty. The steps in apparent core radius were ~ 0.10 arc-seconds. Therefore for each of the eight semi-axes, one was left with five 'best-fitting' King models. A plot of the RMS deviation/central intensity ratio versus core radius was made for each of the semi-axes, and a smooth curve was fitted by eye through the points. The apparent core radius and central intensity ($r_{c, app}$ and I_0) corresponding to the minimum of the smooth curve were used as the parameters for the overall best fitting King model. This was done for each of the eight semi-axes. Table VIII lists the best fitting apparent core radii and central intensities for each of the semi-axes. Figures 3 to 10 are calibrated intensity profiles for each of the semi-axes. Also on each of the figures are the best fitting King models.

Naturally, the goodness of the fit of the models is determined by seeing effects and instrumental smearing of the observed data. By inspection of Figures 3 to 10, one sees that the best fitting portions of the King models is found in the same radial interval as the region used for matching profiles in the stacking process (see Section 3.5). This is natural as the uncertainties in the data are minimized in this region. Inspection of the stacking runs (see Appendix 2) indicates that the central regions of a profile are fainter in intensity for longer exposure plates than shorter exposure ones. This is in part caused by seeing effects and slit smearing in the microdensitometer and is partly the cause of the RMS deviation calculated in Section III. However,

stacking the plates was done partly to eliminate this very problem as fitting models to unaveraged profiles would lead one to conclude that the central intensity would be fainter for progressively longer exposures. By fitting standard King models to averaged profiles, one is minimizing the seeing and instrumental uncertainties, and it is felt that the best fitting King models found in this study are not substantially affected by the above uncertainties.

Finally, it should be noted that in the modelling fitting process, all the points on the observed intensity profiles were used, with the exception of points which defined identified field objects intersecting the intensity profile. These points were omitted and replaced by points representing an eye interpolation of the galaxy's profile. An example of this process is seen in Figure 3. The reason for using all the points on a profile [even in light of Schweizer's (1979) work, which indicates the problems involved especially in the central regions] is simple; there were not enough data points to allow one the option of omitting points, either near the centre or in the outskirts. One was obliged to use all the data points one could get.

The apparent core radii found in the above analysis were 2.74 and 1.68 arc-seconds for the NW and SE components respectively. Using a value of $H_0 = 75$ km/sec/Mpc, the linear sizes of these core radii are 3.9 and 2.4 kpc respectively. These values are quite a bit larger than the value of $r_{c, app}$ for M87, a 'typical' elliptical galaxy, of ~ 0.8 kpc, but only half as large as $r_{c, app}$ for the A2029 cD galaxy of ~ 7.5 kpc. Both of these values are calculated assuming $H_0 = 75$ km/sec-/Mpc⁻¹ and are quoted by Dressler (1979).

Figure 3. SE component, NE semi-axis plot of surface brightness versus \log_{10} radius (in arc seconds). The open circles are data points and the full line is the best fitting standard King model. The error bars are from the RMS deviations found in Table VI.

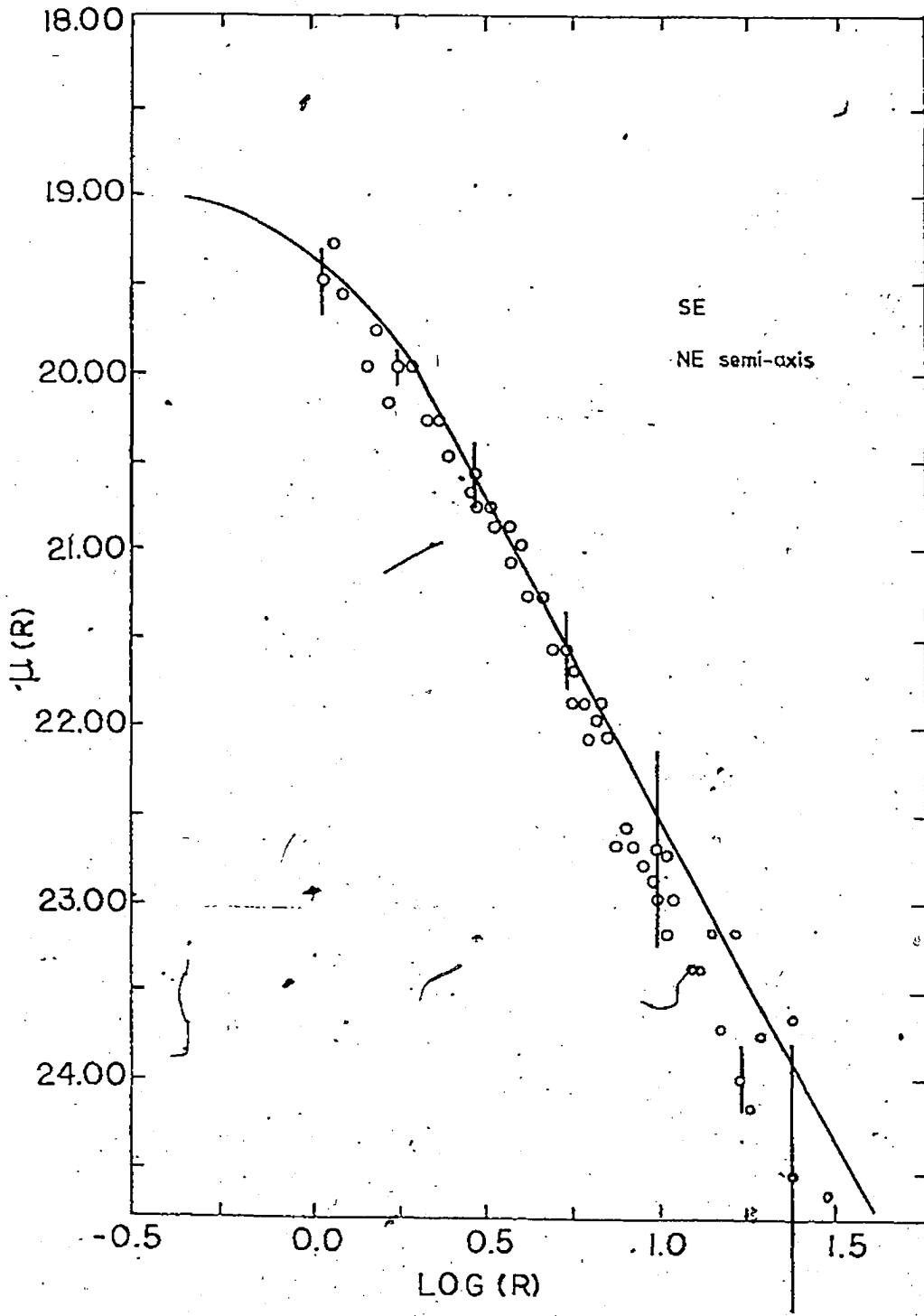
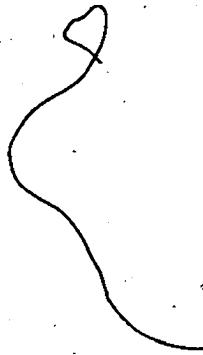


Figure 4. Same as Figure 3 except for SW semi-axis of SE component.



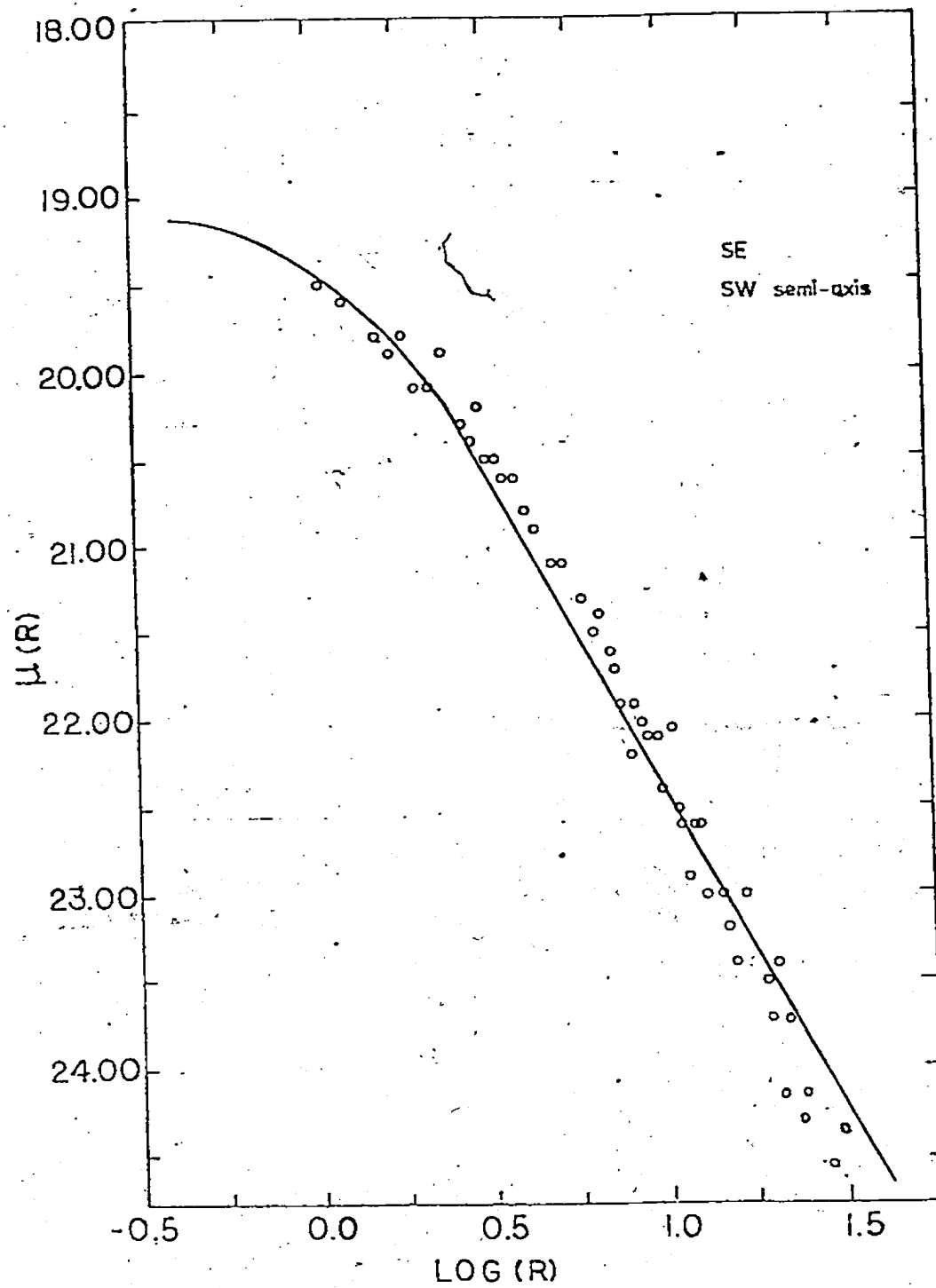
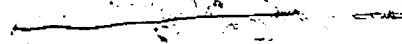




Figure 5. Same as Figure 3 except for NW semi-axis of SE component. Note this semi-axis is between the components and is terminated half way between them.



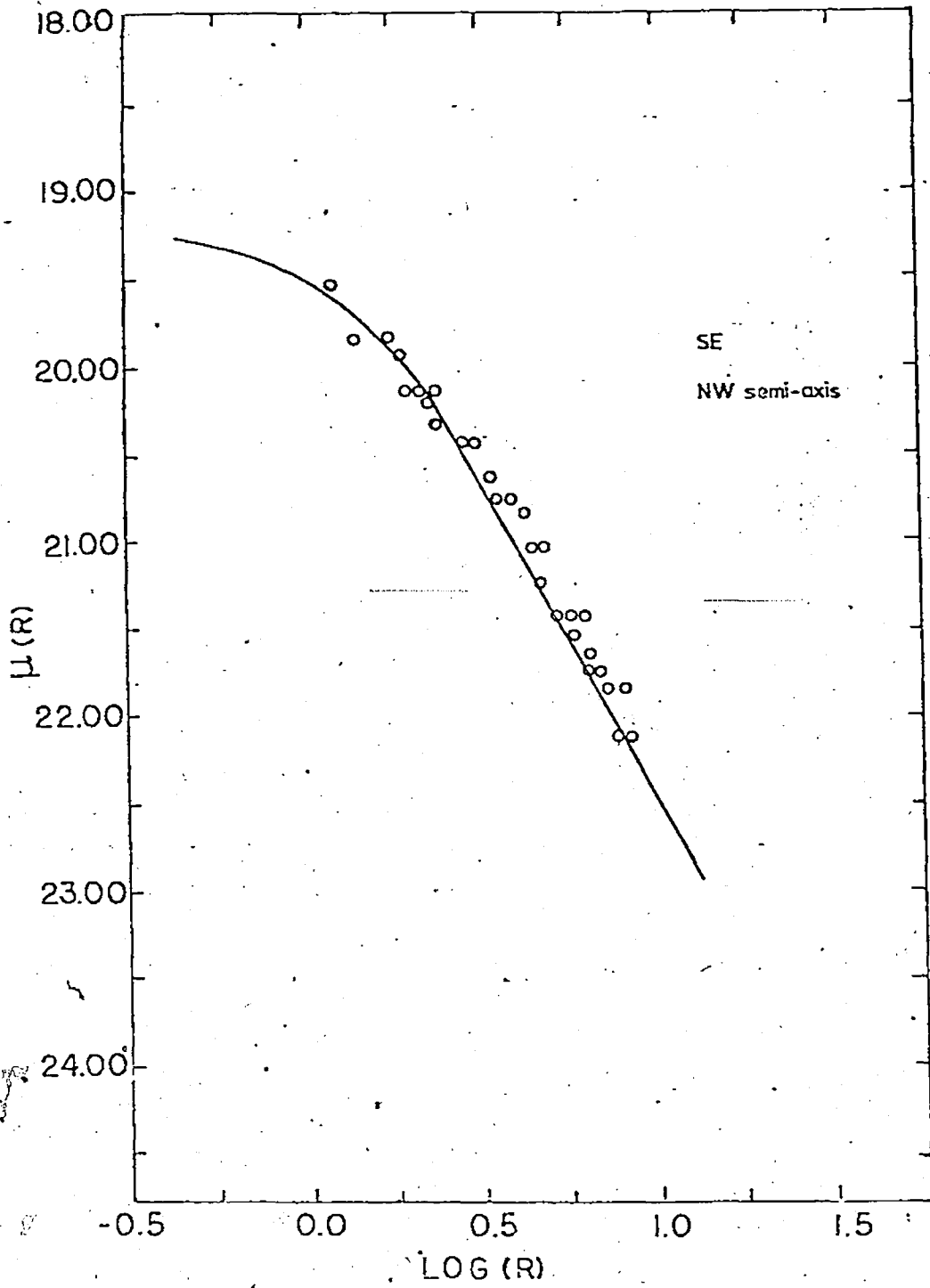


Figure 6. Same as Figure 3 except for SE semi-axis of SE component.

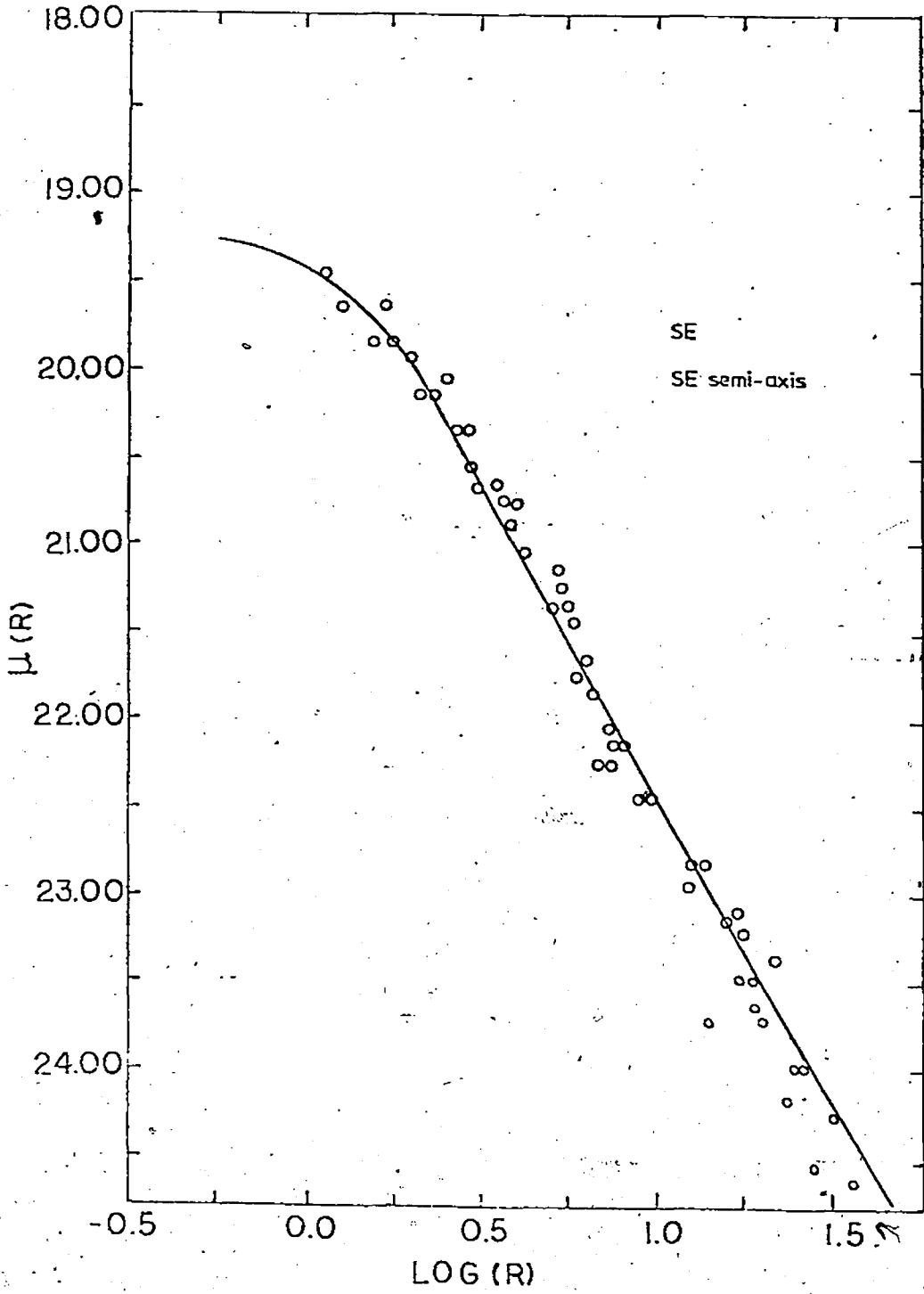


Figure 7. NW component, NW semi-axis; plot of surface brightness versus \log_{10} radius (in arc seconds). The open circles are data points and the full curve is the best fitting standard King model. The error bars are from Table VI. The triangles are interpolated points to avoid the field object.



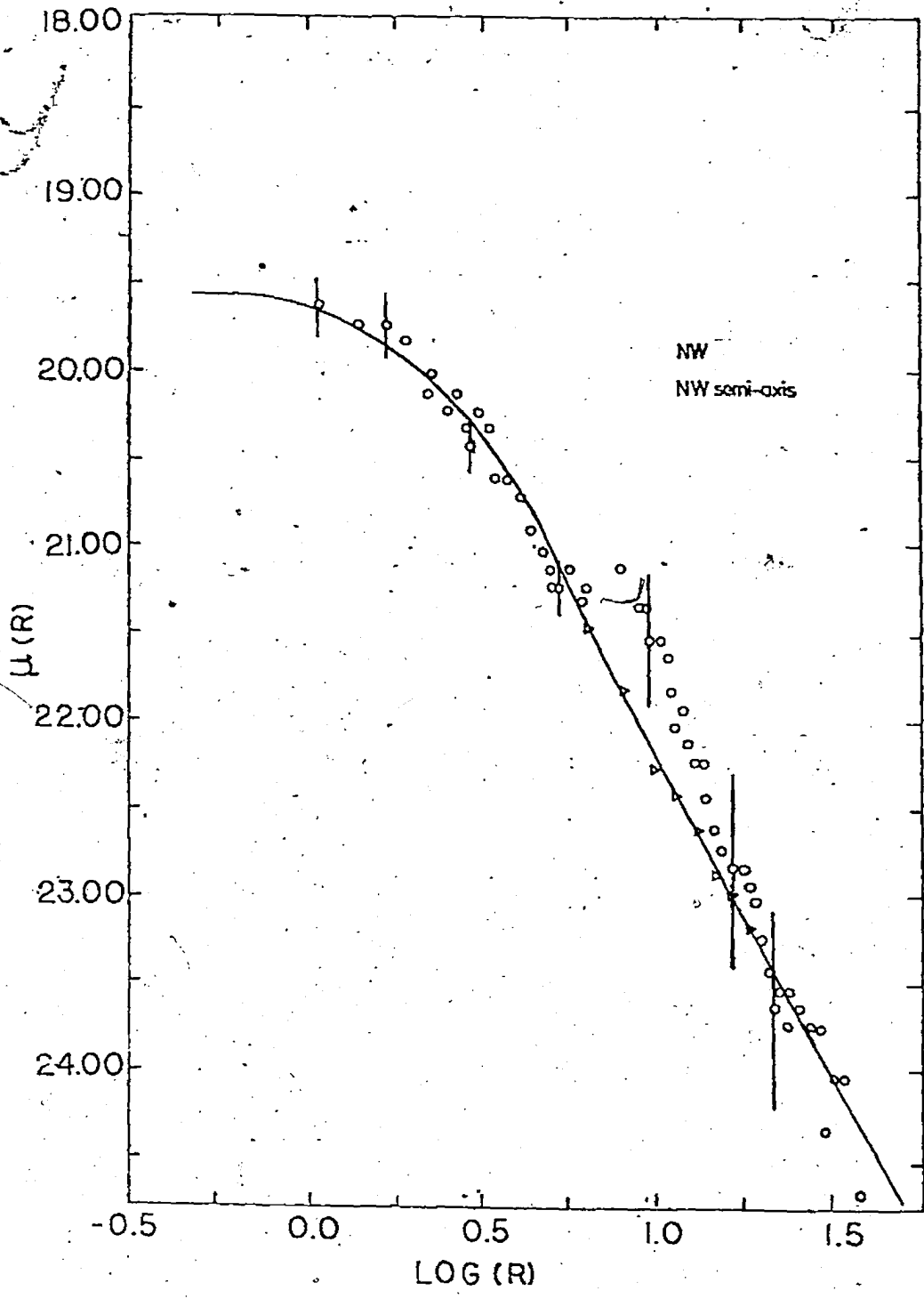


Figure 8. Same as Figure 7 except for SW semi-axis of NW component.

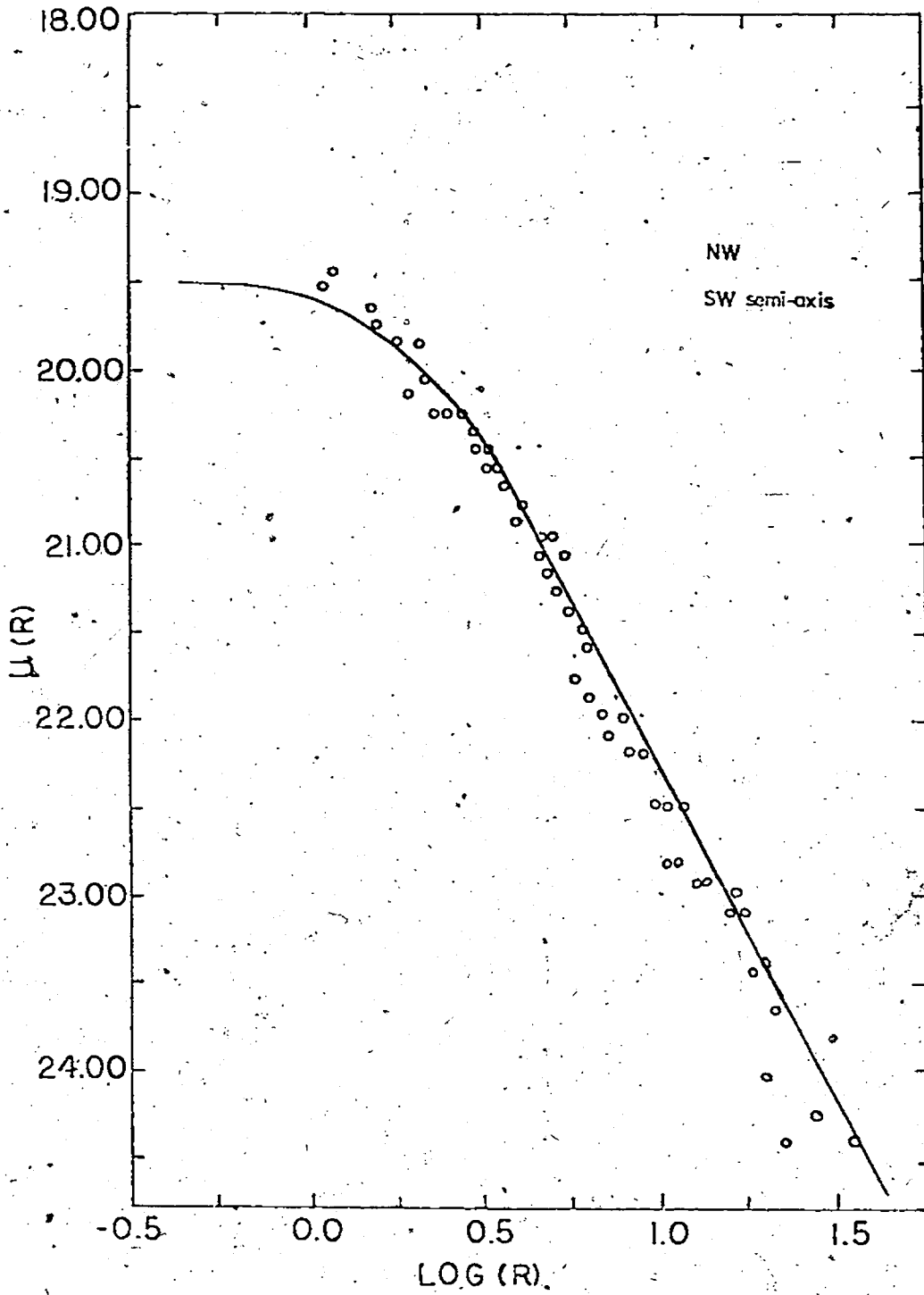


Figure 9. Same as Figure 7 except for NE semi-axis NW component.

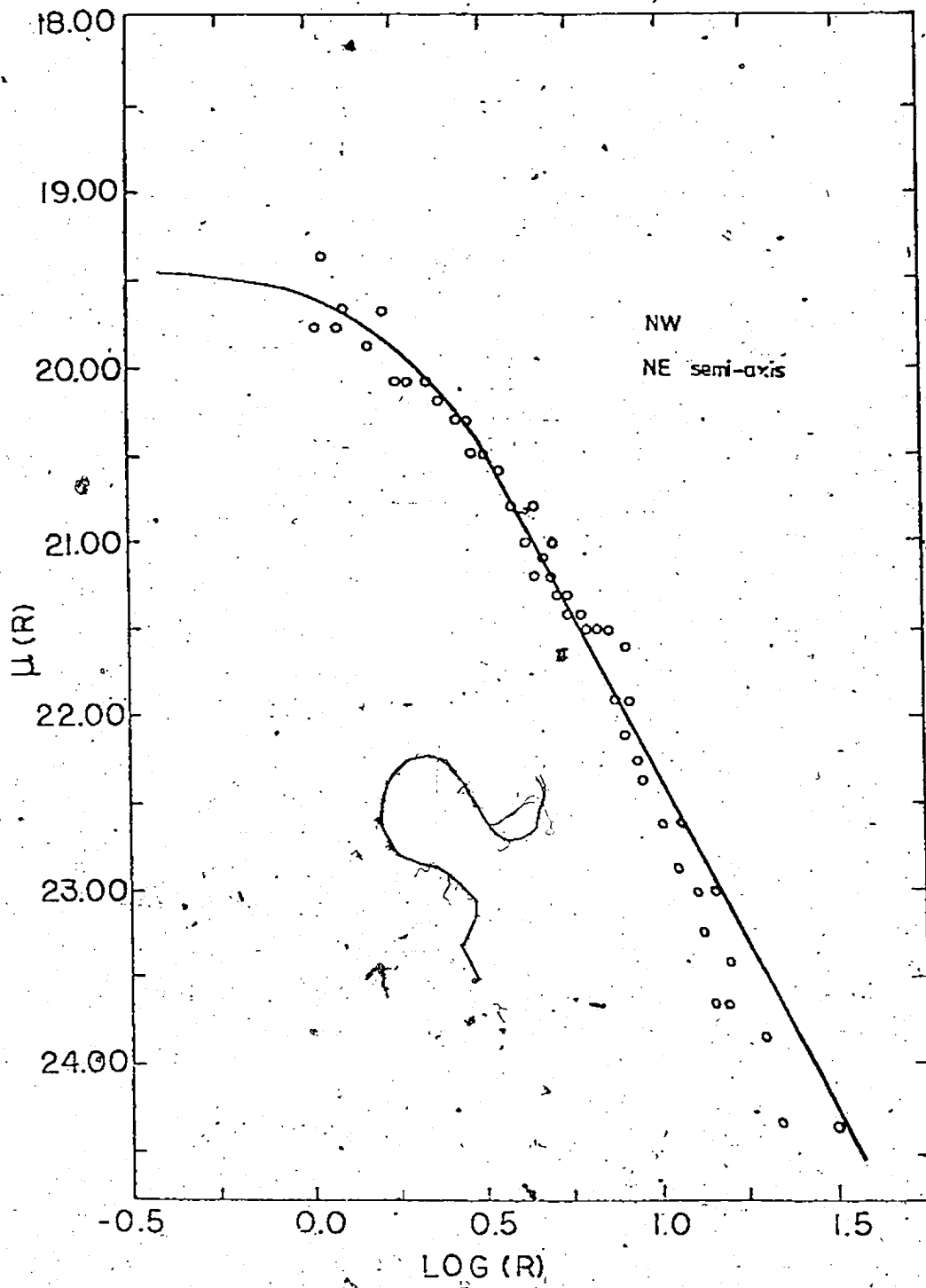
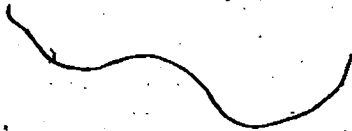
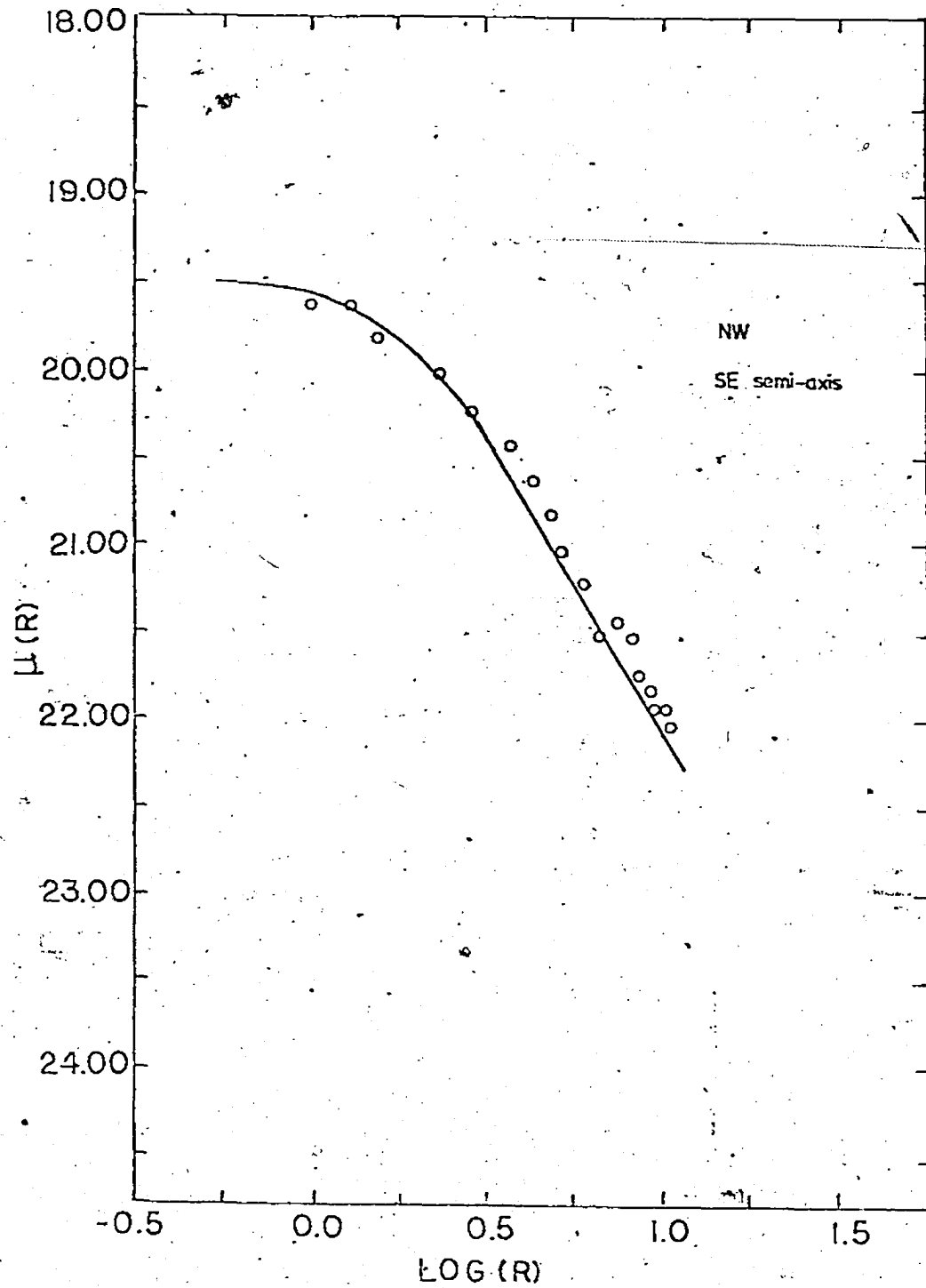


Figure 10. Same as Figure 7 except for SE semi-axis of NW component.
This semi-axis is midway between the components and is truncated at
half way between them.





SECTION V: COMPOSITE MODELS

5.1 Introduction

There are two composite models constructed in this study, and they are constructed using the best fitting King models described in Section IV above. The composite models consist of 2 components and are made up of two parts: (1) an isophotal contour map and; (2) an intensity profile of the system major axis.

5.2 The Composite Models; The CC Model

For ease of notation, the composite models will be denoted by CC and CE.

The CC composite model is composed of two circularly symmetric scaled King models, while the CE model is composed of one circularly symmetric King model and one elliptical King model. The elliptical King model was constructed because it was found by inspecting the isophotes of the A1775 double galaxy that the SE component was elliptical in form (see Figures 2 and 11).

The composite models were constructed in the following manner; standard King models (i.e. $c = 2.25$) were scaled using the averaged values of the apparent core radius and central intensity found in Table VIII for the SE and NW components. The scaling procedure was carried out by means of a computer programme called MODEL (see Appendix 5). The computer programme uses as input the averaged values for the apparent core radius and central intensity for a given component of the A1775 system, and also the points which define the unscaled standard King models. Also used as input is a cut-off radius. The cut off radius is an arbitrary radial limit to the component being modelled. A cut off radius was used

Figure 11. Smoothed isophotes (taken from Figure 2a) of the A1775 double system. The dotted circles are the aperture diaphragms used in the photo-electric photometry of the system.

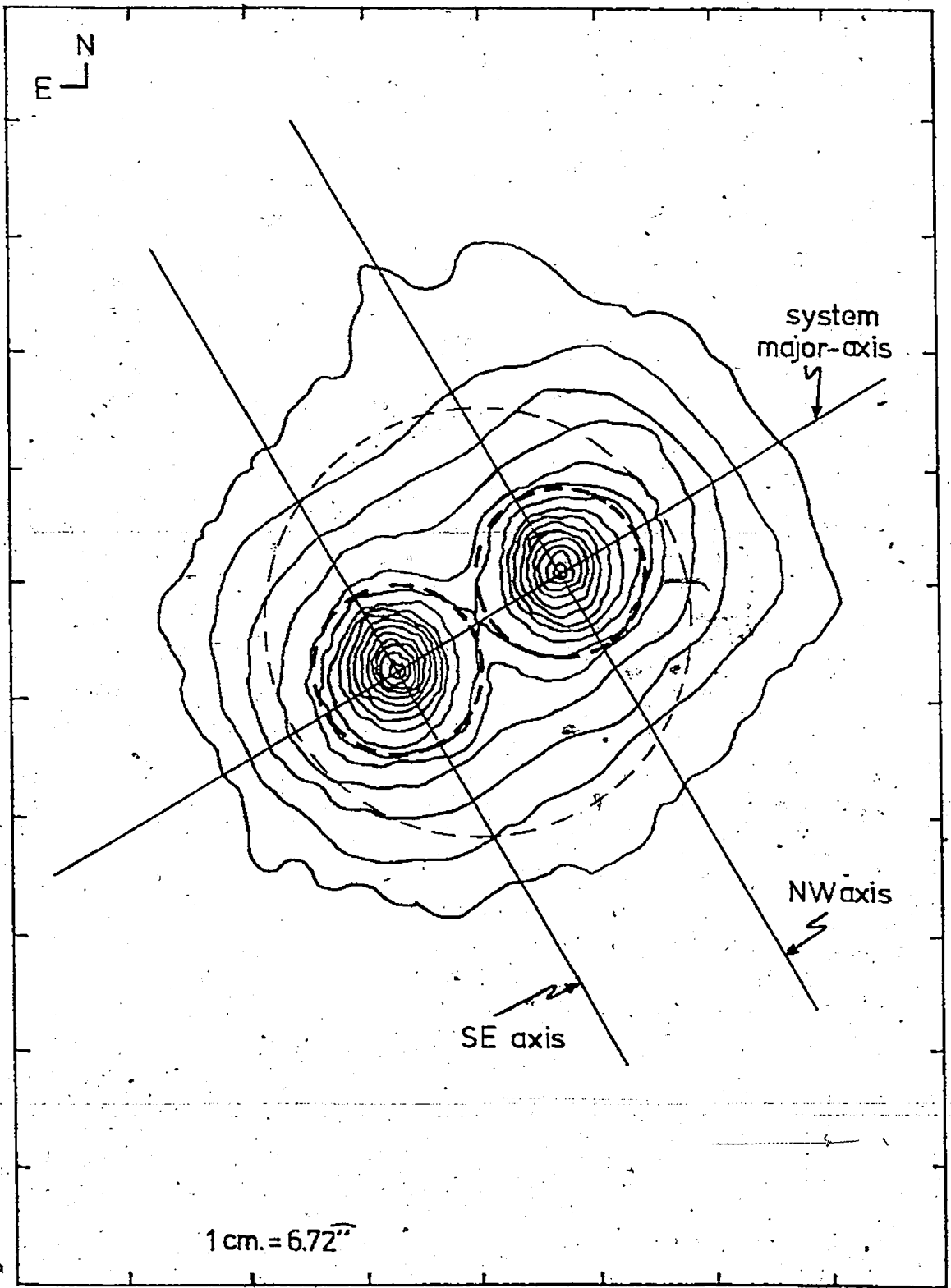


TABLE VIII

Apparent core radii, modelled central intensities and calibrated surface brightnesses for each semi-axis of the A1775 system

semi-axis	Apparent core radius (arc-secs) $r_{c, app}$	Model Central Intensity (as in PROFIL) I_0	Calibrated Surface Brightness (mags/arc ²) μ_V
<u>NW Component</u>			
SE	2.75	948.4	19.55
SW	2.82	912.0	19.46
NW	2.71	949.0	19.50
NE	2.69	898.3	19.60
<u>SE Component</u>			
SE	1.78	1118.9	19.31
SW	1.67	1125.2	19.27
NW	1.70	1168.3	19.24
NE	1.60	1189.4	19.15
<u>Averages*</u>			
	$r_{c, app}$	I_0	μ_V
NW Component	$2^{\text{m}}74 \pm 0^{\text{m}}06$	927 ± 27	19.53 ± 0.05
SE Component	$1^{\text{m}}68 \pm 0^{\text{m}}08$	1178 ± 68	19.24 ± 0.06

*The uncertainties are the standard deviations.

because a scaled King model with $c = 2.25$ and $r_{c, app} = 2$ arc-seconds can be extended out to 356 arc-seconds from the central regions. This angular extent is simply not seen in the present data, which is at most some 50 arc-seconds in extent. Therefore, the cut off radius was imposed upon the scaled King models in order to allow one to model the regions for which data exists. The cut off radii for the components were chosen to be 45 arc-seconds. Larger cut off radii were tried, to determine whether or not the brightness distributions were seriously affected by the cut off. No such problems were encountered.

In constructing the composite models, the model isophotes were constructed first. The centres of the NW and SE model components were separated by an amount, which when scaled, gives the true angular separation of the components in the plane of the sky. This separation was measured to be 20.71 ± 0.05 arc-seconds, and was found by direct measurement of the isophotes in Figure 2.

The next step in the model construction is to use the output of the computer programme MODEL to obtain contours of equal intensity for each of the appropriately scaled components. Radial values are read off the scaled King models for each of the components in 2 arc-second intervals, from the centre to the cut off radius. As these radii are all associated with specific intensities (which is due to the circular symmetry of the models), one may draw in the contours of constant intensity simply by using a compass. This is not true for the CE model, as the SE component is modelled as elliptical. The CE model will be discussed below in more detail. Finally one displaces the centres of the models by the scaled separation. Where the contours of intensity intersect, they are identified and the net intensities (i.e. the sums of the individual intensities) are

calculated. The net intensities are then 'binned' into intervals of 0.10 in the logarithm of the relative intensity. Any points within a given 'bin' were joined together to form the contours of the models. The 'bin' intervals correspond to 0.25 magnitudes per square arc-second in terms of surface brightness. The contours were drawn in by hand using French curves.

5.3 The CE Model

The same procedure was carried out for the CE model, except that the SE component was modelled as elliptical in form. As mentioned above, eye inspection of the isophotes of the A1775 system (Figures 2 or 11) show that the SE component is elliptical in form. The eccentricity of the elliptical contours was found by measuring major/minor axis pairs of the 10 inner-most smoothed isophotes (see Figure 11). The eccentricity was found for each major/minor axis pair, and from these calculated eccentricities, an average value was found. The value of the average eccentricity was found to be

$$\langle e \rangle = 0.28 \pm 0.02.$$

The same process was carried out for the NW component, and it was found to be essentially circular.

In constructing the elliptical intensity contours of the SE component, the profile of the intensity along the system major axis was constructed first. By eye inspection, the major axis of the SE component was found to be in an essentially north-south orientation, as opposed to the system major axis, which had a position angle of $128^\circ \pm 0.5^\circ$ (by direct measurement). Then, given the known difference in orientation between the system and component major axes, one could calculate radial values on the SE component's major and minor axes by the relations

$$a_i = \frac{r_i (1 + e \cos D)}{(1 - e^2)} \quad (5.1)$$

and

$$b_i = \frac{r_i (1 + e \cos D)}{(1 - e^2)^{1/2}} \quad (5.2)$$

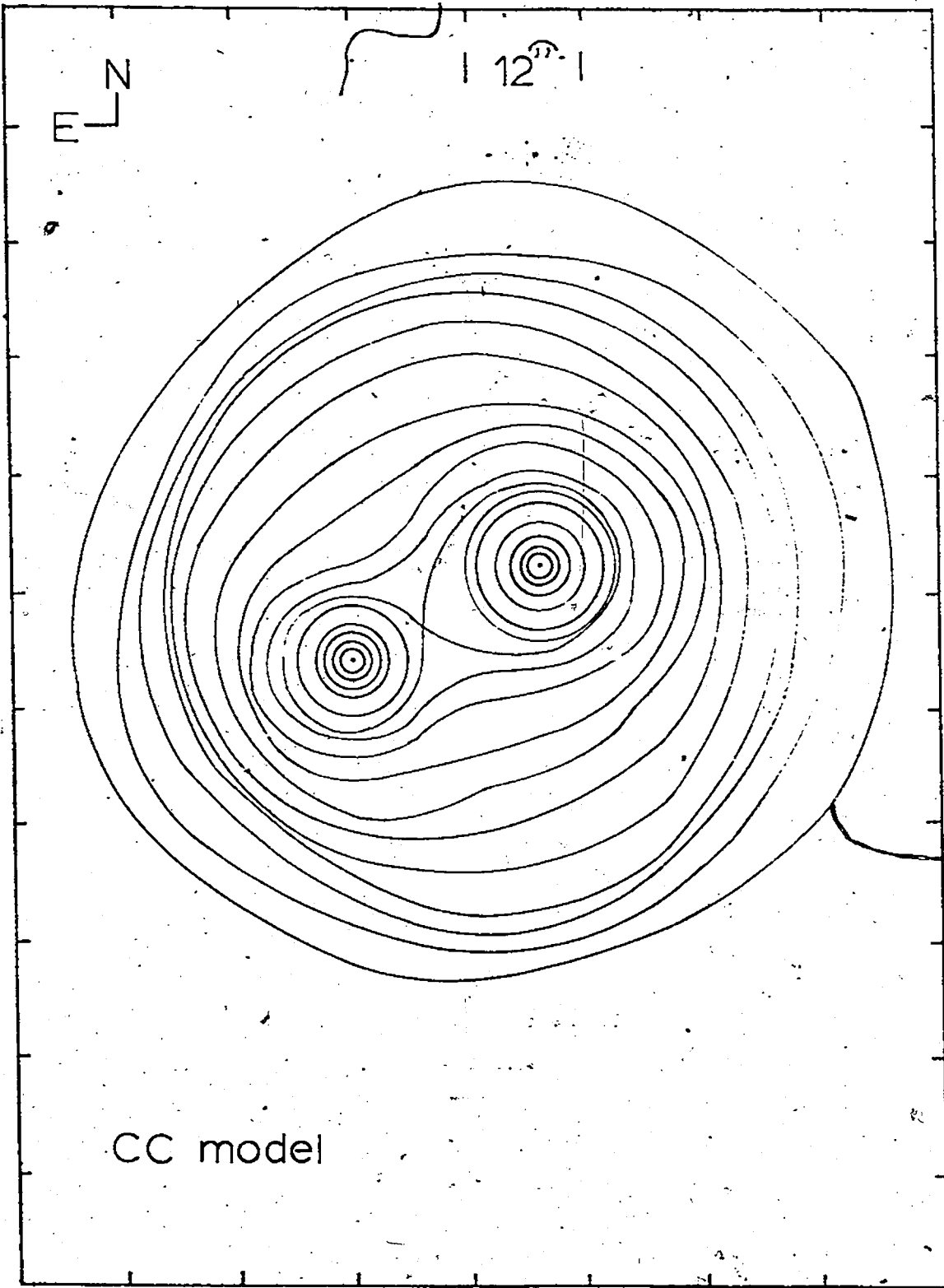
where D is the angle between the system and component major axes, and r_i is a radial position along the system major axis. With the use of the above equations it was then possible to construct an elliptical model of the SE component which fitted the observed intensity profile along the system major axis, and hence it was possible to draw contours of intensity with an ellipsograph. The model contours were constructed in the same fashion as those for the CC model outlined above. The model system major axes were constructed from the isophotal contour maps of both the CC and CE models. These model system major axes are plotted along with the data points defining the observed system major axis. The parameters for both the CC and CE models are found in Table IX. The CC model is found in Figures 12 and 13, and the CE model is found in Figures 14 and 15.

5.4 Other Models

The CC and CE models were constructed by fitting each of the components separately, and then super-imposing them to form the composite models. By inspecting Figures 13 and 15, one notes that the outskirts of the profiles along the system major axis are over-estimated by the composite models by ~ 0.5 mags/arc-sec². Therefore, modifications were made to the composite models to see if the problem in the outskirts could be rectified.

The approach taken was to try to fit the overall brightness profile

Figure 12. Model isophotes for the CC model of the A1775 system.
The scale is $2 \text{ cm} = 12''$. The contour interval is $0.25 \text{ mag}/\square''$.



CC model

Figure 13: Model system major axis for the CC model. The dashed line is the model and the filled circles are the observed points of the profile.

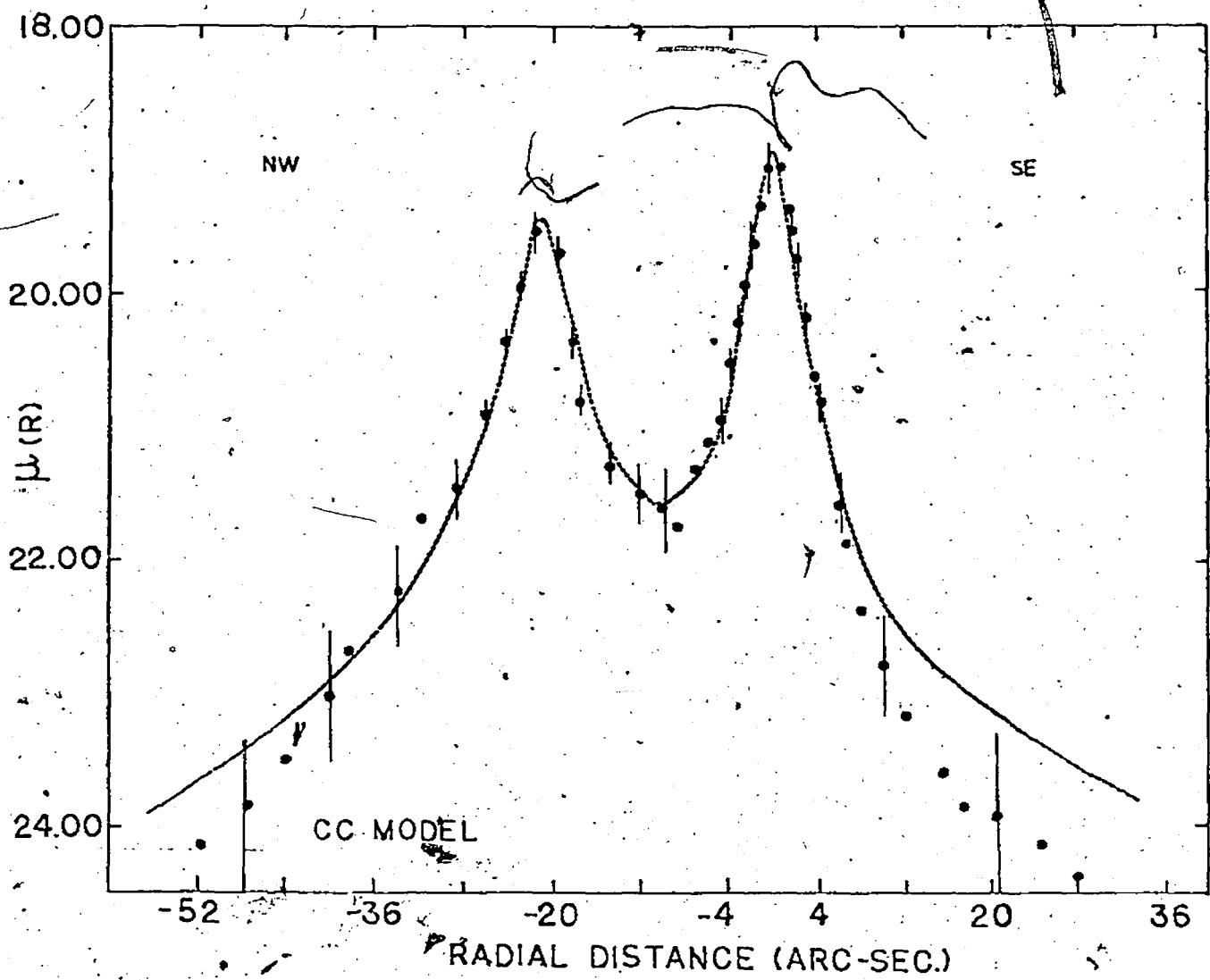
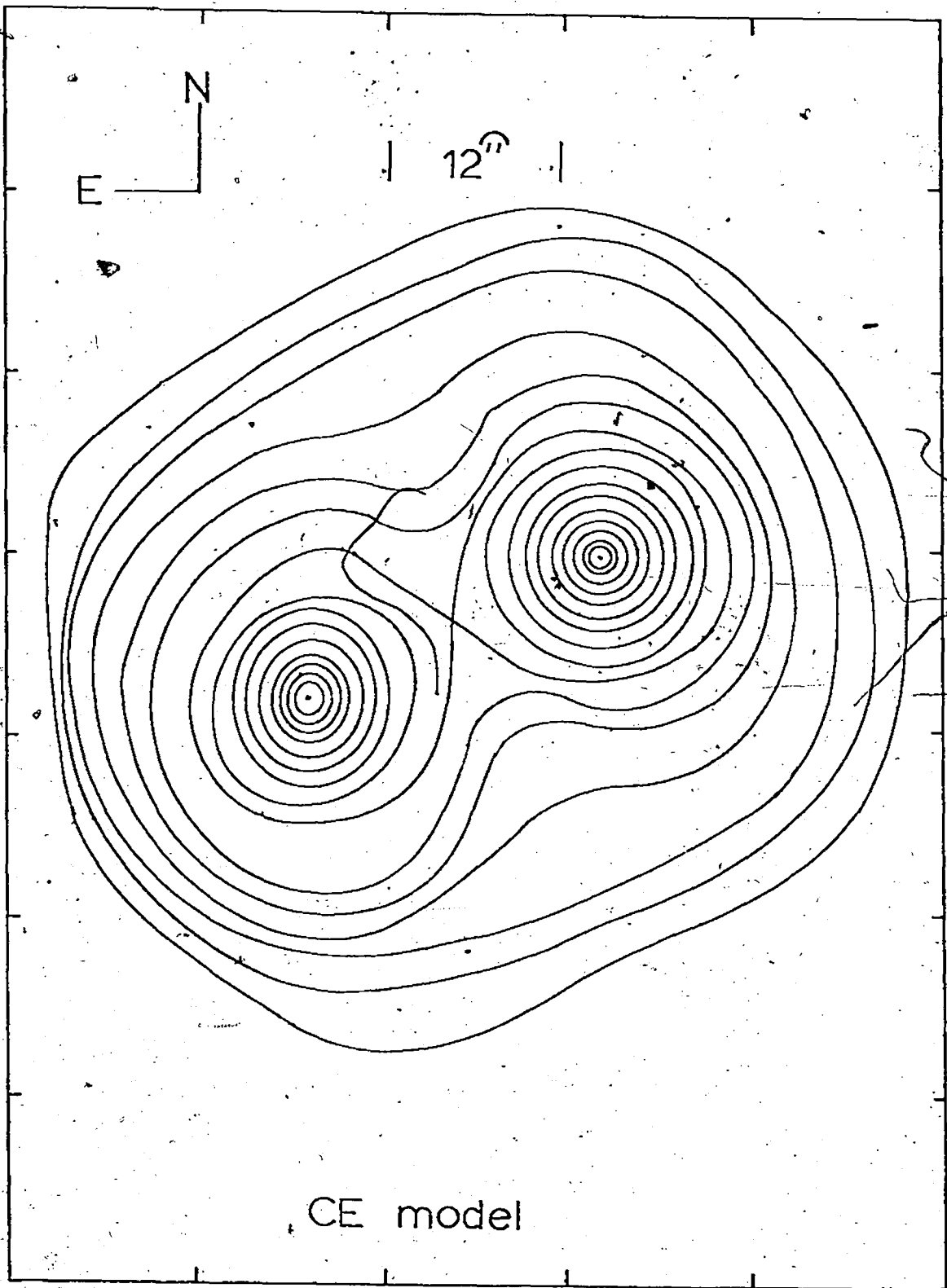


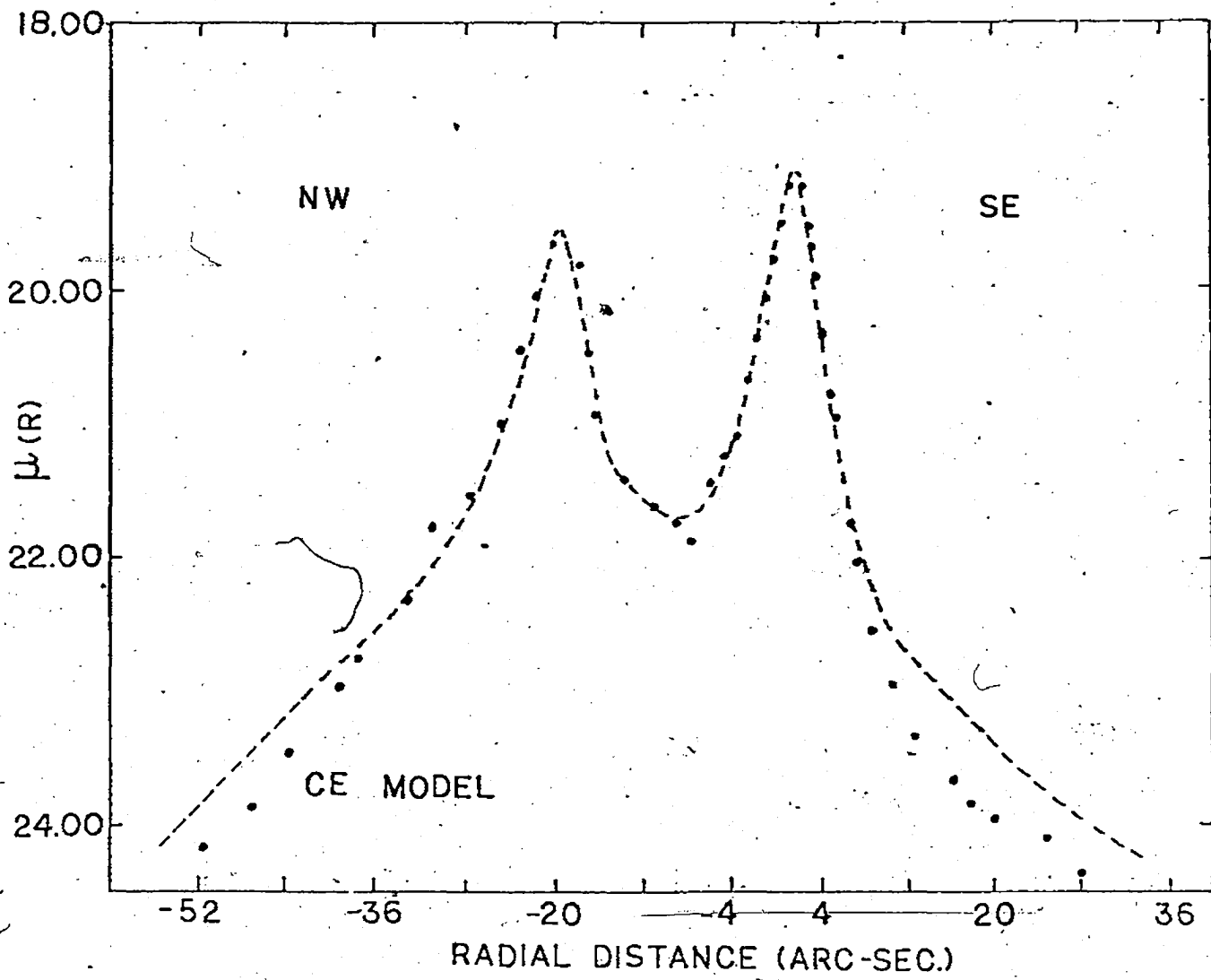


Figure 14. Model isophotes of the CE model. The SE component is modelled as elliptical. Same contour interval as Figure 12 and the scale is $3 \text{ cm} = 12''$.



CE model

Figure 15. Model system major axis for the CE model. The symbols have the same meaning as in Figure 13.



without worrying about whether or not the individual components were well modelled. To do so, the apparent core radii of each component was changed. The central intensities (and therefore the surface brightnesses) were not changed, although it is certain that the values found under-estimate the true surface brightnesses at the centres, due to seeing and instrumentation effects. The reason for not changing the central surface brightnesses, is that the intermediate regions of the profiles (i.e. $r = 2$ arc-sec to $r = 8$ arc-sec) are fairly well modelled, and in these regions the seeing and smearing effects of the instruments should be small, implying that the distribution of brightness seen is the true distribution of light.

The values of the apparent core radii were reduced to one-half and 3/4 of the values found in Table IX, for each component. With these modifications, model system major axes were constructed. It was found that by reducing the apparent core radii of each component by 1/2, the brightness profile produced badly under-estimated the observed profile everywhere, including the outskirts (see Figure 16). By reducing the apparent core radii by a factor of 1/4, the outskirts of the profile were fairly well modelled, but the inner portions of the profile were, again, underestimated (see Figure 17).

To sum up then, in decreasing the apparent core radii, the fit to the observed brightness profile was not at all improved. One simply ended up exchanging an over-estimation in brightness in the outskirts for an under-estimation in the inner portions of the profile. As one is only redistributing the bad fit of the models and not eliminating it, it was decided to retain the CC and CE models as originally constructed.

TABLE IX

Components of the Composite Models

Model	Components	Apparent Core Radius $r_{c,app.}$ (arc-sec)	Central Intensity (as in PROFIL)	Surface Brightness μ_V (mag/ \square^m)
CC	SE	1.68	1189	19.24
	NW	2.75	927	19.53
CE	SE	1.68	1189	19.24
	NW	2.74	927	19.53

Figure 16. The model system major axis of the A1775 system, with the values of the apparent core radii of the two components reduced by a factor of one-half.

The model is the dotted line, while the observed data are the filled circles.

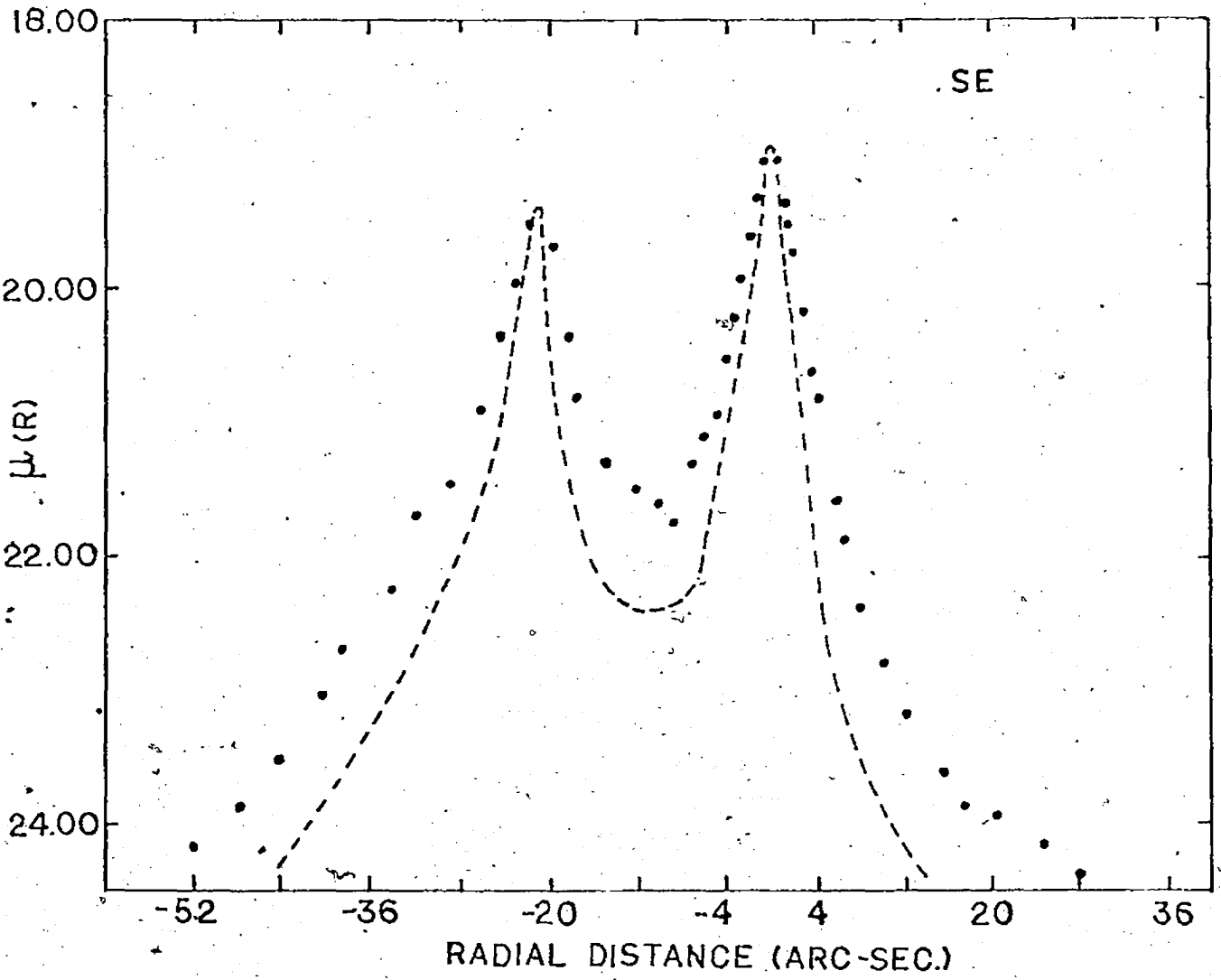
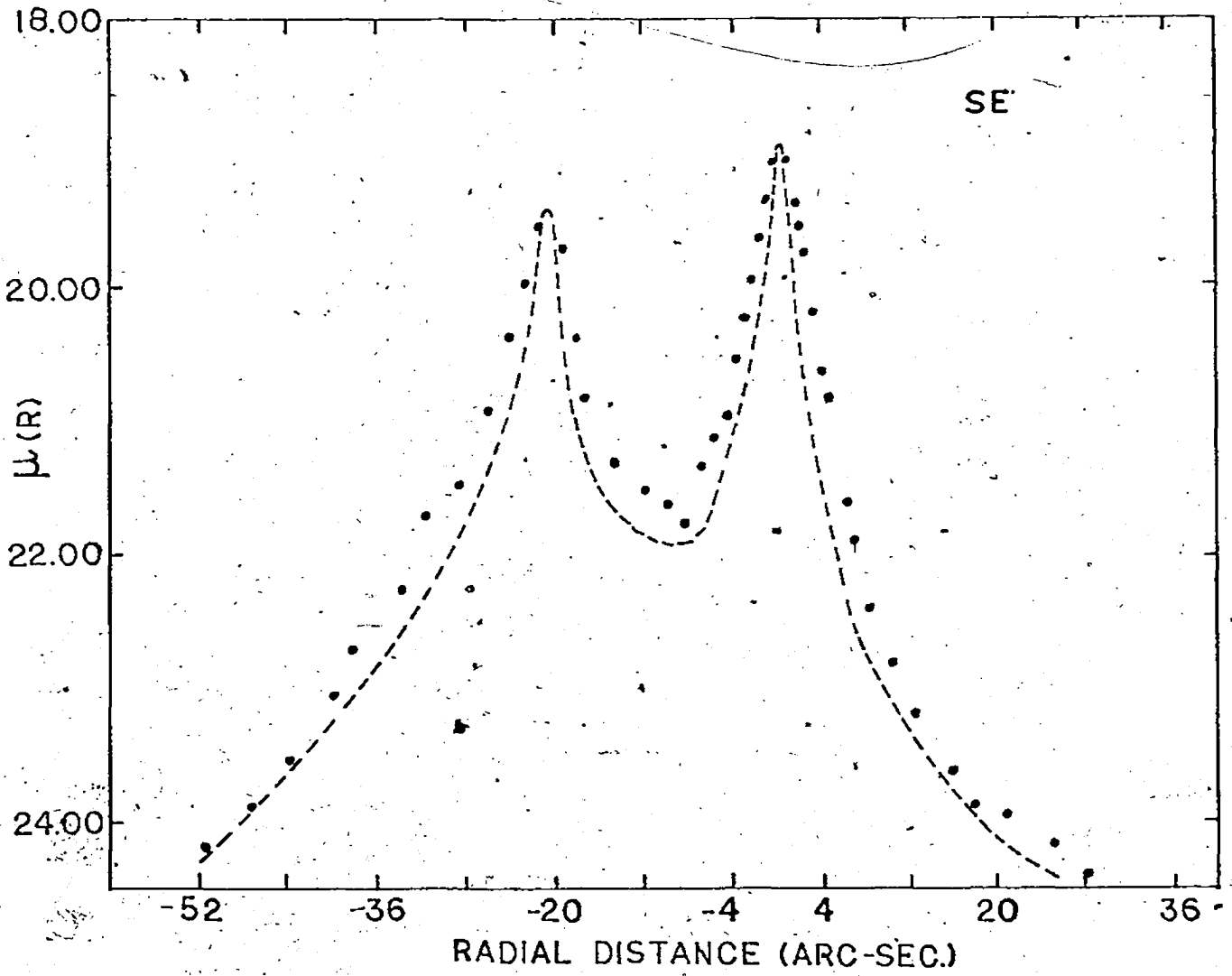


Figure 17. The model system major-axis with the values of the apparent core radii reduced by a factor of one-quarter.

Symbols have the same meaning as in Figure 16.



SECTION VI: CONCLUSIONS AND DISCUSSION

It is possible to draw a few conclusions about the A1775 double galaxy upon the basis of the composite models constructed in Section V above.

Consider Figure 11, the smoothed isophotes of the A1775 double. One notes that the most distinctive feature of these isophotes is the fact that the two centres of light are surrounded by a halo with a very distinct 'box' shape. This box-shaped halo is qualitatively well reproduced by the isophotes of the CE model (Figure 14).

By modelling the SE component of the A1775 system as elliptical, the fit to the observed isophotes in both the central regions of the SE component and in the halo, is significantly improved over the isophotes of the CC model. On the face of it, this is what would be expected in the case of the superposition of two unrelated elliptical galaxies, but it may be possible to form such a distinctively box-like halo through a gravitational interaction as well.

If one now considers the brightness profile of the A1775 system along the system major axis, one notices immediately that in both the CC and CE models (Figures 13 and 15 respectively), the outskirts of the profile are over-estimated by about 3 times (or roughly 1 magnitude). As outlined in Section 5.4 above, experiments were carried out to see if it was possible to eliminate or at least minimize this over-estimation by adjusting the apparent core radii of each of the components. The results of these experiments were either to shift the portion of the brightness profile where the composite models were bad fits or to make the overall fit to the observed profile worse.

A couple of points can be made in light of the results of the models constructed. These points can best be outlined under the two major possibilities concerning the nature of the A1775 double system. The two possibilities are that: 1) the A1775 system is the result of a superposition of unrelated and non-interacting galaxies or; 2) the system is interacting (and is either bound or unbound).

Consider the case if the A1775 system is a superposition of two unrelated galaxies. From the results of the models and the results of trying to modify these models, as outlined in Section 5.4 above, one can conclude that both of the galaxies which are superimposed must have brightness profiles which are different than those of most other large isolated elliptical systems. This conclusion is unattractive for two reasons. First, if both of the components are members of the A1775 cluster, then the photometry is such as to indicate that each is about as luminous as a typical bright elliptical galaxy. One would therefore expect the standard ($c = 2.25$) King model to be appropriate. The second reason is that this sets up a special case for the A1775 cluster. However, it should be pointed out that throughout this study, it has been tacitly assumed that the standard King model is appropriate. While this seems to be the case in light of the present photometry, some investigators (e.g. King 1978) have found that some elliptical galaxies in rich clusters of galaxies are better fitted by King models with $c = 2.00$ (i.e. with steeper brightness profiles). This possibility does not seem too likely in view of the fact that one was able to get quite good fits to the data by fitting each component individually, using the standard King model. It is for these reasons, that the superposition model for the A1775 system is considered unlikely.

Consider next the possibility that the A1775 double is the result of some sort of interaction. In this case, one might reasonably expect the procedure of fitting the standard King models to each of the components individually and then superimposing them, to break down somewhat. This is because it is either not possible or even valid to individually fit the components in a dynamical system. It might be more realistic to consider the overall profile of the system and try to fit it without any regard to how good the fit is to the individual components.

By way of a qualitative example, consider a King model with $\log_{10} r_t/r_c \equiv c = 2.00$. This model has a steeper brightness gradient, but in the central regions of the model, there is not too much difference from the standard ($c = 2.25$) King model. It is only in the outskirts (as is to be expected) where the differences of the profiles manifest themselves (see Figure A1 in Appendix 3). Indeed, at the point where the present data cuts off (at $\mu_v = 24.5$ mags/arc-sec² or $r = 32$ arc-sec), the difference between the two King models is about a factor of 3 in intensity, with the $c = 2.25$ model being brighter. One might reasonably expect a composite model formed from two appropriately scaled King models with $c = 2.00$ to be almost the same as the CC and CE models constructed using $c = 2.25$, in the inner portions, but to be fainter in the outskirts. Moreover, not only might the fit be better to the observed brightness profile, but one would also have a plausible explanation for the existence of the steeper gradients in the central regions of the profile. The steeper gradients would be attributable to tidal interaction effects, which would cause the surface brightness to fall off more rapidly than in an isolated system. This sort of tidal steepening of the brightness profile has been seen in

NGC 4486B and NGC 5846A (e.g. Faber 1973).

Another interesting point which can be brought out is to consider the A1775 system not only to be interacting but to be bound. If this were the case, then one would expect the centres of light to be surrounded and embedded in a large diffuse halo. The halo could be formed by one of two mechanisms. If a binary galaxy is formed out of a proto-galactic nebula, then some of the original material may not have collapsed into the central regions. Assuming little overall net rotation (Illingsworth 1977), this material could be quite extensive and its distribution isotropic. If on the other hand, the A1775 system was formed by a tidal merger, then the halo may be stripped material which, while lost to the individual galaxies, is retained by both in common. In any event, one would expect a large diffuse common halo about the A1775 system such as is seen in the A2029 and A2670 cD galaxies.

Unfortunately, Dressler's (1979) study of the A2029 cD galaxy only goes down to $\mu_V = 24$ mags/arc-sec², which is to about the same surface brightness as the present study. Comparing the A1775 and A2029 systems does not lead to any useful results, as the A2029 system looks just like the A1775 system except it has been radially scaled larger. There is no evidence in Dressler's data for A2029, that the halo has been detected. The study of the A2670 cD by Oemler (1973) is far more promising in that his data extends down to $\mu_V = 30$ mags/arc-sec², and there is definite evidence for a large diffuse halo.

Unfortunately, the evidence for the halo first appears at $\mu_V = 26$ mags/arc-sec², which is about a magnitude-and-a-half fainter than the cut off of the surface-brightness data in this present data. Again no useful conclusions can be drawn by comparing the A1775 and A2670 systems due to

the lack of surface brightness data on the A1775 system. One cannot say anything about the existence of a large faint halo which may surround the A1775 system.

To sum up then, the A1775 double seems to be some sort of interacting system. It is unlikely to be a superposition of two unrelated ellipticals as these objects would not be fitted by a standard King model, and this would require these ellipticals to have surface brightness profiles different than other isolated elliptical galaxies. Due to the lack of surface brightness data, no conclusions can be drawn about the nature of the interaction that the A1775 system is undergoing, nor can information be gained about the interaction by comparing the A1775 data with other large galaxies.

Further study of the A1775 double system, and systems like it, are desirable as these systems may be intermediate between isolated ellipticals in clusters in rich clusters, and the large cannibalistic CD galaxies seen in the centres of rich clusters. Such a study will need to be carried out on large instruments (e.g. the KPNO 4 metre) in order to obtain high resolution and to reach fainter surface brightness levels. Thus, one may be able to come to more positive conclusions concerning the nature of these types of systems.

NOTE TO APPENDICIES

All the programmes used in this study are listed excepting the programmes GALAXY and PROFIL. More information on these two programmes may be obtained from their respective authors. Mr. T. J. Deveau and Dr. G. A. Welch.

All the programmes are written in FORTRAN IV, except GALAXY which is written in PDP BASIC. All of the FORTRAN programmes were run in the BATCH mode on the Dalhousie University Cyber 170. A sample BATCH command programme is found in Appendix 2. The programme GALAXY was run on a time-sharing basis on the St. Mary's University PDP 11/70. All of the out-puts of the BATCH-run programmes were directed to the line printer at St. Mary's University.

APPENDIX 1: SUBSYSTEM GALAXY

The subsystem GALAXY is a computer routine written for the St. Mary's University PDP 11/70 computer and uses a Tekronix 4662 plotter. The subsystem was written by Mr. T. J. Deveau and is used to digitize microdensitometer tracings, forming data files which may be processed further.

The digitizing process is as follows, the microdensitometer tracing is placed on the Tekronix plotter, which is set in data transmission mode, and the system GALAXY is called. Three points are selected to form a co-ordinate axis on the tracing, and these points are digitized. Starting at the extreme left end of the tracing, points along the tracing are digitized at 1 mm intervals. The 3 points defining the co-ordinate axis are redigitized to check for any movement of the tracing during the digitization process. Upon successfully digitizing a tracing, one enters a name for the data file which has been created and stored on the PDP 11/70. These data files may be transferred to the Dalhousie University Cyber 170 by calling the programme CDC.QUE and the file name of the data one wishes transmitted.

Further information concerning this subsystem may be obtained from either the present writer or Mr. Deveau.

APPENDIX 2: THE PROGRAMME PROFIL

The programme PROFIL converts the densities of the digitized microdensitometer tracings into relative intensity-radius profiles. The programme can plot the intensity profiles individually, or averaged together.

The input data cards, formats and type of data being entered into the programme are listed below. More information concerning PROFIL can be found from English (1979). Included in this appendix are the file used to submit the programme and any data files to the Dalhousie University Cyber 170 computer and a sample run of PROFIL in the averaging mode. The run is of 5 plates on the system major axis and is the NW semi-axis of the NW component.

Input Data Cards (In order of appearance)

<u>NAME</u>	<u>FORMAT</u>	<u># CARDS</u>	<u>COMMENTS</u>
NPLATE	I2	1	-# of plates to be reduced
COMBIN	A10	1	-governs the way the data is processed.
OBJT	A4	1	-If = STAR the programme will bypass the 3x smear of the projected slit width
NPRINT	I2	1	00 = full printout 01 = minimum printout 10 = both data pts and plots
NPTS, DINIT	I3, F8.1	1	-the # of points in the characteristic curve and the initial density
CURVE	10F8.2	3	-relative intensity at 1 cm intervals of density points on the characteristic curve

APPENDIX 2 (cont.)

<u>NAME</u>	<u>FORMAT</u>	<u># CARDS</u>	<u>COMMENTS</u>
SKYCAL	F5.1	1	-density of sky (in mm) above clear plate level
ISKY	20I4	≤ 28	-digitized sky tracing
IGAL	2I4	1	-location of galaxy nucleus on sky tracing
IOBJ	20I4	≤ 28	-digitized galaxy tracing
ICENTR	2I4	1	-location of nucleus on galaxy tracing
NPLOT	I2	1	-00 = no plots 01 = plots on a plotter 10 = plots on a line printer
DEL	F4.2	1	-included if NPLOT \neq 00. It governs the increment for selecting the points to be plotted.

Sample Run of PROFIL

NW component, NW semi-axis.

All five plates of this study have been stacked (averaged) to form the 10th profile found in this run.

/JOB
AGLXY, T070, CH110000.
USER, SMA5004, GALAXY.
PRINTAT(SMU)
GET(BINBRT1)
GET(MJAXIS)
BINBRT1(MJAXIS)
REPLACE(OUTPUT=OUTFILE/N0)
NOTIFY, TRACING RAN OK.
SKIP,EOJ.
EXIT,
NOTIFY, TRACING BOMBED
ENDIF,EOJ.
DAYFILE(DAYFILE)
REPLACE(DAYFILE)
/EOF
/

CHARACTERISTIC CURVE DATA

Table with 11 columns of numerical values representing characteristic curve data.

WITH FIRST POINT AT DENSITY 2.0 MM ABOVE CLEAR PLATE

INPUT VALUES OF ISKY

Large table of input values for ISKY, containing multiple rows of numerical data.

HACK HAS THROWN OUT 3 POINTS. THEY ARE....

600. 123. 640. 117. 873. 123.

ROTATE FINDS .0 DEGREES BETWEEN COORDINATE SYSTEMS

ROTATE FINDS .0 DEGREES BETWEEN COORDINATE SYSTEMS

LEAST-SQUARES FIT TO SKY LEVEL SHOWS DENSITY CHANGE OF .2E-01 MM PER CENTIMETER OF TRACING

SKY DENSITY AT GALAXY POSITION = 7.3 MM PLUS OR MINUS 1.1 MM IN COORD. SYSTEM OF TRACING

SKY DENSITY EXCEEDS CLEAR PLATE BY 11.9MM

INPUT VALUES OF IORJ

Large table of input values for IORJ, containing multiple rows of numerical data.

HACK HAS THROWN OUT 0 POINTS. THEY ARE....

0.

ROTATE FINDS .0 DEGREES BETWEEN COORDINATE SYSTEMS

ROTATE FINDS .0 DEGREES BETWEEN COORDINATE SYSTEMS

CHARACTERISTIC CURVE DATA

Table with 8 columns of numerical data: 1.00, 5.75, R.91, 11.22, 15.14, 17.18, 19.28, 21.63, 24.27, 27.23, 30.55, 33.88, 38.90, 43.65, 48.98, 54.95, 61.66, 69.18, 78.52, 88.10, 98.85, 110.41, 124.17, 0.00, 0.00, 0.00, 0.00, 0.00, 0.00, 0.00, 0.00.

WITH FIRST POINT AT DENSITY 1.8 MM ABOVE CLEAR PLATE

INPUT VALUES OF ISKY

Large table of input values for ISKY, with columns labeled 10, 10.1560, 10.21, 10.2610, 10.27, 21, 44, 29, 38, 40, 41, 51, 38, 60, 57, 69, 64, 79, 27, 91, 39, 101, 50, 111, 45, 121, 22, 128, 42, 140, 43, 152, 41, 160, 48, 173, 38, 182, 70, 191, 41, 200, 47, 208, 41, 221, 61, 230, 47, 239, 52, 249, 38, 259, 52, 270, 68, 282, 78, 290, 41, 299, 70, 308, 53, 320, 49, 331, 43, 340, 36, 349, 37, 360, 55, 369, 72, 378, 52, 389, 34, 401, 61, 411, 52, 423, 61, 429, 54, 441, 61, 450, 40, 459, 52, 472, 39, 481, 57, 492, 50, 501, 47, 510, 43, 520, 60, 529, 67, 540, 32, 550, 41, 559, 51, 569, 47, 579, 50, 592, 41, 602, 38, 611, 43, 621, 31, 632, 40, 641, 37, 652, 31, 659, 18, 669, 47, 680, 56, 692, 49, 700, 45, 709, 41, 718, 47, 730, 43, 837, 40, 851, 61, 860, 60, 871, 40, 880, 44, 891, 53, 898, 46, 909, 40, 920, 35, 931, 60, 941, 48, 952, 40, 961, 62, 970, 48, 979, 40, 990, 47, 997, 44, 1008, 52, 1020, 47, 1027, 87, 1038, 69, 1050, 39, 1058, 34, 1069, 38, 1082, 53, 1089, 48, 1099, 48, 1109, 37, 1114, 30, 1121, 51, 1128, 45, 1141, 35, 1152, 57, 1163, 74, 1169, 53, 1179, 59, 1191, 40, 1202, 46, 1212, 51, 1221, 58, 1229, 41, 1400, 50, 1409, 44, 1420, 55, 1427, 45, 1439, 39, 1452, 57, 1461, 48, 1468, 39, 1478, 61, 1490, 37, 1501, 33, 1510, 46, 62, 1520, 56, 1528, 51, 1537, 59, 1549, 38, 1560, 41, 1569, 52, 1580, 47, 1582, 45, 1594, 37, 1612, 28, 1621, 46, 1631, 72, 1639, 50, 1652, 57, 1659, 51, 1669, 58, 1680, 48, 1689, 46, 1699, 58, 1708, 71, 1720, 45, 1729, 43, 1739, 47, 1747, 47, 1759, 47, 1769, 54, 1778, 58, 1789, 35, 1799, 43, 1808, 50, 1818, 36, 1828, 41, 1840, 32, 1851, 43, 1861, 49, 1869, 74, 1879, 41, 1889, 62, 1900, 36, 1908, 32, 1920, 39, 1931, 30, 1940, 36, 1950, 40, 1960, 30, 1969, 43, 1981, 38, 1990, 38, 1999, 38, 2008, 49, 2022, 43, 2031, 56, 2040, 47, 2050, 52, 2058, 45, 2071, 54, 2079, 40, 2092, 45, 2099, 38, 2111, 47, 2122, 42, 2130, 51, 2141, 47, 2148, 65, 2159, 50, 2170, 54, 2180, 46, 2190, 40, 2201, 42, 2210, 32, 29, 2211, 45, 2222, 50, 2231, 47, 2240, 41, 2249, 58, 2258, 33, 2270, 54, 2280, 46, 2290, 40, 2301, 42, 2310, 38, 2322, 42, 2332, 37, 2340, 62, 2350, 51, 2362, 42, 2370, 76, 2382, 33, 2501, 51, 2510, 56, 2518, 42, 2532, 38, 2542, 30, 2551, 33, 2558, 42, 2569, 57, 2579, 67, 10, 15, 63, 10, 10, 2609, 10.

HACK HAS THROWN OUT 2 POINTS. THEY ARE....

282, 79, 1027, 87.

ROTATE FINDS 0.0 DEGREES BETWEEN COORDINATE SYSTEMS

ROTATE FINDS 0.0 DEGREES BETWEEN COORDINATE SYSTEMS

LEAST-SQUARES FIT TO SKY LEVEL SHOWS DENSITY CHANGE OF -.0E-02 MM PFR CENTIMETER OF TRACING

SKY DENSITY AT GALAXY POSITION = 3.7 MM PLUS OR MINUS 1.0 MM IN COORD. SYSTEM OF TRACING

SKY DENSITY EXCEEDS CLEAR PLATE BY 6.1MM

INPUT VALUES OF IOPJ

Large table of input values for IOPJ, with columns labeled 10, 10.1810, 10.21, 10.2610, 10.27, 21, 44, 29, 38, 40, 41, 51, 38, 60, 57, 69, 64, 79, 27, 91, 39, 101, 50, 111, 45, 121, 22, 128, 42, 140, 43, 152, 41, 160, 48, 173, 38, 182, 70, 191, 41, 200, 47, 208, 41, 221, 61, 230, 47, 239, 52, 249, 38, 259, 52, 270, 68, 282, 78, 290, 41, 299, 70, 308, 53, 320, 49, 331, 43, 340, 36, 349, 37, 360, 55, 369, 72, 378, 52, 389, 34, 401, 61, 411, 52, 423, 61, 429, 54, 441, 61, 450, 40, 459, 52, 472, 39, 481, 57, 492, 50, 501, 47, 510, 43, 520, 60, 529, 67, 540, 32, 550, 41, 559, 51, 569, 47, 579, 50, 592, 41, 602, 38, 611, 43, 621, 31, 632, 40, 641, 37, 652, 31, 659, 18, 669, 47, 680, 56, 692, 49, 700, 45, 709, 41, 718, 47, 730, 43, 837, 40, 851, 61, 860, 60, 871, 40, 880, 44, 891, 53, 898, 46, 909, 40, 920, 35, 931, 60, 941, 48, 952, 40, 961, 62, 970, 48, 979, 40, 990, 47, 997, 44, 1008, 52, 1020, 47, 1027, 87, 1038, 69, 1050, 39, 1058, 34, 1069, 38, 1082, 53, 1089, 48, 1099, 48, 1109, 37, 1114, 30, 1121, 51, 1128, 45, 1141, 35, 1152, 57, 1163, 74, 1169, 53, 1179, 59, 1191, 40, 1202, 46, 1212, 51, 1221, 58, 1229, 41, 1400, 50, 1409, 44, 1420, 55, 1427, 45, 1439, 39, 1452, 57, 1461, 48, 1468, 39, 1478, 61, 1490, 37, 1501, 33, 1510, 46, 1409, 574, 1417, 671, 1428, 784, 1437, 908, 1447, 980, 1457, 1161, 1470, 1279, 1476, 1264, 1486, 1274, 1499, 1199, 1510, 1129, 1518, 985, 1527, 890, 1538, 727, 1547, 601, 1556, 518, 1569, 415, 1578, 369, 1586, 334, 1598, 291, 1605, 254, 1613, 234, 1627, 207, 1639, 181, 1650, 160, 1660, 126, 1667, 101, 1679, 106, 1689, 94, 1698, 88, 1708, 81, 1722, 86, 1728, 87, 1734, 104, 1750, 91, 1756, 81, 1765, 75, 1780, 75, 1786, 71, 1803, 77, 1814, 77, 1815, 84, 1828, 75, 1840, 70, 1848, 61, 1861, 55, 1869, 58, 1880, 57, 1889, 46, 1900, 40, 1909, 48, 1919, 54, 1933, 54, 1937, 48, 1946, 60, 1959, 53, 1967, 71, 1979, 62, 1988, 58, 1999, 60, 2008, 60, 2018, 57, 2027, 57, 2038, 42, 2048, 34, 2058, 31, 2069, 30, 2080, 31, 2090, 33, 2100, 34, 2110, 43, 2118, 52, 2128, 46, 2146, 42, 2161, 49, 2168, 43, 2174, 40, 2188, 40, 2195, 49, 2207, 56, 2215, 60, 2226, 67, 2238, 76, 2247, 88, 2258, 72, 2268, 70, 2278, 67, 2290, 58, 2299, 51, 2312, 48, 2323, 40, 2330, 45, 2340, 45, 2349, 52, 2358, 56, 2369, 52, 2379, 49, 2391, 41, 2400, 41, 2408, 41, 2418, 41, 2427, 39, 2436, 38, 2449, 36, 2460, 36, 2468, 36, 2474, 41, 2481, 39, 2487, 44, 2490, 41, 10, 1809, 10, 11, 2558, 17.

HACK HAS THROWN OUT 0 POINTS. THEY ARE....

0.

ROTATE FINDS 0.0 DEGREES BETWEEN COORDINATE SYSTEMS

ROTATE FINDS 0.0 DEGREES BETWEEN COORDINATE SYSTEMS

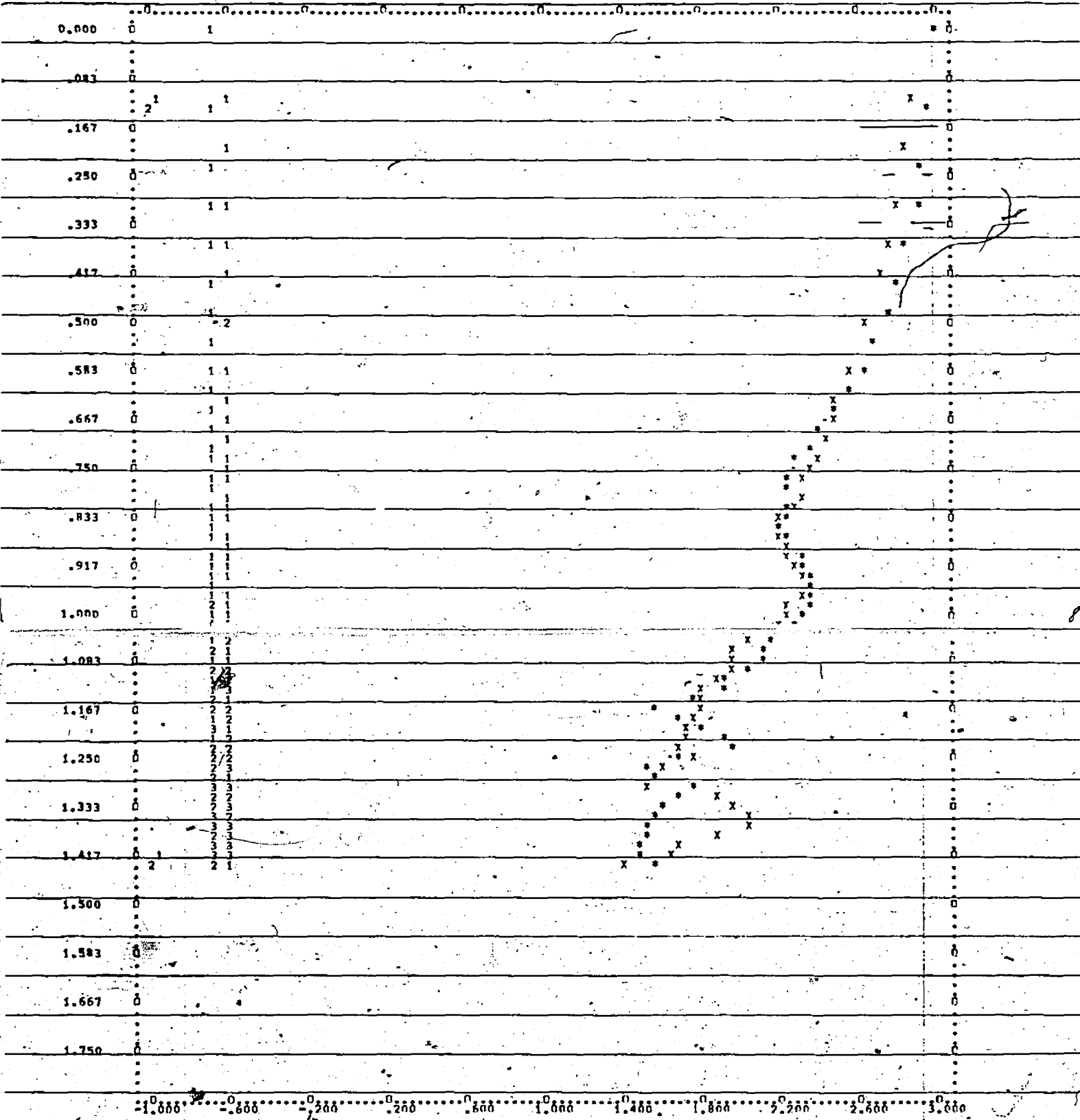
CURVE FITTING FOR AVERAGE NUMBER 1 USES INTERVAL .133 THROUGH .417 INCLUSIVE IN LOGR

FOLLOWING POINTS ARE USED IN FORMING SECOND APPROXIMATION IN FITTING PROCESS

Table with 3 columns: PASS, DELTA, S0SUM, DELTA, S0SUM, DELTA, S0SUM. Row 1: 1, -.23853, 3.40057, -.03853, 1.42654, .16147, 2.87252. Row 2: 2, -.13853, 2.17356, .06147, 1.65953, .26147, 5.06550.

FITTING PROCEDURE FOR AVERAGE NUMBER 1 GIVES -.03853 -.0123 -.0123 -.0123 FOR FIRST APPROXIMATION SECOND GUESSES 1 AND 2 AND FINAL APPROXIMATION RESPECTIVELY FOR INCREMENT IN LOG I NECESSARY TO MATCH PRESENT TRACING WITH FIRST TRACING OR PREVIOUS AVERAGE

2 of



SYMBOLS X REPRESENT AVERAGE OF NW SEMIAXES OF FOLLOWING PLATES.

ABELL1775 PS5720 V05 LEVER ARM = 199.30 PROJECTED SLIT = 35X 35 MU

SYMBOLS * REPRESENT NW SEMIAXIS OF FOLLOWING PLATE TO BE AVERAGED IN.

ABELL1775 PS5720 V05 LEVER ARM = 199.30 PROJECTED SLIT = 35X 35 MU

SYMBOLS 1 AND 2 DENOTE RESPECTIVELY BOUNDARY POINTS ASSIGNED TO AVERAGE UP PREVIOUS PLATE AND TO PRESENT PLATE

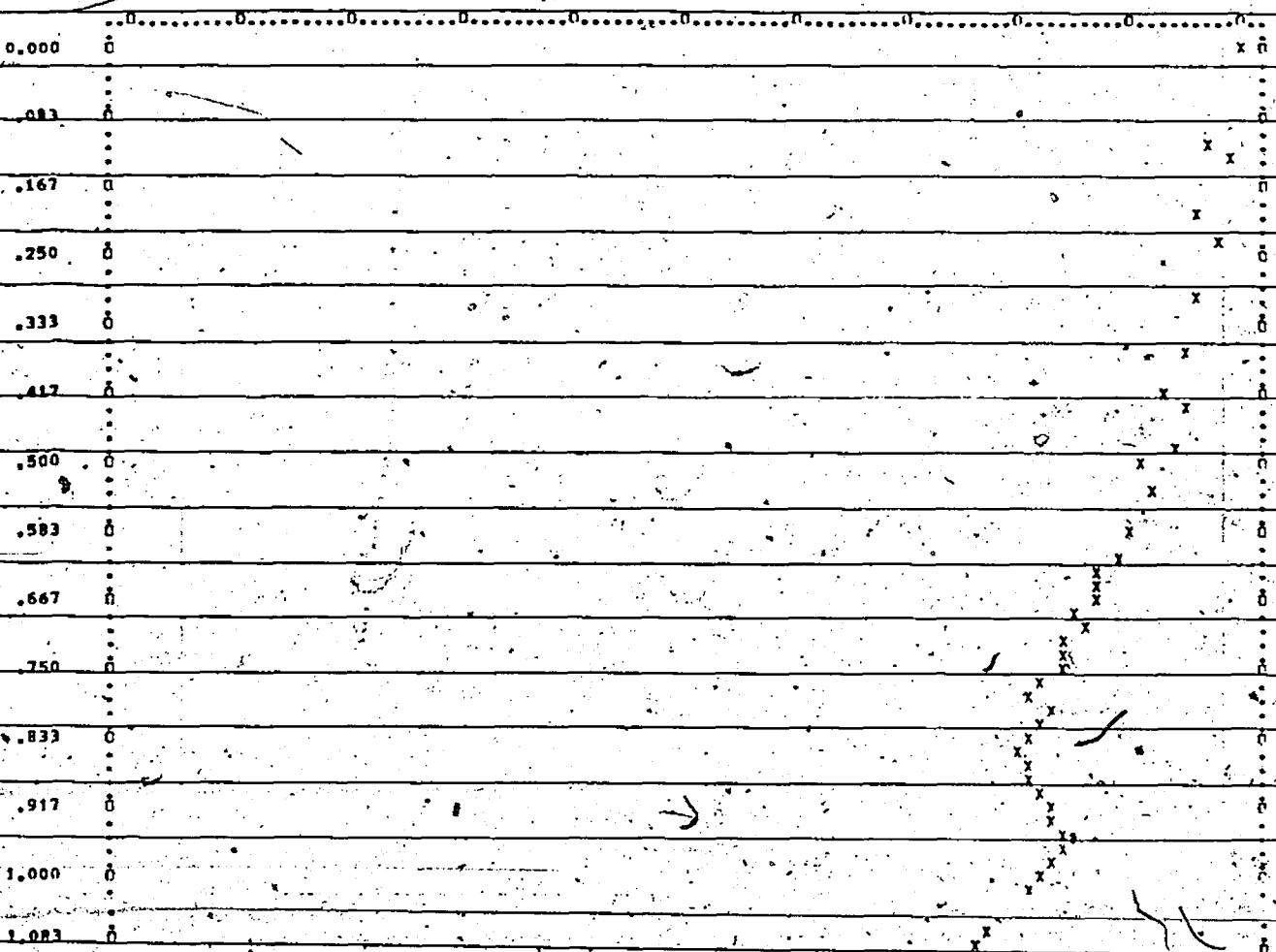
INTENSITIES OF CURRENT TRACING ASSIGNED FOLLOWING RELATIVE WEIGHTS FOR AVERAGING

3 OF

0.000	0.000	0.000	1.000	0.000	0.000	0.000	1.000	0.000	0.000	0.000	1.000	0.000	0.000	1.000	0.000	1.000
0.000	0.000	1.000	0.000	0.000	1.000	0.000	1.000	0.000	1.000	0.000	1.000	0.000	1.000	0.000	1.000	1.414
0.000	1.000	1.000	0.000	1.000	1.000	1.000	1.000	0.000	1.000	1.000	1.000	1.000	1.000	1.000	1.000	1.414
1.000	1.000	1.000	.707	1.414	1.000	1.000	1.000	.577	1.414	1.000	.707	1.732	.707	1.000	1.000	
1.000	.816	1.414	1.000	1.000	.816	1.225	1.000	.816	1.000	1.000	1.414	1.000	1.000	1.000	1.000	

LENGTH OF PRESENT TRACING AND PREVIOUS AVERAGE DIFFER BY LESS THAN 50 PERCENT. SET ALL WEIGHTS W TO 1.0

4 OF



1.000 0

1.083 0

1.167 0

1.250 0

1.333 0

1.417 0

1.500 0

1.583 0

1.667 0

1.750 0

0.000 0.500 1.000 1.500 2.000 2.500 3.000

SYMBOLS X REPRESENT AVERAGE OF NM SEMIAXES OF FOLLOWING PLATES.

ARELL1775 PS5720 V05 LEVER ARM = 199.30 PROJECTED SLIT = 35X 35 MU
ARELL1775 PS5748 V05 LEVER ARM = 199.30 PROJECTED SLIT = 35X 35 MU

ARELL1775 PLATE PS5724 RANDPASS-EXPOSURE = V20 RATIO ARM = 104.07 PROJECTED SLIT = 70X 70 MICRONS

CHARACTERISTIC CURVE DATA

1.99 5.82 7.59 9.12 10.59 11.89 13.18 15.31 17.38 19.49
22.13 24.83 27.86 31.62 35.69 40.27 45.71 51.29 57.88 64.94
72.85 83.18 93.33 104.71 118.85 0.00 0.00 0.00 0.00 0.00

WITH FIRST POINT AT DENSITY 4.0 NM ABOVE CLEAR PLATE

INPUT VALUES OF TSKY

10.1710 10. 10.2610 10. 144. 133. 153. 145. 160. 212. 169. 140. 180. 84. 192. 105. 200. 161. 209. 183. 221.
146. 228. 82. 219. 145. 250. 222. 261. 149. 270. 159. 280. 167. 290. 95. 307. 104. 318. 138. 325. 162. 342. 144.
350. 135. 361. 142. 372. 142. 380. 131. 392. 138. 399. 127. 409. 187. 422. 136. 433. 144. 441. 99. 450. 107. 461.
158. 467. 88. 481. 145. 492. 188. 498. 106. 511. 109. 520. 152. 530. 133. 539. 117. 549. 156. 558. 197. 572. 169.
581. 152. 590. 144. 600. 89. 610. 147. 620. 102. 627. 164. 639. 137. 652. 124. 662. 145. 670. 152. 681. 132. 689.
154. 698. 132. 709. 160. 716. 107. 725. 156. 731. 129. 737. 109. 746. 90. 756. 137. 770. 99. 777. 88. 788. 170.
799. 127. 811. 99. 817. 163. 829. 124. 838. 146. 849. 124. 859. 111. 868. 140. 881. 129. 890. 146. 902. 111. 908.
137. 921. 109. 931. 133. 939. 109. 948. 154. 981. 87. 991. 131. 1004. 145. 1015. 158. 1024. 135. 1035. 141. 1043. 117.
1048. 151. 1057. 124. 1065. 147. 1075. 156. 1087. 113. 1096. 142. 1109. 127. 1117. 158. 1127. 149. 1134. 160. 1148. 136. 1157.
144. 1170. 184. 1179. 141. 1155. 186. 1367. 154. 1380. 161. 1395. 128. 1410. 120. 1421. 108. 1431. 113. 1440. 151. 1449. 140.
1462. 38. 1473. 131. 1482. 116. 1489. 147. 1501. 117. 1506. 146. 1520. 115. 1532. 151. 1539. 133. 1552. 184. 1561. 128. 1572.
160. 1581. 136. 1593. 172. 1598. 160. 1610. 133. 1622. 163. 1630. 179. 1641. 158. 1650. 117. 1663. 146. 1668. 130. 1679. 167.
1690. 135. 1699. 144. 1711. 137. 1718. 167. 1728. 137. 1740. 160. 1749. 140. 1761. 152. 1772. 141. 1779. 133. 1787. 117. 1799.
182. 1810. 111. 1819. 161. 1828. 107. 1839. 154. 1846. 129. 1857. 141. 1869. 149. 1880. 124. 1891. 152. 1907. 120. 1921. 164.
1937. 185. 1951. 146. 1957. 124. 1973. 152. 1985. 163. 1999. 155. 2009. 136. 2017. 165. 2031. 91. 2041. 120. 2048. 151. 2060.
182. 2070. 142. 2079. 116. 2088. 131. 2100. 120. 2109. 151. 2117. 129. 2127. 142. 2140. 124. 2147. 149. 2160. 122. 2172. 108.
218. 2179. 2190. 148. 2201. 122. 2211. 147. 2270. 117. 2234. 102. 2242. 137. 2248. 113. 2258. 164. 2269. 154. 2278. 144. 2289.
131. 2298. 141. 2304. 151. 2313. 129. 2324. 115. 2335. 180. 2344. 136. 2351. 172. 2361. 133. 2367. 141. 2385. 129. 2399. 115.
2411. 128. 2418. 115. 2469. 137. 2479. 184. 2495. 136. 2506. 142. 2520. 159. 2534. 137. 2545. 139. 2558. 164. 2563. 100. 2568.
144. 2579. 159. 2591. 145. 10.1710. 10. 10.2610. 10.

HACK HAS THROWN OUT 2 POINTS. THEY ARE....

160. 212. 250. 227.

ROTATE FINDS 0.0 DEGREES BETWEEN COORDINATE SYSTEMS

ROTATE FINDS 0.0 DEGREES BETWEEN COORDINATE SYSTEMS

LEAST-SQUARES FIT TO SKY LEVEL SHOWS DENSITY CHANGE OF .2E-01 NM PER CENTIMETER OF TRACING

SKY DENSITY AT GALAXY POSITION = 12.7 NM PLUS OR MINUS 2.2 NM IN COORD. SYSTEM OF TRACING

SKY DENSITY EXCEEDS CLEAR PLATE BY .733MP

INPUT VALUES OF TORJ

10.1910 10. 10.2510 10. 134. 124. 141. 125. 151. 132. 162. 116. 164. 87. 180. 98. 194. 79. 201. 184. 212. 182.
100. 110. 133. 122. 143. 132. 138. 141. 125. 151. 132. 162. 116. 164. 87. 180. 98. 194. 79. 201. 184. 212. 182.
221. 159. 212. 157. 241. 142. 249. 181. 260. 214. 269. 226. 282. 231. 289. 200. 299. 257. 308. 231. 315. 270. 330.
218. 339. 157. 351. 136. 359. 107. 368. 158. 381. 139. 388. 161. 398. 170. 408. 178. 422. 186. 431. 147. 440. 184.
450. 156. 459. 148. 470. 163. 481. 172. 491. 192. 500. 206. 510. 242. 518. 276. 532. 296. 541. 276. 549. 251. 558.
212. 572. 187. 584. 197. 590. 174. 597. 185. 610. 182. 617. 164. 631. 211. 641. 210. 650. 205. 658. 182. 667. 160.
642. 677. 690. 220. 703. 240. 711. 303. 721. 316. 728. 310. 738. 338. 748. 341. 758. 341. 768. 205. 658. 182. 667. 160.

5 of

54

14

10.1910	10.	10.2910	14.	21.	241.	31.	237.	40.	200.	49.	100.	81.	180.	11.	134.	79.	167.	50.	40.	163.		
100.	110.	133.	122.	143.	132.	138.	141.	125.	151.	132.	162.	116.	169.	87.	180.	98.	189.	120.	201.	189.	217.	187.
271.	159.	232.	152.	241.	147.	240.	181.	260.	214.	268.	226.	287.	231.	288.	200.	208.	257.	308.	231.	314.	275.	330.
218.	339.	157.	351.	136.	359.	107.	388.	158.	381.	139.	388.	161.	378.	170.	408.	178.	422.	186.	431.	107.	440.	188.
450.	156.	459.	148.	470.	163.	481.	172.	481.	197.	500.	206.	510.	247.	518.	276.	532.	296.	541.	276.	540.	251.	558.
212.	572.	187.	584.	197.	590.	174.	597.	185.	610.	182.	617.	164.	631.	211.	641.	210.	650.	205.	658.	187.	667.	189.
679.	187.	680.	220.	703.	240.	711.	303.	721.	316.	728.	339.	739.	318.	749.	278.	760.	250.	768.	266.	780.	329.	789.
179.	800.	393.	812.	423.	821.	458.	830.	549.	842.	619.	851.	607.	860.	824.	867.	846.	878.	860.	892.	808.	899.	781.
908.	789.	919.	798.	930.	873.	940.	995.	952.	1144.	959.	1323.	968.	1525.	981.	1607.	987.	1668.	998.	1733.	1010.	1620.	1619.
1544.	1030.	1419.	1040.	1354.	1050.	1229.	1058.	1104.	1067.	1007.	1078.	932.	1090.	842.	1098.	777.	1109.	707.	1118.	647.	1130.	575.
1140.	577.	1148.	521.	1158.	610.	1170.	546.	1181.	515.	1191.	505.	1199.	520.	1209.	641.	1218.	586.	1229.	767.	1230.	893.	1250.
1123.	1260.	1316.	1271.	1494.	1279.	1693.	1290.	1824.	1299.	1853.	1306.	1829.	1317.	1785.	1328.	1641.	1338.	1514.	1350.	1357.	1359.	1140.
1370.	964.	1379.	856.	1387.	706.	1396.	533.	1411.	488.	1420.	359.	1430.	352.	1439.	313.	1447.	291.	1456.	277.	1460.	268.	1477.
221.	1486.	741.	1502.	219.	1508.	233.	1518.	207.	1534.	246.	1543.	239.	1547.	250.	1558.	205.	1568.	198.	1582.	187.	1590.	158.
1601.	149.	1611.	164.	1621.	134.	1631.	125.	1638.	103.	1653.	126.	1662.	153.	1669.	146.	1681.	134.	1691.	141.	1699.	161.	1713.
159.	1721.	141.	1730.	178.	1743.	126.	1751.	114.	1758.	126.	1768.	146.	1779.	180.	1792.	178.	1800.	141.	1812.	150.	1821.	166.
1834.	145.	1839.	141.	1848.	161.	1861.	173.	1868.	154.	1882.	145.	1891.	139.	1900.	137.	1907.	117.	1918.	108.	1927.	101.	1940.
153.	1948.	169.	1958.	197.	1972.	125.	1979.	140.	1990.	137.	1997.	128.	2001.	116.	2010.	136.	2020.	128.	2029.	126.	2042.	161.
2049.	144.	2056.	164.	2072.	145.	2080.	139.	2088.	139.	2097.	164.	2106.	134.	2111.	140.	2124.	141.	2130.	145.	2139.	184.	2148.
183.	2153.	179.	2159.	175.	2168.	187.	2177.	208.	2189.	189.	2200.	182.	2210.	195.	2217.	173.	2233.	154.	2241.	132.	2248.	108.
2258.	108.	2271.	126.	2280.	146.	2294.	148.	2299.	134.	2307.	150.	2316.	128.	2327.	163.	2343.	133.	2351.	151.	2357.	165.	2368.
222.	2379.	206.	2392.	186.	2400.	140.	2411.	131.	2422.	138.	2432.	128.	2439.	146.	2450.	131.	2461.	116.	10.	1910.	10.	12.
2510.	10.																					

DATA HAS THROWN OUT - 0 POINTS. THEY ARE

D.

ROTATE FINDS - 0 DEGREES BETWEEN COORDINATE SYSTEMS

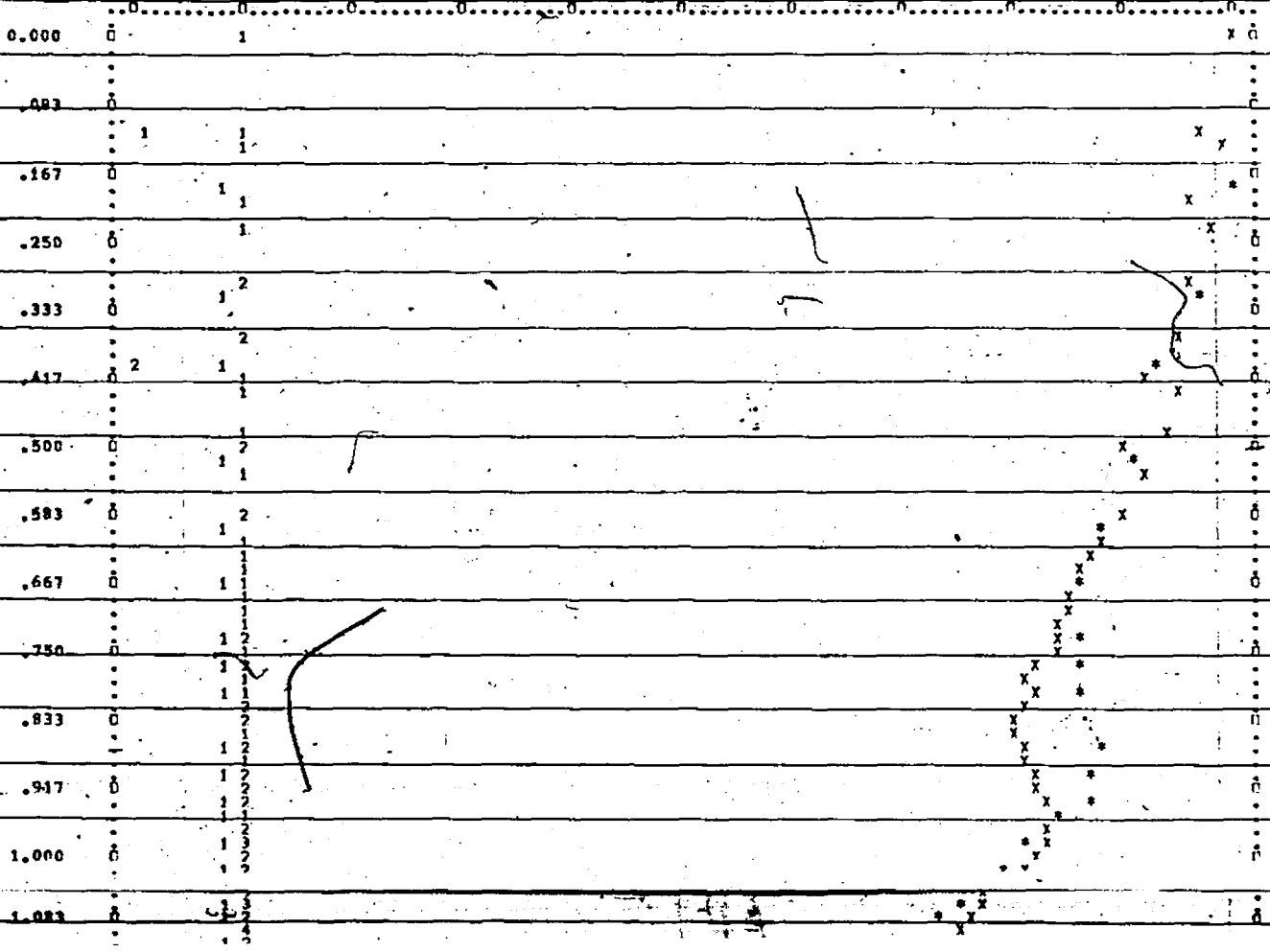
ROTATE FINDS - 0 DEGREES BETWEEN COORDINATE SYSTEMS

CURVE FITTING FOR AVERAGE NUMBER 2 USES INTERVAL .400 THROUGH 1.300 INCLUSIVE IN LOGR

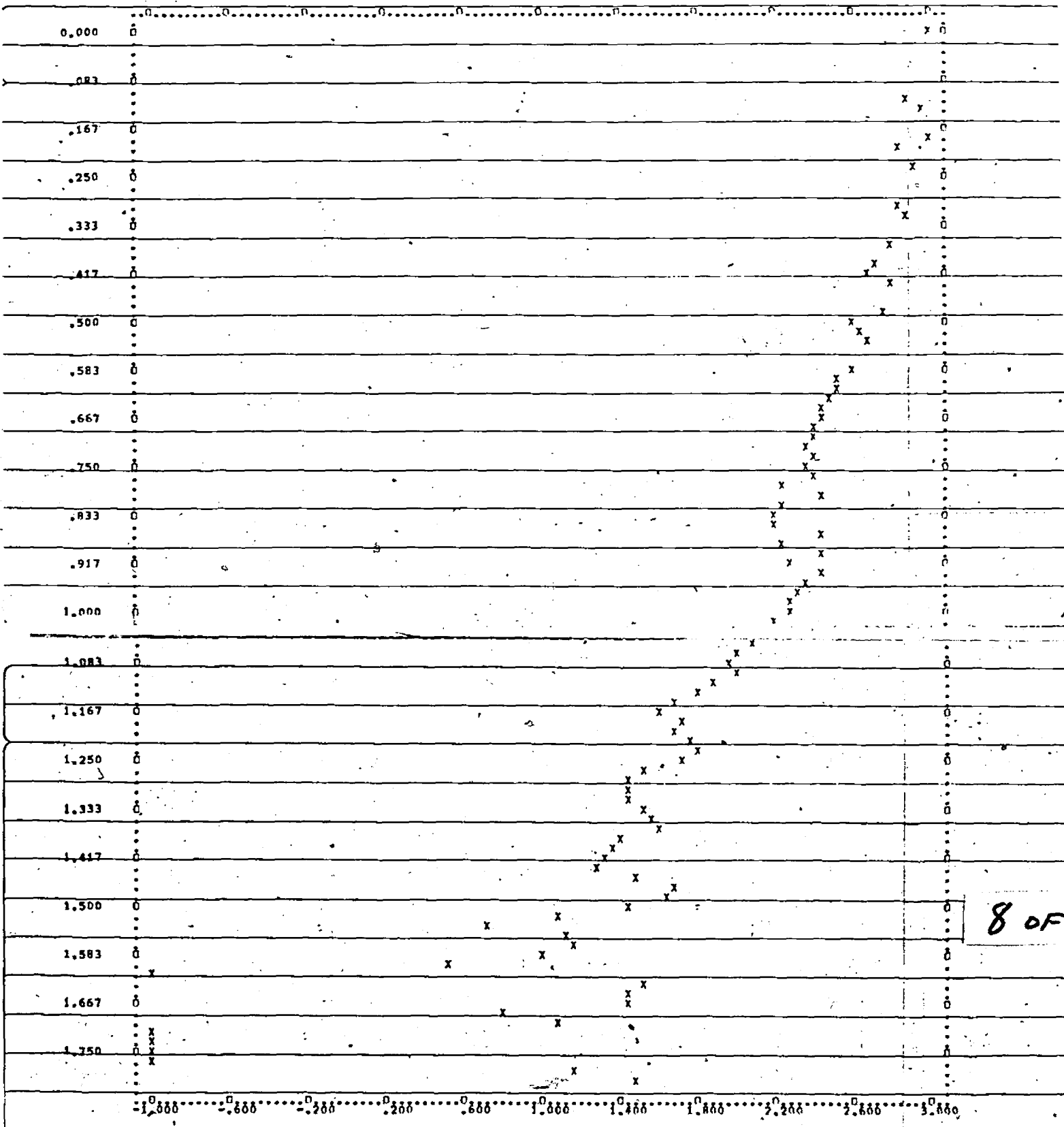
FOLLOWING POINTS ARE USED IN FORMING SECOND APPROXIMATION IN FITTING PROCESS

PASS	DELM	SOSIMM	DELS	SOSIM	DELP	SOSIMP
1	03405	46910	23405	78876	43405	3.10843
2	-06595	1.05927	13405	37893	33405	1.60860

FITTING PROCEDURE FOR AVERAGE NUMBER 2 GIVES .2341 .1021 .1021 .1021 FOR FIRST APPROXIMATION,
 SECOND GUESSES 1 AND 2 AND FINAL APPROXIMATION RESPECTIVELY FOR INCREMENT IN LOG Y NECESSARY TO MATCH
 PRESENT TRACING WITH FIRST TRACING OR PREVIOUS AVERAGE.



6 OF



8 OF

SYMBOLS X REPRESENT AVERAGE OF NW SEMIAXES OF FOLLOWING PLATES.				
ABELL1775	PS5720	V06	LEVER ARM = 199.30	PROJECTED SLIT = 35x 35 MU
ABELL1775	PS5748	V05	LEVER ARM = 199.30	PROJECTED SLIT = 35x 35 MU
ABELL1775	PS5724	V20	LEVER ARM = 104.07	PROJECTED SLIT = 70x 70 MU

CHARACTERISTIC CURVE DATA

5.62	9.2R	17.47	15.27	17.46	19.41	21.63	24.04	26.55	29.44
32.66	36.39	40.53	45.81	51.8R	59.15	67.76	76.03	90.16	105.44
122.46	142.58	0.00	0.00	0.00	0.00	0.00	0.00	0.00	0.00

WITH FIRST POINT AT DENSITY 7.1 MM ABOVE CLEAR PLATE

INPUT VALUES OF ISKY

10.1810.	10.	10.2660.	10.	69.	114.	81.	150.	88.	137.	100.	109.	112.	115.	119.	141.	129.	165.	138.	132.	149.		
101.	157.	118.	169.	147.	188.	98.	189.	137.	209.	178.	219.	122.	228.	131.	239.	183.	248.	127.	259.	120.		
268.	106.	279.	136.	289.	147.	390.	160.	400.	134.	409.	114.	419.	177.	429.	140.	440.	127.	449.	147.	461.	122.	470.
143.	480.	123.	490.	163.	499.	109.	509.	114.	520.	142.	529.	148.	540.	124.	549.	143.	560.	138.	570.	116.	580.	132.
700.	111.	710.	134.	720.	127.	730.	122.	741.	135.	748.	134.	759.	141.	770.	148.	780.	201.	780.	144.	799.	68.	810.
114.	819.	161.	829.	152.	847.	134.	850.	141.	864.	108.	873.	144.	882.	123.	892.	144.	1007.	10.	1015.	86.	1024.	124.
1329.	140.	1340.	172.	1349.	134.	1359.	129.	1369.	147.	1378.	134.	1380.	136.	1399.	143.	1411.	120.	1419.	130.	1430.	131.	1439.
139.	1449.	145.	1458.	139.	1469.	124.	1460.	130.	1469.	154.	1500.	174.	1510.	130.	1519.	138.	1530.	134.	1541.	118.	1550.	98.
1560.	175.	1570.	119.	1578.	171.	1591.	157.	1599.	117.	1611.	129.	1620.	139.	1630.	146.	1641.	139.	1649.	87.	1659.	100.	1670.
171.	1681.	139.	1690.	168.	1700.	152.	1710.	102.	1724.	143.	1740.	128.	1749.	75.	1759.	116.	1768.	162.	1778.	105.	1788.	102.
1800.	121.	1808.	102.	1820.	97.	1830.	159.	1839.	172.	1848.	157.	1859.	120.	1869.	117.	1880.	110.	1890.	114.	1900.	117.	1909.
144.	1919.	155.	1930.	120.	1939.	157.	1951.	92.	1960.	148.	1970.	125.	1980.	144.	1989.	171.	2000.	157.	2009.	151.	2021.	131.
2030.	96.	2038.	115.	2050.	109.	2061.	146.	2070.	178.	2079.	109.	2090.	136.	2100.	152.	2110.	110.	2118.	97.	2129.	131.	2140.
110.	2151.	149.	2161.	145.	2171.	126.	2240.	177.	2249.	122.	2261.	108.	2270.	138.	2279.	135.	2289.	129.	2301.	110.	2310.	138.
2319.	108.	2331.	150.	2339.	134.	2351.	130.	2360.	78.	2370.	61.	2370.	130.	2391.	111.	2400.	100.	2410.	125.	2420.	166.	2430.
134.	2441.	69.	2450.	100.	2461.	154.	2470.	158.	2481.	154.	2491.	130.	2499.	166.	2510.	159.	2520.	84.	2532.	132.	2540.	157.
2551.	105.	2560.	114.	2571.	143.	2580.	173.	2590.	138.	2602.	84.	2612.	118.	2620.	141.	2632.	130.	2641.	110.	2651.	107.	12.
1817.	10.	11.	2660.	10.																		

HACK HAS THROWN OUT 2 POINTS. THEY ARE...

780. 201.2370. 61.

ROTATE FINDS --0 DEGREES BETWEEN COORDINATE SYSTEMS

ROTATE FINDS --0 DEGREES BETWEEN COORDINATE SYSTEMS

LEAST-SQUARES FIT TO SKY LEVEL SHOWS DENSITY CHANGE OF -.1E-01 MM PER CENTIMETER OF TRACING

SKY DENSITY AT GALAXY POSITION = 12.1 MM PLUS OR MINUS 2.2 MM IN COORD. SYSTEM OF TRACING

SKY DENSITY EXCEEDS CLEAR PLATE BY 101.4MM

INPUT VALUES OF IOBJ

10.1910.	10.	10.2710.	16.	119.	193.	128.	384.	134.	185.	150.	161.	160.	148.	171.	141.	178.	139.	191.	142.	198.		
144.	209.	159.	220.	147.	242.	145.	246.	131.	250.	157.	260.	140.	268.	148.	280.	141.	288.	172.	311.	176.		
321.	191.	331.	201.	347.	207.	352.	201.	360.	177.	371.	340.	200.	378.	206.	407.	215.	418.	214.	429.	479.		
207.	441.	196.	449.	197.	461.	203.	467.	212.	481.	228.	490.	237.	500.	234.	509.	230.	518.	214.	542.	227.		
551.	221.	560.	226.	570.	222.	578.	228.	590.	226.	602.	223.	610.	218.	619.	206.	627.	210.	640.	213.	651.	208.	658.
210.	668.	203.	680.	170.	690.	134.	699.	131.	708.	136.	717.	149.	728.	163.	738.	174.	749.	201.	760.	204.	771.	198.
779.	190.	789.	193.	798.	210.	810.	213.	819.	206.	828.	210.	841.	227.	851.	247.	859.	253.	868.	277.	883.	337.	900.
349.	912.	341.	920.	347.	929.	365.	938.	394.	948.	420.	961.	426.	970.	499.	980.	552.	989.	560.	1000.	541.	1007.	535.
1018.	310.	1032.	541.	1039.	556.	1050.	602.	1059.	655.	1071.	759.	1082.	837.	1090.	1003.	1103.	1165.	1110.	1211.	1120.	1247.	1133.
1237.	1140.	1180.	1150.	1115.	1162.	1044.	1169.	954.	1182.	870.	1192.	775.	1200.	681.	1209.	582.	1218.	547.	1229.	521.	1240.	504.
1250.	470.	1258.	466.	1268.	472.	1277.	469.	1290.	441.	1299.	431.	1308.	443.	1317.	452.	1330.	452.	1339.	443.	1351.	484.	1362.
525.	1371.	557.	1386.	601.	1389.	698.	1401.	838.	1413.	1001.	1423.	1126.	1431.	1265.	1438.	1382.	1451.	1388.	1461.	1316.	1470.	1184.
1479.	1036.	1492.	931.	1500.	831.	1512.	694.	1519.	631.	1529.	557.	1539.	452.	1550.	384.	1558.	384.	1571.	346.	1586.	128.	1588.
296.	1680.	255.	1610.	249.	1618.	250.	1620.	242.	1641.	233.	1650.	236.	1658.	241.	1671.	236.	1679.	218.	1690.	235.	1699.	229.
1711.	209.	1720.	206.	1729.	207.	1740.	197.	1750.	191.	1761.	198.	1770.	197.	1781.	182.	1790.	179.	1801.	177.	1810.	180.	1821.
166.	1829.	155.	1842.	148.	1851.	132.	1862.	118.	1869.	116.	1877.	123.	1890.	141.	1903.	159.	1910.	171.	1920.	176.	1931.	169.
1940.	153.	1951.	143.	1964.	146.	1974.	157.	1989.	182.	2000.	201.	2010.	207.	2021.	203.	2030.	200.	2037.	204.	2050.	173.	2062.
155.	2073.	152.	2080.	158.	2089.	155.	2100.	169.	2109.	180.	2120.	188.	2137.	207.	2139.	205.	2151.	197.	2159.	190.	2170.	199.
2182.	207.	2193.	205.	2199.	210.	2212.	205.	2218.	216.	2230.	212.	2240.	206.	2250.	211.	2261.	219.	2270.	216.	2281.	210.	2287.
203.	2301.	199.	2311.	214.	2320.	237.	2330.	240.	2343.	206.	2352.	187.	2359.	165.	2376.	147.	2379.	133.	2388.	136.	2400.	148.
2410.	145.	2418.	186.	2428.	188.	2441.	183.	2454.	162.	2461.	158.	2471.	157.	2481.	165.	2492.	176.	2501.	182.	2511.	155.	2522.
204.	2530.	199.	2542.	189.	2551.	171.	2562.	157.	2569.	150.	2581.	152.	2591.	161.	2601.	199.	2612.	215.	2622.	243.	2633.	239.
2643.	223.	2649.	213.	2661.	200.	2669.	188.	2687.	173.	2689.	162.	12.	1912.	10.	10.	2710.	10.					

HACK HAS THROWN OUT 0 POINTS. THEY ARE....

ROTATE FINDS --0 DEGREES BETWEEN COORDINATE SYSTEMS

ROTATE FINDS --0 DEGREES BETWEEN COORDINATE SYSTEMS

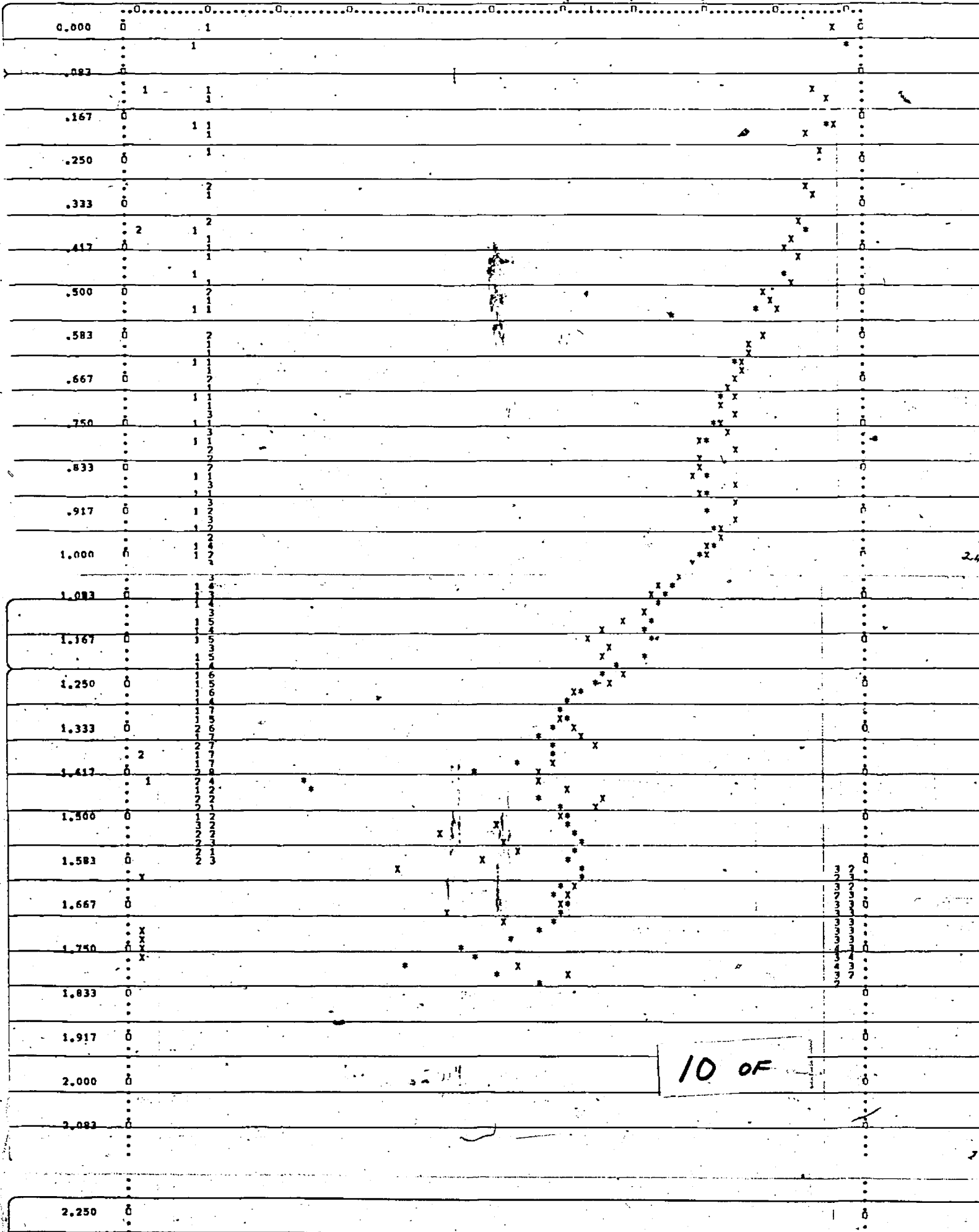
CURVE FITTING FOR AVERAGE NUMMR 3 USES INTERVAL .383 THROUGH 1.383 INCLUSIVE IN LOGR

FOLLOWING POINTS ARE USED IN FORMING SECOND APPROXIMATION IN FITTING PROCESS

PASS	DPLM	SOSIHM	DELI	SOSIHM	DPLP	SOSIHP
1	.0487R	.42006	.2487R	1.20184	.4487R	4.38362
2	-.05122	.9291H	.1487R	.61095	.3487R	2.40973

FITTING PROCEDURE FOR AVERAGE NUMMR 3 GIVES .248R .0836 .0R36 .0R36 FOR FIRST APPROXIMATION SECOND GUESSES 1 AND 2 AND FINAL APPROXIMATION RESPECTIVELY FOR INCREMENT IN LOG-I NECESSARY TO MATCH PRESENT TRACING WITH FIRST TRACING OR PREVIOUS AVERAGE.

9 OF



10 OF

2.250 0

2.333 0

2.417 0

2.500 0

2.583 0

2.667 0

2.750 0

0.000 0.600 1.200 1.800 2.400 3.000 3.600 4.200 4.800 5.400 6.000 6.600 7.200 7.800 8.400 9.000 9.600 10.200

SYMBOLS X REPRESENT AVERAGE OF NW SEMIAXES OF FOLLOWING PLATES.

ABELL1775	PS5720	V05	LEVER ARM = 199.30	PROJECTED SLIT = 35X 35 MU
ABELL1775	PS5748	V05	LEVER ARM = 199.30	PROJECTED SLIT = 35X 35 MU
ABELL1775	PS5724	V20	LEVER ARM = 104.07	PROJECTED SLIT = 70X 70 MU
ABELL1775	PS5719	V20	LEVER ARM = 104.07	PROJECTED SLIT = 62X 62 MU

ABELL1775 PLATE PS6664 PANPASS-EXPOSURE = 12H RATIO ARM = 51.86 PROJECTED SLIT = 140X140 MICRONS

CHARACTERISTIC CURVE DATA

1.00	2.75	4.45	6.31	8.13	10.23	12.45	14.96	16.41	20.07
22.52	25.41	28.57	32.17	35.89	40.50	45.45	51.29	57.54	64.57
72.44	81.29	91.20	102.33	114.14	128.46	136.46	0.00	0.00	0.00

WITH FIRST POINT AT DENSITY 5.5 MM ABOVE CLEAR PLATE

INPUT VALUES OF ISKY

10.1610.	10.	10.2310.	10.	23.	62.	29.	62.	3R.	62.	4H.	62.	59.	5R.	70.	58.	H7.	57.	41.	61.	102.		
69.109.	68.	118.	68.	127.	62.	128.	52.	163.	54.	158.	47.	167.	63.	177.	65.	188.	65.	210.	58.	221.	50.	
230.	61.	240.	61.	249.	60.	258.	60.	269.	61.	280.	6R.	289.	59.	297.	6R.	313.	63.	325.	6R.	333.	61.	341.
57.	352.	59.	359.	59.	433.	64.	440.	64.	446.	60.	457.	60.	469.	60.	478.	56.	579.	61.	592.	5R.	604.	59.
611.	59.	619.	59.	626.	59.	636.	57.	646.	57.	651.	49.	659.	45.	669.	5R.	679.	5R.	691.	6R.	702.	5F.	710.
62.	723.	63.	734.	63.	743.	62.	752.	56.	766.	5R.	772.	5R.	841.	61.	852.	61.	864.	61.	872.	63.	881.	66.
889.	66.	903.	70.	913.	70.	923.	73.	932.	74.	941.	74.	950.	73.	960.	73.	970.	6R.	1237.	71.	1241.	76.	1251.
72.	1260.	69.	1268.	77.	1280.	74.	1293.	69.	1300.	71.	1311.	73.	1324.	67.	1335.	65.	1344.	63.	1502.	64.	1511.	64.
1522.	66.	1532.	77.	1542.	69.	1549.	72.	1561.	72.	1570.	69.	1580.	62.	1594.	62.	1599.	62.	1610.	62.	1622.	64.	1630.
66.	1643.	66.	1655.	59.	1661.	59.	1670.	66.	1680.	66.	1691.	61.	1703.	61.	1713.	62.	1719.	60.	1729.	64.	1739.	64.
1751.	64.	1763.	64.	1774.	64.	1783.	64.	1794.	64.	1804.	64.	1808.	69.	1819.	5R.	1828.	60.	1835.	60.	1847.	60.	1858.
69.	1867.	62.	1873.	62.	1882.	62.	1889.	69.	1900.	62.	1910.	5R.	1921.	63.	1928.	54.	1938.	54.	1950.	54.	1958.	54.
1958.	49.	1970.	49.	1982.	56.	1991.	56.	2000.	56.	2014.	48.	2022.	45.	2089.	56.	2101.	51.	2112.	64.	2123.	64.	2129.
59.	2141.	59.	2152.	60.	2158.	60.	2166.	60.	2177.	60.	2186.	64.	2202.	68.	2214.	71.	2229.	60.	2240.	60.	2253.	62.
12.1610.	9.	10.2310.	11.																			

HACK HAS THROWN OUT 1 POINTS. THEY ARE....

1958. 49.

ROTATE FINDS -0 DEGREES BETWEEN COORDINATE SYSTEMS

ROTATE FINDS -0 DEGREES BETWEEN COORDINATE SYSTEMS

LEAST-SQUARES FIT TO SKY LEVEL SHOWS DENSITY CHANGE OF .RE-02 MM PER CENTIMETER OF TRACING

SKY DENSITY AT GALAXY POSITION = 5.3 MM PLUS OR MINUS .6 MM IN COORD. SYSTEM OF TRACING

SKY DENSITY EXCEEDS CLEAR PLATE BY 109.5MM

INPUT VALUES OF IOBJ

10.1660.	10.	10.2310.	10.	29.	35.	39.	3R.	50.	3R.	61.	3R.	71.	3R.	81.	42.	92.	42.	102.	42.	110.		
42.	118.	42.	127.	42.	139.	42.	149.	43.	156.	43.	171.	43.	178.	43.	186.	43.	203.	43.	210.	43.	220.	43.
233.	43.	241.	43.	251.	43.	264.	43.	271.	43.	282.	43.	291.	44.	298.	44.	309.	44.	316.	44.	329.	45.	340.
442.	43.	441.	43.	451.	43.	464.	43.	471.	43.	482.	43.	491.	44.	498.	44.	509.	44.	516.	44.	529.	45.	540.
455.	3R.	463.	3R.	471.	3R.	482.	3R.	491.	3R.	502.	3R.	511.	3R.	521.	3R.	531.	3R.	541.	3R.	551.	3R.	561.
69.	570.	7R.	571.	7R.	57R.	7R.																
682.	112.	689.	116.	700.	112.	709.	110.	722.	112.	728.	122.	742.	126.	755.	128.	764.	129.	768.	129.	768.	129.	768.

13 OF

233.	43.	241.	43.	251.	43.	264.	43.	271.	43.	282.	43.	291.	44.	298.	44.	309.	44.	316.	44.	329.	45.	340.	
445.	38.	463.	30.	473.	30.	482.	30.	491.	30.	500.	30.	509.	30.	518.	30.	527.	30.	536.	30.	545.	30.	554.	
64.	570.	74.	581.	74.	590.	74.	599.	74.	608.	74.	617.	74.	626.	74.	635.	74.	644.	74.	653.	74.	662.	74.	671.
682.	112.	689.	116.	700.	117.	709.	118.	722.	112.	728.	122.	742.	126.	755.	129.	764.	129.	769.	129.	774.	130.	781.	130.
129.	802.	110.	811.	140.	820.	140.	829.	140.	840.	140.	849.	140.	858.	140.	867.	140.	876.	140.	885.	140.	894.	140.	903.
911.	380.	918.	435.	931.	531.	940.	627.	950.	723.	961.	844.	970.	954.	980.	1038.	980.	1159.	1000.	1281.	1011.	1334.	1020.	1353.
1031.	1291.	1041.	1113.	1051.	993.	1059.	869.	1071.	777.	1080.	726.	1089.	680.	1101.	674.	1110.	694.	1121.	741.	1130.	825.	1139.	
1139.	908.	1149.	1032.	1149.	1242.	1170.	1477.	1170.	1431.	1192.	1238.	1202.	891.	1211.	706.	1220.	579.	1230.	455.	1241.	360.	1249.	
1290.	1262.	219.	1269.	181.	1278.	151.	1291.	118.	1300.	112.	1310.	100.	1318.	93.	1331.	89.	1340.	83.	1349.	76.	1363.	78.	
1369.	71.	1378.	69.	1390.	62.	1407.	62.	1417.	62.	1421.	62.	1430.	57.	1439.	63.	1450.	63.	1459.	63.	1471.	63.	1481.	
60.	1490.	65.	1499.	65.	1506.	65.	1516.	65.	1529.	66.	1540.	64.	1549.	62.	1558.	55.	1569.	50.	1580.	53.	1587.	51.	
1599.	47.	1612.	46.	1621.	46.	1628.	46.	1641.	44.	1648.	41.	1662.	38.	1669.	38.	1677.	38.	1680.	38.	1699.	38.	1707.	
38.	1719.	38.	1727.	39.	1738.	39.	1752.	36.	1759.	36.	1767.	36.	1777.	36.	1786.	36.	1796.	37.	1809.	45.	1817.	45.	
1826.	45.	1839.	45.	1849.	45.	1860.	45.	1869.	45.	1876.	45.	1886.	45.	1900.	40.	1909.	37.	1916.	37.	1930.	37.	1941.	
38.	1950.	38.	1961.	42.	1968.	43.	1979.	43.	1988.	44.	2000.	44.	2009.	44.	2020.	42.	2031.	38.	2040.	38.	2049.	37.	
2056.	37.	2067.	38.	2078.	38.	2091.	38.	2100.	38.	2107.	38.	2117.	38.	2128.	38.	2139.	38.	2150.	39.	2159.	41.	2168.	
41.	2175.	42.	2186.	42.	2195.	42.	2200.	38.	2211.	39.	2218.	39.	2229.	35.	2236.	35.	2245.	35.	2254.	34.	2262.	34.	
2273.	34.	2281.	30.	2290.	30.	12.	1660.	10.	10.	2308.	11.												

HACK HAS THROWN OUT 3 POINTS. THEY ARE...
415. 39.

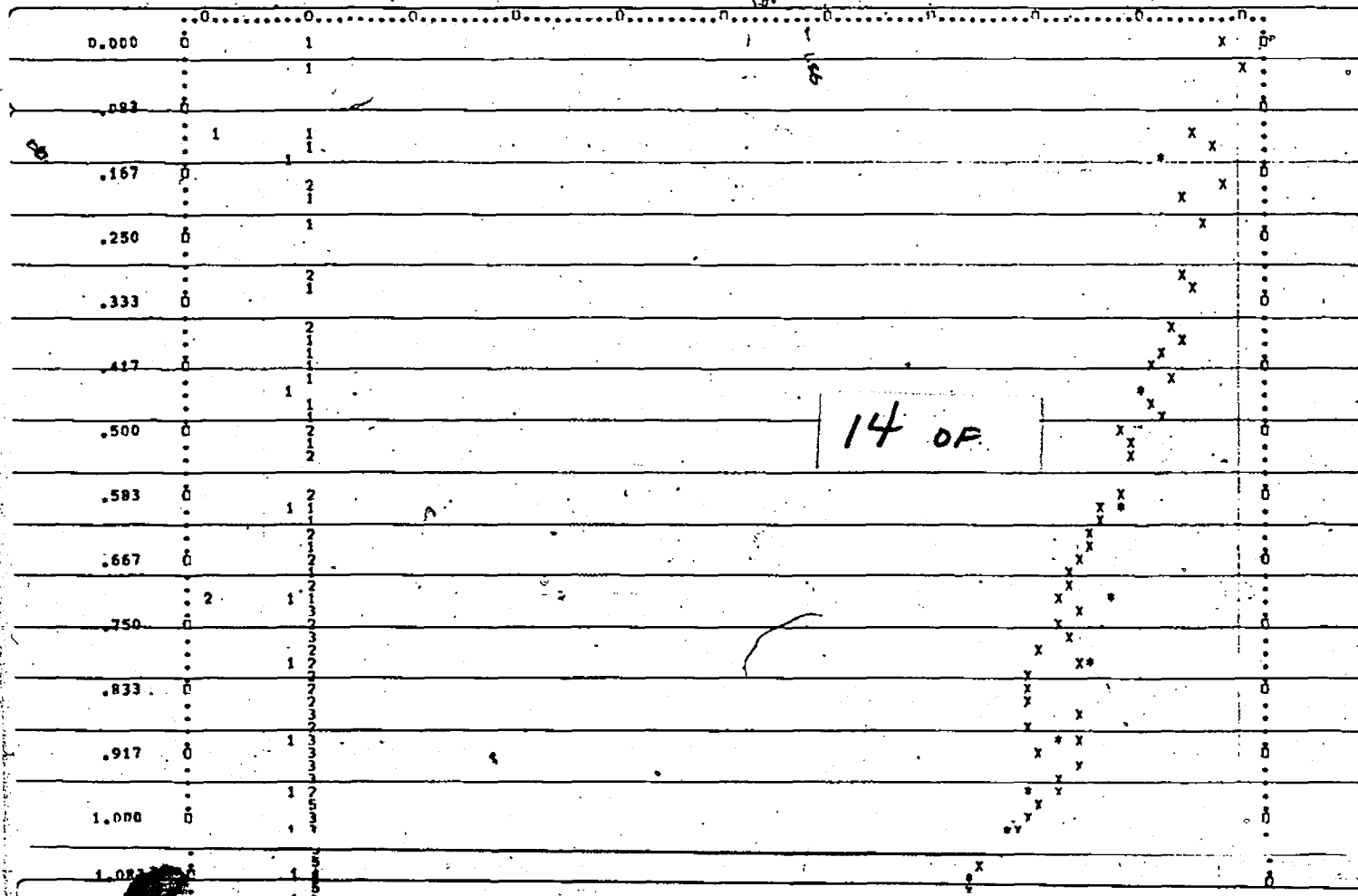
ROTATE FINDS -0.0 DEGREES BETWEEN COORDINATE SYSTEMS
ROTATE FINDS -0.0 DEGREES BETWEEN COORDINATE SYSTEMS

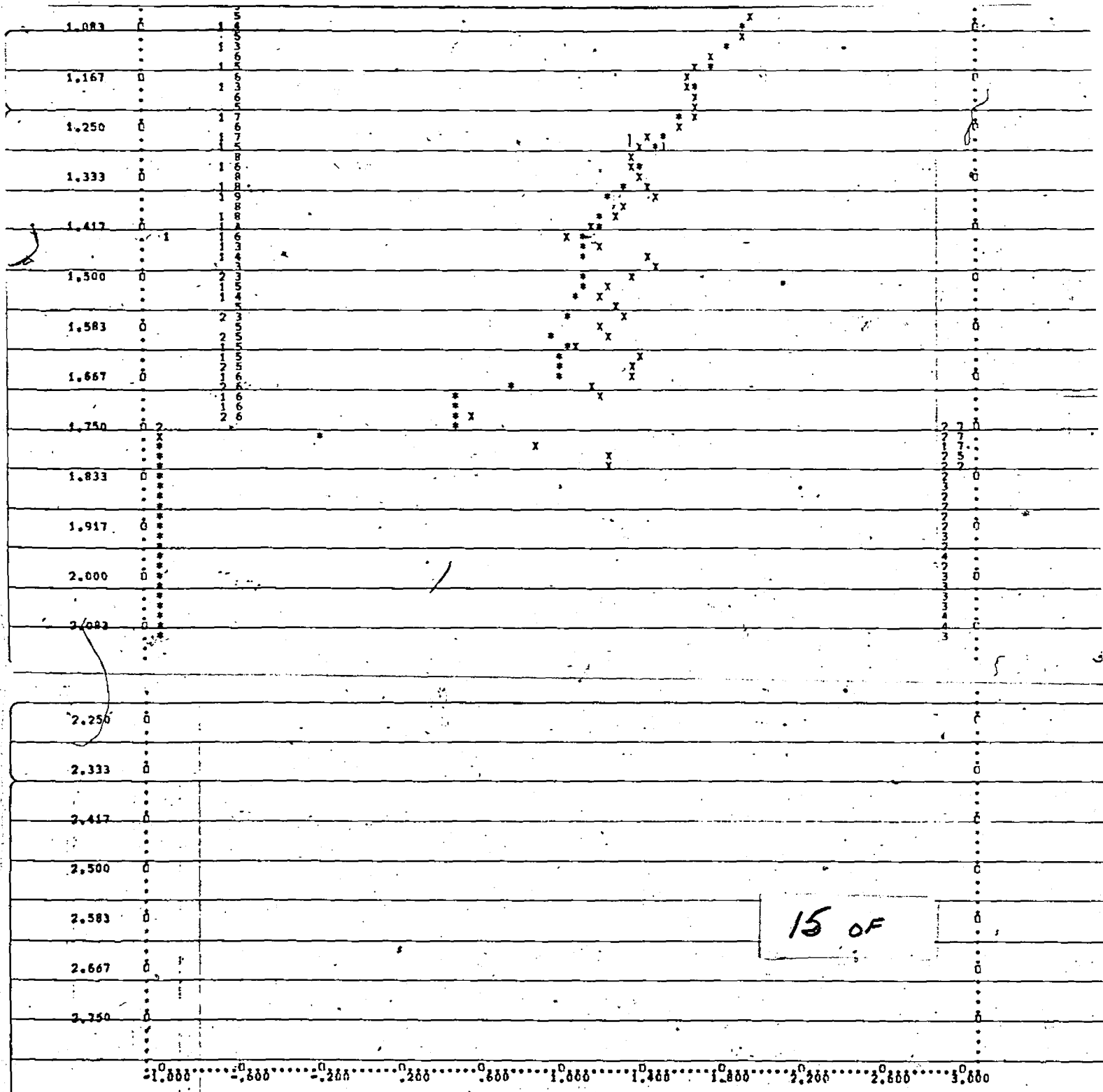
CURVE FITTING FOR AVERAGE NUMBER 4 USES INTERVAL .717 THROUGH 1.433 INCLUSIVE IN LOG

FOLLOWING POINTS ARE USED IN FORMING SECOND APPROXIMATION IN FITTING PROCESS

PASS	DELT	SOSUM	DELT	SOSUM	DELT	SOSUM
1	-.37820	16012	-.12820	66729	.07180	261445
2	-.42820	14654	-.22820	23370	-.07820	146087

FITTING PROCEDURE FOR AVERAGE NUMBER 4 GIVES -1282 - 2386 - 2986 - 2986 FOR FIRST APPROXIMATION
SECOND GUESSES 1 AND 2 AND FINAL APPROXIMATION RESPECTIVELY FOR INCREMENT IN LOG 1 NECESSARY TO MATCH
PRESENT TRACING WITH FIRST TRACING OF PREVIOUS AVERAGE





15 OF

1.000 1.600 2.200 2.800 3.400 4.000 4.600 5.200 5.800 6.400 7.000 7.600 8.200 8.800 9.400 10.000

SYMBOLS X REPRESENT AVERAGE OF NW SEMIAXES OF FOLLOWING PLATES.

ABELL1775	PS5720	V05	LEVER ARM = 199.30	PROJECTED SLIT = 35X 35 MU
ABELL1775	PS5748	V05	LEVER ARM = 199.30	PROJECTED SLIT = 35X 35 MU
ABELL1775	PS5724	V20	LEVER ARM = 104.07	PROJECTED SLIT = 70X 70 MU
ABELL1775	PS5719	V20	LEVER ARM = 164.07	PROJECTED SLIT = 62X 62 MU

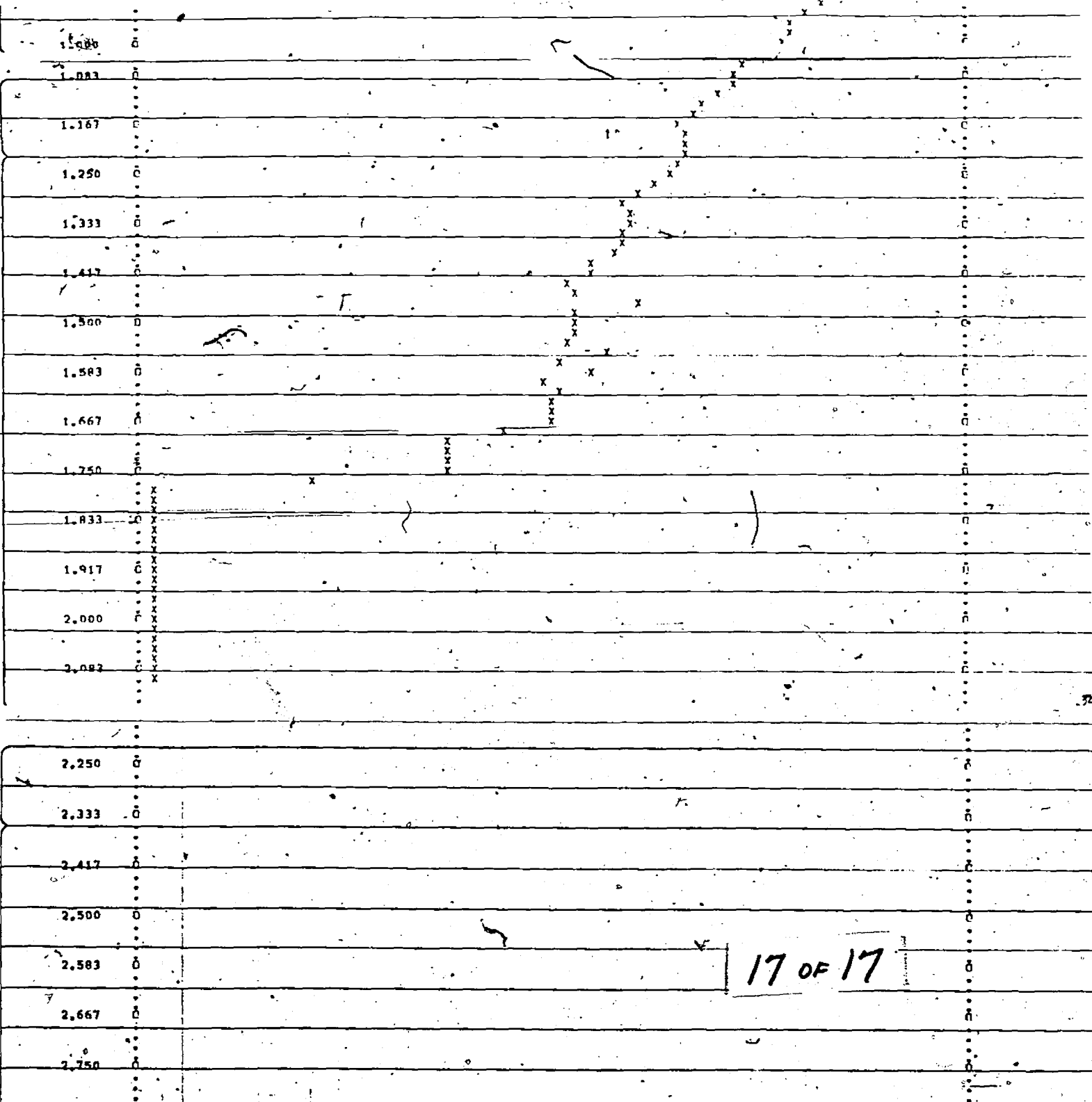
SYMBOLS 0 REPRESENT NW SEMIAXIS OF FOLLOWING PLATE TO BE AVERAGED IN

ABELL1775	PS6864	J7H	LEVER ARM = 51.86	PROJECTED SLIT = 140X140 MU
-----------	--------	-----	-------------------	-----------------------------

SYMBOLS 1 AND 2 DENOTE RESPECTIVELY BOUNDARY POINTS ASSIGNED TO AVERAGE OF PREVIOUS PLATES AND TO PRESENT PLATE

INTENSITIES OF CURRENT TRACING ASSIGNED FOLLOWING RELATIVE WEIGHTS FOR AVERAGING

0.000	0.000	0.000	0.000	0.000	0.000	0.000	0.000	0.000	0.000	1.000	0.000	0.000	0.000	0.000	0.000
0.000	0.000	0.000	0.000	0.000	0.000	0.000	0.000	0.000	0.000	0.000	0.000	0.000	0.000	0.000	0.000
0.000	0.000	0.000	0.000	0.000	0.000	0.000	0.000	0.000	0.000	0.000	0.000	0.000	0.000	0.000	0.000
0.000	2.828	0.000	0.000	0.000	2.449	0.000	0.000	2.828	0.000	2.191	0.000	2.828	0.000	0.000	1.852
0.000	1.852	2.191	0.000	2.000	0.000	1.737	1.633	0.000	1.737	1.549	2.000	2.828	0.000	2.828	0.000
4.000	2.191	2.449	0.000	4.000	0.000	3.098	2.191	2.191	3.098	2.000	2.828	2.000	2.000	2.000	2.828
2.619	2.619	1.852	3.098	4.899	1.000	1.000	1.000	1.000	1.000	1.000	1.000	1.000	1.000	1.000	1.000
1.000	1.000	1.000	1.000	1.000	1.000	1.000	1.000	1.000	1.000	1.000	1.000	1.000	1.000	1.000	1.000



17 OF 17

1.000 1.200 1.400 1.600 1.800 2.000 2.200 2.400 2.600 3.000

	SYMBOLS	X	REPRESENT AVERAGE OF NM SEMIAXES OF FOLLOWING PLATES	
ABELL1775	PS5720	V05	LEVER ARM = 199.30	PROJECTED SLIT = 35X 35 MU
ABELL1775	PS5748	V05	LEVER ARM = 199.30	PROJECTED SLIT = 35X 35 MU
ABELL1775	PS5724	V20	LEVER ARM = 104.07	PROJECTED SLIT = 70X 70 MU
ABELL1775	PS5719	V20	LEVER ARM = 104.07	PROJECTED SLIT = 62X 62 MU
ABELL1775	PS6864	J2H	LEVER ARM = 51.86	PROJECTED SLIT = 140X140 MU

APPENDIX 3: INTRODUCTION

The following appendix deals very briefly with the dynamical arguments used to construct the King models. Only the essential ideas are presented, along with some of the more important equations. The actual description of the construction of a King isothermal model is to be found in King's original paper of 1966.

APPENDIX 3: MATHEMATICAL BACKGROUND FOR STAR CLUSTERS

After a long enough time, an isolated cluster of stars will be in complete statistical equilibrium. Indeed, even the richest star clusters will be in statistical equilibrium in their centres.

Chandrasekhar (1960) and Freeman (1975) have shown that the mean freepath of a star in a cluster is many times the radius of the cluster. Therefore, spatial mixing is more important than relaxation through stellar encounters. Chandrasekhar (1960) has also shown that the structure of a star cluster is closely represented by a solution of the encounterless Liouville equation, with the stellar encounters producing a slow evolution from one solution to another.

The general solution to the steady-state encounterless Liouville equation was given by Jeans (1915). The distribution function in phase space must be expressible as a function of the isolating integrals of the equations of motion of a star. For the case of spherical symmetry in position space the only known isolating integrals for a general potential function $V(r)$ are the energy and angular momentum per unit mass,

$$E = 1/2v^2 + V(r) \quad (1)$$

and

$$h = rv_t \quad (2)$$

In the above, v is the magnitudes of the velocity and v_t , its tangential component. Even after specifying these integrals, Jeans' theorem permits a very large range of cluster models. One needs only to glance at real cluster and galaxies to see that there are strong

similarities between one object of a given class and others. The real clusters and galaxies are best described by a particular set of distribution functions. If one assumes that at the relaxation time at the centre of a galaxy is a small fraction of its age, it is natural for stellar encounters to provide the regularizing mechanism in galaxies. One approach to the problem is to ask that the stellar encounters determine a velocity distribution, which then in turn determines the spatial characteristics of the model. This approach has been used by a number of investigators (Chandrasekhar 1960; Spitzer and Härm 1958; King 1966), each of whom chose somewhat different velocity distributions.

The remainder of this discussion follows the work of King.

To start with, consider the ideal, but unattainable Gaussian velocity distribution. This distribution has been shown by Chandrasekhar (1960) to lead to a density distribution that corresponds to an isothermal gas sphere. The model has a total mass that is infinite; when r is large, the mass contained within that radius increases in direct proportion to r . In fact, the Gaussian distribution could have been rejected initially, as a cluster or galaxy cannot retain stars whose velocity exceeds a finite escape velocity. What is needed is a velocity distribution that will be produced by stellar encounters, yet drops to zero at a finite limiting velocity. The mechanism for solving this problem was provided by Chandrasekhar (1943), who introduced the Fokker-Planck equation into stellar dynamics to calculate the effect of encounters on a velocity distribution. The Fokker-Planck equation is a differential equation involving the probability function governing the occurrence of a velocity at a given time. The probability function must satisfy the diffusion equation:

$$\frac{\partial w}{\partial t} = qv^2 w \quad (3)$$

where q is the diffusion co-efficient and w is the probability function.

To describe the velocity distribution in a cluster, Chandrasekhar found a steady-state solution of the Fokker-Planck equation with a finite cut off velocity. He used this solution only to determine the rate of escape of stars, and not the velocity distribution explicitly.

Spitzer and Härm (1958) tabulated the steady-state velocity distribution and attempted to use this distribution to derive a cluster model but were unsuccessful. No matter what they chose for the central value of the potential, the density of their model went to zero at some finite value of the radius, contradicting their identification of the cut off velocity with the escape velocity of the cluster.

In the approach used by King (1966), the model is constructed by choosing a velocity distribution at the centre of the model of the form,

$$f(0, v) = k[\exp(-j^2 v^2) - \exp(j^2 v_e^2)] \quad (4)$$

where v_e is the escape velocity and j is given by

$$j^2 = 2/3 \langle v \rangle^2, \quad (5)$$

where $\langle v \rangle$ is the mean velocity of a Maxwell-Boltzmann distribution.

The energy integral for a star is

$$E = 1/2 v^2 + V(r) \quad (5)$$

If one lets $V(r)$ equal zero at the surface of the cluster, a star with zero energy then is barely able to reach the surface. The escape velocity is thus given at any point by

$$v_e^2 = -2V(r) \quad (6)$$

Above zero energy, $f(v)$ is taken to be zero since stars of positive energy have escaped from the cluster. Tidal distortion of the shape of the cluster has been neglected in the discussion. It affects only the outermost regions and is taken into account by applying perturbation theory at a later stage.

In terms of E , the distribution function at the centre of the cluster is

$$f(o,v) = k(\exp(-2j^2 \cdot v(o))[\exp(-2Ej^2)-1]). \quad (7)$$

But according to Jeans' theorem, the distribution function must be the same at all points; therefore at any point the distribution is of the form.

$$f(r,v) = k(\exp(-2j^2(v(r)-v(o)))[\exp[-j^2v^2]-\exp(-j^2v_e^2)]) \quad (8)$$

Equation (8) is of the same form as equation (4). That is, the velocity distribution at every point within the cluster is the appropriate steady-state solution to the Fokker-Planck equation for the velocity cut off that applies at that point. Stellar encounters are automatically taken into account everywhere in the cluster, not only at the centre.

The density at any point is found by integrating the velocity distribution $f(r,v)$ with respect to velocity. As a simplification, the following substitutions are made.

$$w = -2V(r)j^2 \quad (9)$$

and

$$\eta = j^2v^2 \quad (10)$$

However, in performing this substitution, one no longer has an equation for the density in terms of potential (and hence radius), but

as a function of the variables w and η . The $w(r)$ relation is solved by using Poisson's equation

$$\frac{\partial^2 w(r)}{\partial r^2} + \frac{2}{r} \frac{\partial w(r)}{\partial r} = 4\pi G \rho \quad (10)$$

In terms of a dimensionless radius R ($\equiv \frac{r}{r_{\text{core}}}$), equation (10) may be rewritten as

$$\frac{\partial^2 w}{\partial R^2} + \frac{2}{R} \frac{\partial w}{\partial R} = -8\pi G \rho_j^2 r_{\text{core}}^2 \quad (11)$$

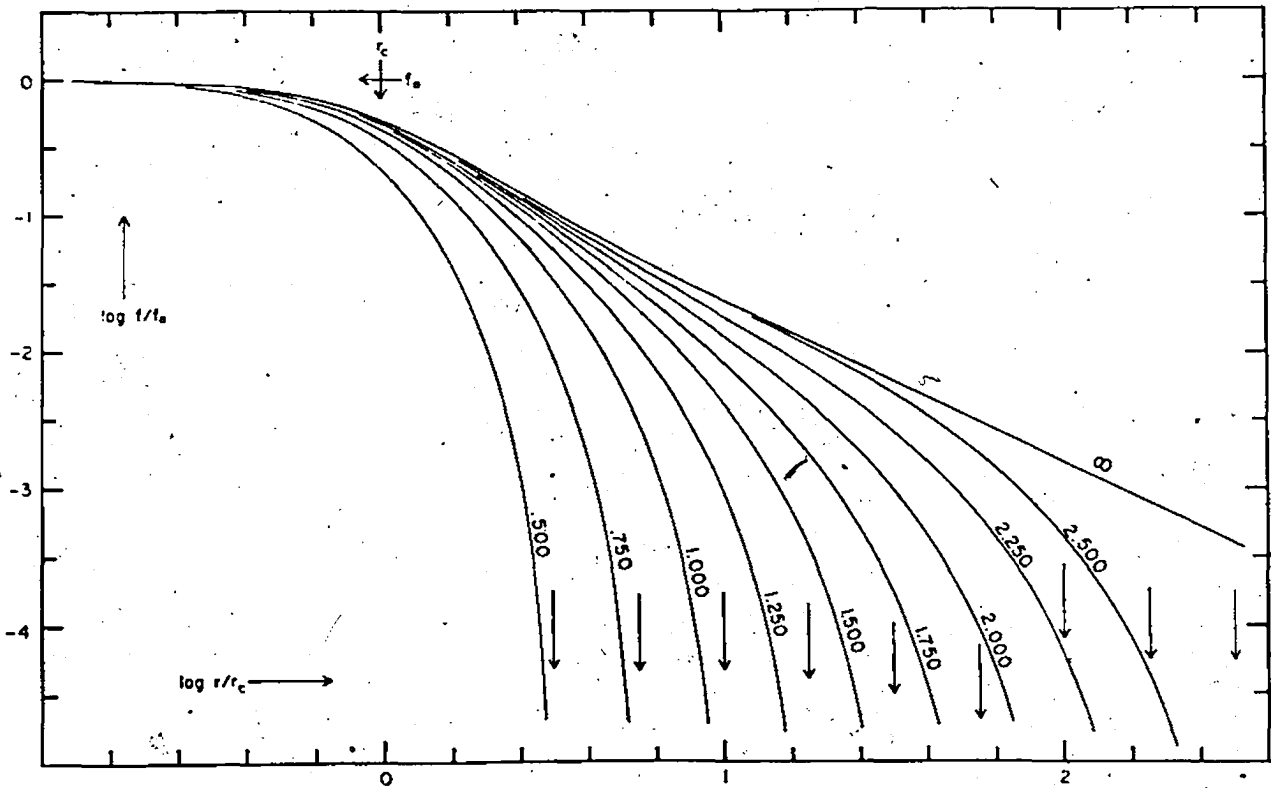
Upon substituting for a power series for the function of $w(R)$, one will obtain values of r which will be close to r_{core} if the central value of the equation (11) is set to -9 . Therefore, if one sets the constant term on the righthand side of (11) to -9 , one only needs the relative values of the density and not the density itself;

$$\text{i.e. } \frac{\partial^2 w}{\partial R^2} + \frac{2}{R} \frac{\partial w}{\partial R} = -9 \rho/\rho_0 \quad (12)$$

The calculations to obtain the relation between intensity and radius are performed from equation (12) on the basis that the density is related to the distribution of light within the cluster. These calculations are found in King (1966). The interested reader may consult that paper for further details.

The resulting models are modifications of an isothermal gas sphere. Near the centre their densities are very close to isothermal, but projected it falls below the isothermal curve and drops to zero. The projected densities are shown in Figure A-1 (taken from Figure 1 of King 1966), where the surface density is called f . The quantities f and r are unitless ratios of the central values f_0 and r_{core} , respectively. The curves are labelled with the values of the parameter c .

Figure A-1. The family of King's isothermal spheres, plotted in terms of brightness relative to the central brightness and radius in terms of the 'core radius' logarithmically.



APPENDIX 4: PROGRAMME REDUCE

The programme REDUCE uses as input a data file containing the points defining a standard King model ($c = 2.25$), and points defining the average intensity-radius profile produced by PROFIL. It then scales the King model in both radius and intensity and compares the observed data points to the fitting King model. The best fitting King model is printed out, a listing of the programme is given below, as is a list of the input data cards.

Input Data Cards (In Order)

<u>NAME</u>	<u>FORMAT</u>	<u># CARDS</u>	<u>COMMENTS</u>
NPKR, NPKB, NPOR, NPOB	4(2X,I3)	1	-number of points in the standard King model and the observed profiles
KINGR	10F8.3	<20	-the radial values of the King model
KINGB	10F8.3	<20	-the intensity values of the King model
OBSR	10F8.3	<20	-the radial value of the data points
OBSB	10F8.3	<20	-the intensity values of the data points
RCORE	F5.2	1	-the value of the core radius of the King model.
BVALU, NSTEPS, AXIS, VALUE, PLATE	F10.3, 3X, I3, 3X, A5, 3X, F5.0, 3X, A6		-the min. value of intensity to start scaling process; the number of steps for the scaling. The semi-axis being fitted. The maximum value of intensity and the name of the galaxy.

cid:reduce
/list

THIS PROGRAMME IS MADE WITH THE REDUCTION OF
DATA AS PRODUCED BY THE PROGRAMME 'PROFILE' OF
G. WELCH. THIS PROGRAMME TAKES THE OUTPUTTED
DATA FROM 'PROFILE' (FORMAT: LOG10(RADIUS FROM CENTRE)
LOG10(INTENSITY, IN ARBITRARY UNITS)) & DOES THE FOLLOWING:
1) CONVERTS THE LOG VALUES TO CARTESIAN CO-ORDS.
2) NORMALISES THE RADIAL VALUE TO THE OBSERVED RADIAL
SIZE OF EACH SPECIFIC CENTRE OF LIGHT.
3) PERFORMS A DO LOOP WHERE A BEST FIT IS ACHIEVED
FOR THE INTENSITY OF THE SYSTEM.
4) A CUBIC SPLINE IS USED TO FIT THE OBSERVED DATA
TO A STANDARD KING MODEL WITH (RTIAL/RCORE)=2.25.
5) PERFORMING STEP (3) WITHIN THE DO LOOP WILL GIVE
DIFFERENCE BETWEEN KING'S VALUES & THE OBSERVED
VALUES AS DETERMINED BY 'PROFILE'. - THE
DIFFERENCE GIVING, EVENTUALLY A LEAST-SQUARES
- THE LOWEST VALUE OF THE LEAST-SQUARES FIT BEING CONSIDERED
THE BEST FIT.

PROGRAM REDUCE(DATA1,OUTPUT,TAPES=DATA1,TAPE6=OUTPUT)
DIMENSION KRAD(155),KBRT(155),ADUMP(155),CBUMP(100),RATIO(50)
1, RADIUS(100),BRTNSS(100),RADKS(153),CHI(50)
2, BNORM(50,155)
DIMENSION CNORM(155),YVALUS(75),RKLOG(155),BKLOG(155)
DIMENSION KINGR(155),KINGB(155),OBSR(100),OBSB(100)
COMMON LAST1, LAST2, LAST3, LAS4
REAL LRADK, LBRTK, KRAD, KBRT, LOGR, LOGI, MAXRAD, MAXBRT
COMMON YVALUS(75)
REAL KINGR, KINGB, OBSR, OBSB
READ(5,11) NPKR, NPKB, NPOR, NPOB
11 FORMAT(4(2X,I3))

THE NEXT PART OF THE PROGRAMME WILL READ IN THE DATA
AND TAKE THE ANTI-LOGS OF BOTH THE
RADIi AND INTENSITIES FOR BOTH THE KING MODEL AND THE
OBSERVED DATA

----- KING MODEL -----
N=1
DO 3000 J=1,20
NN=N+9
1007 READ(5,1007) (KINGR(I),I=N,NN)
FORMAT(10F8.3)
IF (KINGR(NN).EQ.0) GO TO 3001
N=N+10
3000 CONTINUE
3001 CONTINUE
DO 770 I=1,NPKR
IF(KINGR(I).NE.0) GO TO 770
LAST1=I-1
GO TO 780
770 CONTINUE
780 DO 750 I=1, LAST1
ADUMP(I)=KINGR(I)
750 CONTINUE
1032 WRITE(6,1032)
FORMAT(//////,20X,"THE RADIAL VALUES OF THE KING MODEL ARE:")
WRITE(6,1033) (ADUMP(J),J=1, LAST1)
1033 FORMAT(/,2X,10F8.3)
CALL RADUS(KINGR,KRAD, LAST1)
C ----- NOW FOR THE KING MODEL INTENSITY -----
K=1
DO 2000 J=1,20
KK=K+9
1107 READ(5,1107) (KINGB(I),I=K, KK)
FORMAT(10F8.3)
IF(KINGB(KK).EQ.0) GO TO 2001
K=K+10
2000 CONTINUE
2001 CONTINUE
DO 730 I=1,NPKB
IF(KINGB(I).NE.0) GO TO 730
LAST2=I-1
GO TO 740
730 CONTINUE
740 DO 720 I=1, LAST2
ADUMP(I)=KINGB(I)
720 CONTINUE
1634 WRITE(6,1634)
FORMAT(//////,20X,"THE VALUES OF INTENSITY FOR THE"
1,1X,"KING MODEL ARE:")
WRITE(6,1635) (ADUMP(J),J=1, LAST2)
1635 FORMAT(/,2X,10F8.3)
CALL BRGTNS(KINGB,KBRT, LAST2)
C ----- SAME AS ABOVE BUT NOW FOR OBSERVED DATA -----
M=1
DO 5000 J=1,15
MM=M+9
1207 READ(5,1207) (OBSR(I),I=M, MM)
FORMAT(10F8.3)
IF (OBSR(MM).EQ.0) GO TO 5001
M=M+10
5000 CONTINUE
5001 CONTINUE
DO 870 I=1,NPOR

```

1207 READ(5,1207) (OBSR(I),I=M,MH)
      FORMAT(10F8.3)
      IF (OBSR(MH).EQ.0) GO TO 5001
      M=M+10
5000 CONTINUE
5001 CONTINUE
      DO 870 I=1,NPOR
      IF (OBSR(I).NE.0) GO TO 870
      LAST3=I-1
      GO TO 890
870 CONTINUE
890 DO 850 I=1, LAST3
      CDUMP(I)=OBSR(I)
850 CONTINUE
      WRITE(6,1034)
1034 FORMAT(////,20X,'THE RADIAL VALUES OF THE OBSERVED DATA ARE:')
      WRITE(6,1035) (CDUMP(J),J=1, LAST3)
1035 FORMAT(/,2X,10F8.3)
      CALL RADIUS(OBSR,RADIUS, LAST3)
      CALL MAX(RADIUS,RMAX, LAST3)
C
      L=1
      DO 6000 J=1,15
      LL=L+9
      READ(5,1307) (OBSB(I),I=L,LL)
1307 FORMAT(10F8.3)
      IF (OBSB(LL).EQ.0) GO TO 6001
      L=L+10
6000 CONTINUE
6001 CONTINUE
      DO 960 I=1,NPOR
      IF (OBSB(I).NE.0) GO TO 960
      LAST4=I-1
      GO TO 970
960 CONTINUE
970 DO 950 I=1, LAST4
      CDUMP(I)=OBSB(I)
980 CONTINUE
      WRITE(6,1332)
1332 FORMAT(////,20X,'THE INTENSITY VALUES OF THE'
1 1X,'OBSERVED DATA ARE:')
      WRITE(6,1333) (CDUMP(J),J=1, LAST4)
1333 FORMAT(/,2X,10F8.3)
      CALL BRGTNS(OBSB,BRTNSS, LAST4)
C
C NOW TO NORMALIZE THE KING MODEL AS TO RADIUS AND INTENSITY.
C THE CORE RADIUS IN THE KING MODEL IS SET TO RCORE
C IN ARC-SECS. THIS IS THEN USED TO SCALE THE KING MODEL TO THE
C THE OBSERVATIONS.
      READ(5,22) RCORE
22 FORMAT(F5.2)
      DO 10 II=1, LAST1
      RADKS(II)=KRAD(II)*RCORE
      IF (RADKS(II).LE.RMAX) GO TO 10
      IEND=II
      GO TO 12
10 CONTINUE
12 CONTINUE
C
C NEXT TO NORMALIZE FOR THE INTENSITY-ONE WANTS TO HAVE A READ-IN
C VALUE SET EQUAL TO THE MAXIMUM INTENSITY, BUT ONE WISHES TO STEP
C THROUGH A NUMBER OF INTENSITIES, TO GET A BEST FIT.
      READ(5,101) BVALU, NSTEPS, AXIS, VALUE, PLATE
101 FORMAT(F10.3,3X,13,3X,AS,3X,F5.0,3X,A6)
      BOLD=BVALU
      STEPS=FLOAT(NSTEPS)
      DELTA=(VALUE-BVALU)/STEPS
      DELHLD=DELTA
      DO 50 KK=1,NSTEPS
      CALL MAX(KBRT,MAXBRT,IEND)
      DO 15 II=1,IEND
      BNORM(KK,II)=(BVALU/MAXBRT)*KBRT(II)
      CNORM(II)=BNORM(KK,II)
15 CONTINUE
      CALL INTPRL(6,IEND,RADKS,CNORM, LAST3,RADIUS,YVALUS)
      CALL CHISD(YVALUS,BRTNSS, LAST3,CHIONE)
      CHI(KK)=CHIONE
      RATIO(KK)=CHI(KK)/BVALU
      BVALU=BVALU+DELTA
50 CONTINUE
      KMIN=1
      XMIN=RATIO(1)
      DO 51 KK=1,NSTEPS
      IF (XMIN.LE.RATIO(KK)) GO TO 51
      XMIN=RATIO(KK)
      KMIN=KK
51 CONTINUE
      DO 8 I=1,IEND
      RKLOG(I)=ALOG10(RADKS(I))
      BKLOG(I)=ALOG10(BNORM(KMIN,I))
8 CONTINUE
C
C NOW TO WRITE EVERYTHING OUT.
      WRITE(6,80)
      WRITE(6,81)
      WRITE(6,82) (RADKS(II),BNORM(KMIN,II),RKLOG(II),
1 BKLOG(II),II=1,IEND)
      WRITE(6,83) AXIS, PLATE
      WRITE(6,84)
      WRITE(6,88) (RADIUS(J),BRTNSS(J),OBSR(J),OBSB(J),J=1, LAST3)
80 FORMAT(///,25X,'THE VALUES FOR THE NORMALIZED KING MODEL ARE:')
81 FORMAT(/,15X,'RADIUS(ARC-SEC.)',10X,' INTENSITY',10X,
1 10X,'LOG(RADIUS)',10X,'LOG(INTENSITY)')
82 FORMAT(/,16X,F10.4,14X,F10.4,18X,F10.6,12X,F10.6)
83 FORMAT(///,25X,'THE VALUES OF THE TRACING DATA',1X,AS,
1 1X,'AXIS OF THE CLUSTER',A6,' ARE:')
84 FORMAT(/,15X,' RADIUS(ARC-SEC.)',10X,' INTENSITY ',
1 10X,'LOG(RADIUS)',10X,'LOG(INTENSITY)')
88 FORMAT(/,16X,F10.4,14X,F10.4,10X,F10.6,12X,F10.6)
      WRITE(7,85) BYTE

```

29

```

WRITE(6,83) AXIS, PLATE
WRITE(6,84)
- WRITE(6,88) (RADIUS(J),BRTNSS(J),QBSR(J),QBSB(J),J=1,LAST3)
80 FORMAT(///,25X,"THE VALUES FOR THE NORMALIZED KINS MODEL ARE:")
81 FORMAT(//,15X,"RADIUS(ARC-SEC.)",10X," INTENSITY",10X,
1 10X,"LOG(RADIUS)",10X,"LOG(INTENSITY)")
82 FORMAT(Y,16X,F10.4,14X,F10.4,18X,F10.4,12X,F10.6)
83 FORMAT(///,25X,"THE VALUES OF THE TRACING OF",1X,45,
1 1X,"AXIS, OF THE CLUSTER",16," ARE: ")
84 FORMAT(//,15X," RADIUS(ARC-SEC.)",8X," INTENSITY ",
1 10X,"LOG(RADIUS)",10X,"LOG(INTENSITY)")
89 FORMAT(//,16X,F10.4,14X,F10.4,10X,F10.6,12X,F10.6)
WRITE(6,85) AXIS
WRITE(6,99) RCORE
99 FORMAT(//,25X," WITH A CORE RADIUS OF",F5.2," ARC-SECS.")
85 FORMAT(///,10X,"THE VALUE OF THE NUCLEUS BRIGHTNESS AND THE",
2 1X," STD. DEV. PARAMETER ARE",//,33X," FOR THE",1X,40,1X,"AXIS")
WRITE(6,86)
86 FORMAT(//,11X,"NUCLEUS INTENSITY",27X,"STANDARD DEVIATION",
2 1X," RATIO OF DEV./I(CENTRE)",//,12X,"(NORM=1000.0)")
DO 1111 KK=1,NSTEPS
WRITE(6,87) BHOLD, CHI(KK),RATIO(KK)
87 FORMAT(//,15X,F10.5,26X,1PE18.4,18X,1PE12.5)
BHOLD=BHOLD + DELNLD
1111 CONTINUE
STOP
END

```

```

C
C THESE ARE THE SUBROUTINES WHICH FOLLOW.
C

```

```

SUBROUTINE RADUS(LRAD,RAD,NP)
C THIS ROUTINE FINDS THE ANTI-LOG OF THE RADII.
REAL LRAD
DIMENSION LRAD(NP), RAD(NP)
DO 15 IJ=1,NP
RAD(IJ)= 10.**(LRAD(IJ))
15 CONTINUE
RETURN
END

```

```

C
C
SUBROUTINE BRGTNS(LBRT,BRT,NP)
C THIS ROUTINE TAKES THE ANTI-LOG OF LBRT
REAL LBRT
DIMENSION LBRT(NP), BRT(NP)
DO 20 JJ=1,NP
BRT(JJ)= 10.**(LBRT(JJ))
20 CONTINUE
RETURN
END

```

```

C
C
SUBROUTINE MAX(X,XMAX,NP)
C THIS ROUTINE FINDS THE MAXIMUM VALUE OF THE DATA SET INVOLVED AND
C CAUSES THAT MAXIMUM TO BE SET BACK TO THE MAIN PROGRAMME.
DIMENSION X(NP)
XMAX=0.0
DO 111 KI=1,NP
IF(XMAX.LT.X(KI)) GO TO 110
GO TO 111
110 XMAX=X(KI)
111 CONTINUE
RETURN
END

```

```

C
C
C
SUBROUTINE CHISQ(INTPOL,BRTNSS,NTP,STDDEV)
C THIS ROUTINE FINDS THE CHI-SQUARE PARAMETER FOR THE SPLINE FITTING.
REAL INTPOL
DIMENSION INTPOL(NTP), BRTNSS(NTP)
CHI=0.0
DO 8 NN=1,NTP
CHI=CHI+((BRTNSS(NN)-INTPOL(NN))**2)
8 CONTINUE
VAR=CHI/(NN-1)
STDDEV=SQRT(VAR)
RETURN
END

```

```

C
C
SUBROUTINE INTPL(IU,L,X,Y,N,U,V)
DIMENSION X(L),Y(L),U(N),V(N)
C THIS ROUTINE INTERPOLATES Y-VALUES AT A GIVEN X POSITION
C WHICH IS READ IN AS U(N). THE INTERPOLATION IS CARRIED OUT
C BY A SPLINE ON THE READ IN VALUES X(L) & Y(L).
C THE OUTPUT COMES OUT AS V(N), THE ACTUAL INTERPOLATED VALUE.
EQUIVALENCE (PO,X3),(OO,Y3),(Q1,T3)
REAL M1,M2,M3,M4,M5
EQUIVALENCE (UK,DX),(IMN,X2,A1,M1),(IMX,X5,A5,M5),
1 (J,SW,SA),(Y2,W2,W4,O2),(Y5,W3,Q3)
C SETTING UP.
10 LO=L
LM1=LO-1
LM2=LM1-1
LP1=LO+1
NO=N
IF(LM2.LT.0) GO TO 90
IF(NO.LE.0) GO TO 91
DO 11 I=2,LO
IF(X(I-1)-X(I)) 11,95,96
11 CONTINUE
IPV=0
C MAIN DO LOOP.
DO 80 K=1,NO
C TO LOCATE THE DESIRED POINT.
UK=U(K)
20 IF(LM2.EQ.0) GO TO 27
IF(UK.GE.X(LD)) GO TO 26

```

```

C BY A SPLINE ON THE READ IN VALUES X(L) & Y(L).
C THE OUTPUT COMES OUT AS V(N), THE ACTUAL INTERPOLATED VALUE.
EQUIVALENCE (P0,X3),(Q0,Y3),(Q1,T3)
REAL M1,M2,M3,M4,M5
EQUIVALENCE (UK,DX),(IMN,X2,A1,M1),(IMX,X5,A5,M5),
1 (J,SW,SA),(Y2,W2,W4,Q2),(Y5,W3,Q3)
C SETTING UP.
10 LO=L
LM1=LO-1
LM2=LM1-1
LP1=LO+1
ND=N
IF(LM2.LT.0) GO TO 90
IF(ND.LE.0) GO TO 91
DO 11 I=2,LO
IF(X(I-1)-X(I)) 11,95,96
11 CONTINUE
IPV=0
C MAIN DO LOOP.
DO 80 K=1,ND
C TO LOCATE THE DESIRED POINT.
UK=U(K)
20 IF(LM2.EQ.0) GO TO 27
IF(UK.GE.X(LB)) GO TO 26
IF(UK.LT.X(1)) GO TO 25
IMN=2
IMX=LO
21 I=(IMN+IMX)/2
IF(UK.GE.X(I)) GO TO 23
22 IMX=I
GO TO 24
23 IMN=I+1
24 IF(IMX.GT.IMN) GO TO 21
I=IMX
GO TO 30
25 I=1
GO TO 30
26 I=LP1
GO TO 30
27 I=2
C CHECK TO SEE IF I=IPV.
30 IF(I.EQ.IPV) GO TO 70
IPV=I
C ROUTINE TO PICK UP NECESSARY X AND Y VALUES AND
C TO ESTIMATE THEM IF NECESSARY.
40 J=I
IF(J.EQ.1) J=2
IF(J.EQ.LP1) J=LO
X3=X(J-1)
Y3=Y(J-1)
X4=X(J)
Y4=Y(J)
A3=X4-X3
M3=(Y4-Y3)/A3
IF(LM2.EQ.0) GO TO 43
IF(J.EQ.2) GO TO 41
X2=X(J-2)
Y2=Y(J-2)
A2=X3-X2
M2=(Y3-Y2)/A2
IF(J.EQ.LD) GO TO 42
41 X5=X(J+1)
Y5=Y(J+1)
A4=X5-X4
M4=(Y5-Y4)/A4
IF(J.EQ.27) M2=M3+M4-M4
GO TO 45
42 M4=M3+M3-M2
GO TO 45
43 M2=M3
M4=M3
45 IF(J.LE.3) GO TO 46
A1=X2-X(J-3)
M1=(Y2-Y(J-3))/A1
GO TO 47
46 M1=M2+M2-M3
47 IF(J.GE.LM1) GO TO 48
A5=X(J+2)-X5
M5=(Y(J+2)-Y5)/A5
GO TO 50
48 M5=M4+M4-M3
C NUMERICAL DIFFERENTIATION.
50 IF(I.EQ.LP1) GO TO 52
W2=ABS(M4-M3)
W3=ABS(M2-M1)
SW=W2+W3
IF(SW.NE.0.0) GO TO 51
W2=0.5
W3=0.5
SW=1.0
51 T3=(W2*M2+W3*M3)/SW
IF(I.EQ.1) GO TO 54
52 W3=ABS(M5-M4)
W4=ABS(M3-M2)
SW=W3+W4
IF(SW.NE.0.0) GO TO 53
W3=0.5
W4=0.5
SW=1.0
53 T4=(W3*M3+W4*M4)/SW
IF(I.NE.LP1) GO TO 60
T3=T4
SA=A2+A3
T4=0.5*(M4+M5-A2*(A2-A3)*(M2-M3)/(SA*SA))
X3=X4
Y3=Y4
A3=A2
M3=M4
GO TO 60

```

```

GO TO 30
26 I=LP1
GO TO 30
27 I=2
C CHECK TO SEE IF I=IPV.
30 IF(I.EQ.IPV) GO TO 70
IPV=I
C ROUTINE TO PICK UP NECESSARY X AND Y VALUES AND
C TO ESTIMATE THEM IF NECESSARY.
40 J=1
IF(J.EQ.1) J=2
IF(J.EQ.LP1) J=LB
X3=X(J-1)
Y3=Y(J-1)
X4=X(J)
Y4=Y(J)
A3=X4-X3
M3=(Y4-Y3)/A3
IF(LM2.EQ.0) GO TO 43
IF(J.EQ.2) GO TO 41
X2=X(J-2)
Y2=Y(J-2)
A2=X3-X2
M2=(Y3-Y2)/A2
IF(J.EQ.LD) GO TO 42
41 X5=X(J+1)
Y5=Y(J+1)
A4=X5-X4
M4=(Y5-Y4)/A4
IF(J.EQ.2) A2=A3+M3-M4
GO TO 45
42 M4=M3+M3-M2
GO TO 45
43 M2=M3
M4=M3
45 IF(J.LE.3) GO TO 46
A1=X2-X(J-3)
M1=(Y2-Y(J-3))/A1
GO TO 47
46 M1=M2+M2-M3
47 IF(J.GE.LM1) GO TO 48
A5=X(J+2)-X5
M5=(Y(J+2)-Y5)/A5
GO TO 50
48 M5=M4+M4-M3
C NUMERICAL DIFFERENTIATION.
50 IF(I.EQ.LP1) GO TO 52
W2=ABS(M4-M3)
W3=ABS(M2-M1)
SW=W2+W3
IF(SW.NE.0.0) GO TO 51
W2=0.5
W3=0.5
SW=1.0
51 T3=(W2*M2+W3*M3)/SW
IF(I.EQ.1) GO TO 54
52 W3=ABS(M5-M4)
W4=ABS(M3-M2)
SW=W3+W4
IF(SW.NE.0.0) GO TO 53
W3=0.5
W4=0.5
SW=1.0
53 T4=(W3*M3+W4*M4)/SW
IF(I.NE.LP1) GO TO 60
T3=T4
SA=A2+A3
T4=0.5*(M4+M5-A2*(A2-A3)*(M2-M3)/(SA*SA))
X3=X4
Y3=Y4
A3=A2
M3=M4
GO TO 60
54 T4=T3
SA=A3+A4
T3=0.5*(M1+M2-A4*(A3-A4)*(M3-M4)/(SA*SA))
X3=X3-A4
Y3=Y3-M2*A4
A3=A4
M3=M2
C DETERMINATION OF THE CO-EFFICIENTS.
60 Q2=(2.0*(M3-T3)+M3-T4)/A3
C COMPUTATION OF THE POLYNOMIAL.
70 DX=UK-PO
80 V(K)=00+DX*(D1+DX*(D2+DX*Q3)).
RETURN
C IF ERROR, EXIT.
90 WRITE(IU,2090)
GO TO 99
91 WRITE(IU,2091)
GO TO 99
95 WRITE(IU,2095)
GO TO 97
96 WRITE(IU,2096)
97 WRITE(IU,2097) I,X(I)
99 WRITE(IU,2099) LD,NO
RETURN
C FORMATS.
2090 FORMAT(1X, /22H *** L = 1 OR LESS. /)
2091 FORMAT(1X, " *** N=0 OR LESS. ")
2095 FORMAT(1X, " *** IDENTICAL X VALUES. ")
2096 FORMAT(1X, " *** X VALUES OUT OF SEQUENCE.")
2097 FORMAT(" I= '17,10X,' X(I)= ',E12.3)
2099 FORMAT(1X, " L='17,10X,' N= '17,///
1 "ERROR DETECTED IN SUBROUTINE INTPRL")
END

```

5 OF 5

/IDLE

APPENDIX 5: PROGRAMME MODEL

After all 4 semi-axes of each nucleus have been fitted using the programme REDUCE (Appendix 3), one obtains average values for the core radius and the central intensity. The programme MODEL is designed to scale a King model from the average core radii and central intensities. These model nuclei are then used to construct the model system major ones and isoplates.

A listing of the programme and the input data cards is given below.

Input Data Cards (In Order)

<u>NAME</u>	<u>FORMAT</u>	<u># CARDS</u>	<u>COMMENTS</u>
NPKR, NPKB	2(2X,I3)	1	-The number of pts (radial and intensity) of the standard King model.
KINGR	10F8.3	<20	-The radial values of the King model
KINGB	10F8.3	<20	-The intensity values of the King model
RMAX	F6.2	1	-The maximum extent of the model desired
RCORE	F5.2	1	-average value of the core radius
BVALU	F6.0	1	-average value of the central intensity

```

old,model
/list
C THIS PROGRAMME IS MADE FOR THE REDUCTION OF
C DATA AS PRODUCED BY THE PROGRAMME 'REDUCE' AS
C WRITTEN BY J. HAYES. THIS PROGRAMME TAKES THE
C DATA POINTS OF THE KING MODEL AND NORMALIZES THEM TO
C THE OBSERVED CORE RADIUS AND CENTRAL INTENSITY.
C THE OUTPUT FORMAT OF THIS PROGRAMME IS THE SAME AS THAT
C OF THE PROGRAMME 'REDUCE'.
PROGRAM MODEL(INPUT,OUTPUT,TAPE5=INPUT,TAPE6=OUTPUT)
DIMENSION KRAD(155),KBRT(155),ADUMP(155),CDUMP(100)
1 RADKS(155),BNORM(155)
DIMENSION KINGR(155),KINGB(155),RKLOG(155),BKLOG(155)
COMMON LAST1, LAST2
REAL KRAD,KBRT,MAXBRT
REAL KINGR, KINGB
READ(5,11) NPKR, NPKB
11 FORMAT(2(2X,I3))

C
C THE NEXT PART OF THE PROGRAMME WILL READ IN THE DATA
C AND TAKE THE ANTI-LOGS OF BOTH THE
C RADII AND INTENSITIES FOR THE KING MODEL.
C
C ----- KING MODEL RADIAL VALUES -----
N=1
DO 3000 J=1,20
NN=N+9
1007 READ(5,1007) (KINGR(I),I=N,NN)
      FORMAT(10F8.3)
      IF (KINGR(NN).EQ.0) GO TO 3001
N=N+10
3000 CONTINUE
3001 CONTINUE
      DO 770 I=1,NPKR
      IF(KINGR(I).NE.0) GO TO 770
      LAST1=I-1
      GO TO 780
770 CONTINUE
780 DO 750 I=1, LAST1
      ADUMP(I)=KINGR(I)
750 CONTINUE
      WRITE(6,1032)
1032 FORMAT(//////,20X,'THE RADIAL VALUES OF THE KING MODEL ARE:')
1033 WRITE(6,1033) (ADUMP(J),J=1, LAST1)
      FORMAT(/,2X,10F8.3)
      CALL RADUS(KINGR,KRAD, LAST1)
C ----- THE KING MODEL INTENSITY -----
K=1
DO 2000 J=1,20
KK=K+9
1107 READ(5,1107) (KINGB(I),I=K,KK)
      FORMAT(10F8.3)
      IF(KINGB(KK).EQ.0) GO TO 2001
K=K+10
2000 CONTINUE
2001 CONTINUE
      DO 730 I=1,NPKB
      IF(KINGB(I).NE.0) GO TO 730
      LAST2=I-1
      GO TO 740
730 CONTINUE
740 DO 720 I=1, LAST2
      ADUMP(I)=KINGB(I)
720 CONTINUE
      WRITE(6,1634)
1634 FORMAT(//////,20X,'THE VALUES OF INTENSITY FOR THE'
1 ,1X,'KING MODEL ARE:')
      WRITE(6,1635) (ADUMP(J),J=1, LAST2)
1635 FORMAT(/,2X,10F8.3)
      CALL BRTNS(KINGB,KBRT, LAST2)
C
C NOW TO NORMALIZE THE KING MODEL AS TO RADIUS AND INTENSITY.
C THE CORE RADIUS IN THE KING MODEL IS SET TO RCORE
C IN ARC-SECONDS. THIS IS THEN USED TO SCALE THE KING MODEL.
23 READ(5,23) RMAX
   23 FORMAT(F6.2)
   22 READ(5,22) RCORE
   22 FORMAT(F5.2)
      DO 10 II=1, LAST1
      RADKS(II)=KRAD(II)*RCORE
      IF(RADKS(II).LE.RMAX) GO TO 10
      IEND=II
      GO TO 12
10 CONTINUE
12 CONTINUE
C
C NEXT TO NORMALIZE FOR THE INTENSITY. WE WISH TO SET THE CENTRAL
C INTENSITY VALUE OF THE KING MODEL TO A RELATIVE INTENSITY WHICH
C IS THE BEST AVERAGE OF THE FITTING PROCESS PERFORMED BY THE
C PROGRAMME 'REDUCE'. (IE, THE AVERAGE BEST FIT OF A KING MODEL AND THE
C OBSERVED TRACING).
101 READ(5,101) BVALU
   101 FORMAT(F6.0)
      CALL MAX(KBRT,MAXBRT,IEND)
      DO 15 II=1,IEND
      BNORM(II)=(BVALU/MAXBRT)*KBRT(II)
15 CONTINUE
      DO 8 I=1,IEND
      RKLOG(II)=ALOG10(RADKS(II))
      BKLOG(II)=ALOG10(BNORM(II))
8 CONTINUE
C
C NOW TO WRITE EVERYTHING OUT.
      WRITE(6,83)
      WRITE(6,84) RCORE, BVALU
      WRITE(6,80)
      WRITE(6,81)

```

109

```

2001 CONTINUE
DO 730 I=1,NPKB
IF(KINGB(I).NE.0) GO TO 730
LAST2=I-1
GO TO 740
730 CONTINUE
740 DO 720 I=1, LAST2
ADUMP(I)=KINGB(I)
720 CONTINUE
WRITE(6,1634)
1634 FORMAT(////,20X,"THE VALUES OF INTENSITY FOR THE"
1 ,IX,"KING MODEL ARE:")
WRITE(6,1635) (ADUMP(J),J=1, LAST2)
1635 FORMAT(/,2X,10F8.3)
CALL BRGTNS(KINGB,KBRT, LAST2)
C
C NOW TO NORMALIZE THE KING MODEL AS TO PARTIAL INTENSITY.
C THE CORE RADIUS IN THE KING MODEL IS SET TO RCORE
C IN ARC-SECONDS. THIS IS THEN USED TO SCALE THE KING MODEL.
READ(5,23)RMAX
23 FORMAT(F6.2)
READ(5,22) RCORE
22 FORMAT(F5.2)
DO 10 II=1, LAST1
RADKS(II)=KRAD(II)*RCORE
IF(RADKS(II).LE.RMAX) GO TO 10
IEND=II
GO TO 12
10 CONTINUE
12 CONTINUE
C
C NEXT TO NORMALIZE FOR THE INTENSITY, WE WISH TO SET THE CENTRAL
C INTENSITY VALUE OF THE KING MODEL TO A RELATIVE INTENSITY WHICH
C IS THE BEST AVERAGE OF THE FITTING PROCESS PERFORMED BY THE
C PROGRAMME 'REDUCE'. (IE, THE AVERAGE BEST FIT OF A KING MODEL AND THE
C OBSERVED TRACING).
READ(5,101) BVALU
101 FORMAT(F6.0)
CALL MAX(KBRT,MAXBRT,IEND)
DO 15 II=1,IEND
BNORM(II)=(BVALU/MAXBRT)*KBRT(II)
15 CONTINUE
DO 8 I=1,IEND
RKLOG(I)=ALOG10(RADKS(I))
BKLOG(I)=ALOG10(BNORM(I))
8 CONTINUE
C
C NOW TO WRITE EVERYTHING OUT.
WRITE(6,83)
WRITE(6,84) RCORE, BVALU
WRITE(6,80)
WRITE(6,81)
WRITE(6,82) (RADKS(II),BNORM(II),RKLOG(II),
1 BKLOG(II),II=1,IEND)
80 FORMAT(////,25X,"THE VALUES FOR THE NORMALIZED KING MODEL ARE:")
81 FORMAT(////,15X,"RADIUS(ARC-SEC.)",10X," INTENSITY",17X,
1 "LOG(RADIUS)",10X,"LOG(INTENSITY)")
82 FORMAT(/,16X,F10.4,14X,F10.4,18X,F10.6,12X,F10.6)
83 FORMAT(////,20X," THE MODEL GALAXY , USING A NORMALIZED"
1 ,IX,"KING MODEL IS LISTED BELOW.",//,35X," NOTE: LOG10(R/RCORE)"
1 , " = 2.25 ")
84 FORMAT(////,15X," THE VALUE OF THE CORE RADIUS USED IS ",F5.2,
1 " ARC-SEC. AND THE VALUE OF THE CENTRAL INTENSITY IS ",F6.0)
WRITE(6,98) (RADKS(I),I=1,IEND)
WRITE(6,99) (BNORM(I),I=1,IEND)
98 FORMAT(10F8.3)
99 FORMAT(10F8.3)
STOP
END
C
C THESE ARE THE SUBROUTINES WHICH FOLLOW.
C
C SUBROUTINE RADUS(LRAD,RAD,NP)
C THIS ROUTINE FINDS THE ANTI-LOG OF THE RADII.
REAL LRAD
DIMENSION LRAD(NP), RAD(NP)
DO 15 IJ=1,NP
RAD(IJ)= 10.**(LRAD(IJ))
15 CONTINUE
RETURN
END
C
C SUBROUTINE BRGTNS(LBRT,BRT,NP)
C THIS ROUTINE TAKES THE ANTI-LOG OF LBRT
REAL LBRT
DIMENSION LBRT(NP), BRT(NP)
DO 20 JJ=1,NP
BRT(JJ)= 10.**(LBRT(JJ))
20 CONTINUE
RETURN
END
C
C SUBROUTINE MAX(X,XMAX,NP)
C THIS ROUTINE FINDS THE MAXIMUM VALUE OF THE DATA SET INVOLVED AND
C CAUSES THAT MAXIMUM TO BE SET BACK TO THE MAIN PROGRAMME.
DIMENSION X(NP)
XMAX=0.0
DO 111 KI=1,NP
IF(XMAX.LT.X(KI)) GO TO 110
GO TO 111
110 XMAX=X(KI)
111 CONTINUE
RETURN
END

```

REFERENCES

1. Binney, J.; (1978) *Comments Astrophys.* 8, #2.
2. Carter, D.; (1977) *Mon. Not. RAS.* 178, 137.
3. Chandrasekhar, S.; (1960) "Principles of Stellar Dynamics", Dover, New York, N.Y., Chapter II.
4. Chandrasekhar, S.; (1943) *Rev. Mod. Phys.* 15, 1.
5. Chincarini, G.; Rood, H.J.; Sastry, G.N.; Welch, G.A.; (1971) *Ap.J.* 168, 11.
6. de Vaucouleurs, G.; (1959) *Hdbk. der Physik* LIII, 311.
7. Dressler, A.; (1979) *A.J.* 231, 659.
8. English, D.; (1979) M. Sc. Thesis, St. Mary's University, Halifax.
9. Faber, S.M.; (1973) *Ap.J.* 179, 423.
10. Freeman, K.C.; (1975) in "Stars and Stellar Systems" Vol. IX, eds A. Sandage, M. Sandage and J. Kristian; Univ. of Chicago Press.
11. Hintzen, P.; (1979) *Pub. A.S.P.* 91, 426.
12. Hodge, P.W.; (1971) *Ann. Rev. Ast. & Ap.* 9, 35.
13. Hubble, E.; (1930) *Ap.J.* 71, 231.
14. Huchra, J. (1982) private communication.
15. Illingsworth, G.; (1977) *Ap.J. Letts.* 218, L43.
16. Jeans, J.; (1915) *Mon. Not. RAS.* 76, 70.
17. King, I.R.; (1962) *A.J.* 67, 471.
18. King, I.R.; (1966) *A.J.* 71, 64.
19. King, I.R.; (1978) *Ap.J.* 222, 1.
20. King, I.R.; (1980) private communication.
21. Kodak Corp.; (1967) in "Kodak Plates and Films" Eastman Kodak Co., Rochester, N.Y.

22. Kormendy, J.; (1977) Ap.J. 218, 333.
23. Miley, G.K., and Harris, D.E.; (1977) Ast & Ap 61, L23.
24. Demler, A.; (1973) Ap.J. 180, 11.
25. Demler, A.; (1976) Ap.J. 209, 693.
26. Schweizer, F.; (1979) Ap.J. 233, 23.
27. Schweizer, F.; (1981) A.J. 86, 662.
28. Spitzer, L. and Harm, R.; (1958) Ap.J. 127, 544.
29. White, S.D.M.; (1976) Mon. Not. RAS. 174, 19.